

401 890

63-3-2

①

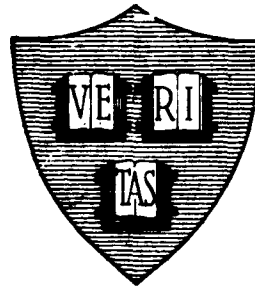
Office of Naval Research

Contract Nonr-1866(16)

NR-372-012

AD No. 401 890
ASTIA FILE COPY

**ELECTRIC FIELD EFFECTS
IN PARAMAGNETIC RESONANCE**



By
E. B. Royce

February 12, 1963

Technical Report No. 379

Cruft Laboratory
Harvard University
Cambridge, Massachusetts

R //, 00

MAY 3 1963

RECEIVED
TISIA A

Office of Naval Research

Contracts

(12) Nonr-1866(16) ^{Part} NR - 372 - 012

and

Nonr-1866(28) ^{Part} NR - 372 - 013

(7)

Technical Report

(6)

ELECTRIC FIELD EFFECTS IN PARAMAGNETIC RESONANCE

(8)

by

E. B. Royce

(9)

February 12 1963

The research reported in this document was made possible through support extended Cruft Laboratory, Harvard University, jointly by the Navy Department (Office of Naval Research), the Signal Corps of the U. S. Army, and the U. S. Air Force, under ONR Contracts Nonr-1866(16) and (28). Reproduction in whole or in part is permitted for any purpose of the United States Government.

(10) iv. incl.
illus. Tables,
ref

(13)

NA

(14)

Uncl

(15) NA

(11)

Technical Report No. 379

Cruft Laboratory

Harvard University

Cambridge, Massachusetts

(5)

234 300

etc

TABLE OF CONTENTS

Table of Contents	iii
List of Figures	v
List of Tables	vi
Abstract	vii
CHAPTER I	
Introduction, Survey of the Thesis, and Miscellaneous Topics	1-1
The Paramagnetic Resonance Phenomenon	1-1
Electric Field Effects in Paramagnetic Resonance	1-5
Linear Electric Field Effects	1-8
Second Order Effects	1-13
Permanent Electric Dipole Moments	1-14
CHAPTER II	
Experimental Procedures, Apparatus, and Results	2-1
Practical Considerations in Paramagnetic Resonance Experiments	2-1
The Absorption Spectrometer	2-3
The Dispersion Spectrometer	2-9
Experimental Work	2-10
CHAPTER III	
Experimental Results, Ruby Electric Field Experiment	3-1

CHAPTER IV

Theory of the Electric Field Effect in MgO:Cr and Al ₂ O ₃ :Cr	4-1
Digression on the Theory of Dielectrics	4-9
Primitive Crystal Field Theory for MgO:Cr	4-21
Crystal Field Theory of Al ₂ O ₃ :Cr	4-26
Semi-Empirical Molecular Orbital Theory of Al ₂ O ₃ :Cr	4-33
Improved Theory of MgO:Cr	4-49
Quadratic Electric Field Effects in Ruby and MgO	4-52
Discussion and Conclusions	4-54

CHAPTER V

Theory of the Quadratic Electric Field Effect in TiO ₂ :Cr and TiO ₂ :Fe	5-1
Molecular Orbital Theory for TiO ₂ :Cr	5-3
Crystal Field Theory for TiO ₂ :Fe	5-5
Molecular Orbital Theory for TiO ₂ :Fe	5-8

CHAPTER VI

On the Electric Dipole Moment of the Electron	6-1
Theoretical Considerations	6-2
Experimental Procedures and Results	6-7
Acknowledgments	6-12
References	R-1

LIST OF FIGURES

<u>Figure Number</u>		<u>After Page</u>
2-1	Detail of microwave cavity	2-4
2-2	Block diagram of the paramagnetic resonance absorption spectrometer	2-4
2-3	Block diagram of the paramagnetic resonance dispersion spectrometer	2-10
3-1	Experimental absorption derivative curve showing electric field induced splitting of Cr^{+3} $1/2 \rightarrow 3/2$ resonance line	3-2
3-2	Linear variation of electric field induced line splitting	3-2
3-3	Quadratic variation of electric field induced line broadening for splittings less than one line width	3-2
3-4	Portion of Al_2O_3 lattice showing the coordinate system used in this work	3-4
3-5	Angular dependence of the electric field induced splitting, where the magnetic field is rotated about the y-axis. E is parallel to the x-axis.	3-8
3-6	Angular dependence of the electric field induced splitting, where the magnetic field is rotated about the y-axis. E is parallel to the y-axis.	3-8
3-7	Angular dependence of the electric field induced splitting, where the magnetic field is rotated about the z-axis. Electric field along the x- and y-axes, respectively	3-8
4-1	One-electron crystal field splitting in ruby for cubic and trigonal fields	On Page 4-27
4-2	Energy levels for d^3 in a cubic field	4-28
4-3	One-electron splittings in MgO:Cr in cubic and tetragonal fields	4-49
5-1	Ti site in TiO_2	5-2

LIST OF TABLES

<u>Table Number</u>		<u>After Page</u>
3-I	Values of elements of the R-tensor for two types of site in ruby	3-10
		<u>On Page</u>
4-I	Dielectric parameters	4-20
4-II	Crystal field splittings in the molecular orbital formulation	4-40
4-III	$R_{ijk}(\lambda)$ in Eq. 4-69	4-45
4-IV	Calculated values of the elements of the R-tensor	4-46
		<u>After Page</u>
6-I	Electronic electric dipole moment	6-2
6-II	Electric dipole moments of the elementary particles	6-2

ABSTRACT

↙ The electric field effects in paramagnetic resonance consist of shifts in resonance frequency produced by the application of a uniform electric field to the magnetic resonance sample. These electric field shifts arise through variations in the crystal field splittings under the influence of the applied electric field. In a non-piezoelectric sample, two mechanisms are considered to be important in producing the electric field induced variation in crystal field. The optical mode ionic polarization of the crystal lattice, in which the anion and cation sublattices move with respect to each other, produces a variation in the local crystalline environment of the magnetic ion and, hence, in its crystal field interaction; the electronic polarization of the magnetic ion alters its interaction with its crystalline surroundings, again producing a variation in the crystal-field interaction. Effects of electrostriction and piezoelectric distortion are mentioned but not treated in this work.

If the magnetic ion is at a crystalline lattice site which is not a center of inversion symmetry, there may be an electric field effect which is linear in the applied electric field. A linear splitting of the paramagnetic resonance lines of Cr^{+3} in ruby by 38 gauss was induced by an electric field of 10^5 volts/cm parallel to the c-axis. The splitting arises from an equal but oppositely directed shift of the Cr^{+3} spin energy levels for two sites related to each other by the symmetry operation of inversion. The complete angular dependence of the effect is described phenomenologically ↗

by the addition of a term to the spin Hamiltonian $(1/2) R_{ijk} E_i (S_j S_k + S_k S_j)$, $j \leq k$. The symmetry of the R-tensor is discussed in terms of the symmetry of the magnetic ion site. For ruby, this symmetry is C_3 , and the five independent components of the R-tensor were evaluated experimentally by taking the applied electric and magnetic fields at several different orientations with respect to each other and to the c-axis. These values indicate that one of the two oxygen ion triangles forming the nearest neighbor oxygen octahedron dominates the other triangle in producing the crystal field splitting.

The theory of the electric field effect in ruby is discussed, first, in terms of a point-charge crystal field theory. Such a theory is inadequate to account for the spectrum of the Cr^{+3} ion in ruby unless adjustable parameters are introduced. Even with adjustable parameters, however, the crystal field theory is still inadequate to account for the microwave spectrum or for the electric field effects on the microwave spectrum. Turning to a semi-empirical molecular orbital formulation, the microwave spectrum and the electric field effects are successfully accounted for. The semi-empirical procedure consists of diagonalizing an approximate Hamiltonian, whose diagonal elements \mathcal{H}_{ii} are determined by free ion ionization potentials and whose off-diagonal elements are given by $\mathcal{H}_{ij} = -2 (\mathcal{H}_{ii} \mathcal{H}_{jj})^{1/2} S_{ij}$. S_{ij} is the overlap matrix of the atomic orbital basis functions. The spin-orbit interaction is introduced as a perturbation using the molecular orbital wave functions as a

basis set, and it is found that the microwave splittings and electric field effect arise from an anisotropy in the spin-orbit interaction. The ionic effect is found to be much larger than the electronic effect.

For Cr^{+3} in a defect site in MgO , a linear electric field splitting of the resonance line from two sites is predicted by the molecular orbital theory to be 0.9 gauss for an applied field of 10^5 volts/cm. The sensitivity of the experiment was not sufficient to detect the effect. If by the extreme adjustment of suitable parameters, the crystal field theory is forced to yield the experimental values of the electric field effect in ruby, the same theory then yields an effect in MgO which would have been large enough to be easily detectable. This constitutes an additional piece of evidence for the superiority of the molecular orbital theory over the crystal field theory.

A quadratic electric field shift in the Cr^{+3} and Fe^{+3} magnetic resonance spectrum in TiO_2 is calculated by the molecular orbital theory. The failure to detect this effect experimentally for Fe^{+3} is analyzed to give information about the polarizability of the impurity in a foreign host lattice.

In addition to the electric field effects discussed, the possible existence of an electronic electric dipole moment would cause a lifting of the Kramers degeneracy in the presence of an electric potential of odd symmetry. By attempting to detect the lifting of the Kramers degeneracy in the odd part of the crystalline electric field for Cr^{+3} in ruby, it was possible to set a new

experimental upper bound of 1.4×10^{-15} cm e on the electric dipole moment of the electron. The ordinary electric field effect was used to lift the degeneracy of the two kinds of sites in ruby. The significance of this result lies in the fact that the existence of a permanent electric dipole moment for an elementary particle would violate both parity and time-reversal symmetry.

Chapter I

INTRODUCTION, SURVEY OF THE THESIS, AND MISCELLANEOUS TOPICS

Electron paramagnetic resonance provides a sensitive probe of the surroundings of a magnetic ion in a diamagnetic host lattice. In general, a paramagnetic ion with spin greater than one half is influenced by the electrostatic field of its crystalline surroundings through the spin-orbit interaction. Thus, the Zeeman resonance condition on the magnetic field and microwave frequency is modified to include the effect of the crystalline-field interaction. Under the action of a uniform electric field applied to the sample, there is a change in the interaction of the magnetic ion with its surroundings, and a shift in magnetic resonance occurs. In the usual spin Hamiltonian formulation, all parameters become a function of the applied electric field.

The Paramagnetic Resonance Phenomenon

The paramagnetic resonance phenomenon has been described in several review articles [1-1], and the reader is referred to these articles or to the more elementary texts [1-2] for details.

Consider a free ion. The electron has a spin angular momentum whose magnitude is given by $[S(S+1)]^{1/2} \hbar$, where S is an integer or half integer. Similarly, the orbital angular momentum of the electron is given by $[L(L+1)]^{1/2} \hbar$, and the total angular momentum by $[J(J+1)]^{1/2} \hbar$. The spin and orbital angular momenta combine so that $J = L + S$ for shells more than half filled or $J = |L - S|$ for shells less than half filled. The spin-orbit interaction energy,

$\lambda \underline{L} \cdot \underline{S}$, and the electrostatic forces between electrons split these J levels.

The spin angular momentum gives rise to a magnetic dipole moment

$$\mu = 2 \frac{e\hbar}{2mc} [S(S+1)]^{1/2} \quad (1-1)$$

If we define the Bohr magneton $\beta = \frac{e\hbar}{2mc}$, we have

$$\mu = 2\beta [S(S+1)]^{1/2} \quad (1-2)$$

The magnetic moment associated with the orbital angular momentum is

$$\mu = \beta [L(L+1)]^{1/2}, \quad (1-3)$$

and because of the anomalous factor of two in the spin equation, we

write for the total magnetic moment

$$\mu = g\beta [J(J+1)]^{1/2} \quad (1-4)$$

g is given by the well-known Landé formula

$$g = \frac{3J(J+1) + S(S+1) - L(L+1)}{2J(J+1)} \quad (1-5)$$

The Zeeman effect gives an energy on the application of a magnetic field

$$W = -\underline{\mu} \cdot \underline{H} \quad (1-6)$$

If the projection of \underline{J} on the z-axis (the z-axis being taken along H) is

M_J , and the projection of $\underline{\mu}$ is $\mu_z = g\beta M_J$, the Zeeman energy is

$$W = -g\beta M_J H \quad (1-7)$$

Noting that M_J must be an integer or half integer, we have $2J + 1$

levels separated by

$$\Delta W = g\beta H \quad (1-8)$$

From the Bohr frequency condition and noting that $\Delta M_J = 1$, we have the absorption of power at a frequency

$$\nu = g\beta H/h \quad (1-9)$$

In a paramagnetic resonance experiment we measure the absorption of electromagnetic energy as a function of frequency or magnetic field, and hence, determine an experimental value of g from the position of an absorption line.

For free ions or atoms, g is given by the Landé formula, but for atoms in a solid, the situation is very different. The ligands, or ions surrounding the ion under consideration, produce local electric fields which act on the orbital angular momentum. This crystalline electric field interacts with the nonspherical distribution of electrons, which is characterized by the orbital quantum number. If this interaction is stronger than the spin-orbit interaction, the $\underline{L} \cdot \underline{S}$ coupling is broken down, J is no longer a good quantum number, and the $2L + 1$ degeneracy of the orbital angular momentum is lifted. The crystalline field in some cases is comparable to the electrostatic repulsion between electrons, in which case the Russell-Saunders coupling is partially destroyed. In this case, L is no longer a good quantum number either, and orbital wave functions are characterized by the eigenvalues of the crystalline field. For the transition metal ions of the iron group this is the case, and the combined crystalline-field interaction and electron repulsion energy yield orbital energy levels split by optical frequencies. For the ions of interest here, the ground state is an orbital

singlet, whose multiplicity is given by the spin. In this case the diagonal elements of L are "quenched", and the angular momentum and magnetic moment are simply given by the spin-only formulas, namely, $g = 2$. There are, however, small splittings of the ground state produced by the off-diagonal elements of L between the optical levels, which in turn are split to a smaller degree by low symmetry components of the crystal field. In second-order perturbation theory one has

$$\Delta W = \lambda^2 / \Delta W_{\text{opt}} \quad (1-10)$$

These splittings are typically comparable to the Zeeman energy and are called zero (magnetic) field or crystal field splittings. There may, also, be g -value shifts. As an example, in ruby the $M_S = \pm 1/2$ and $M_S = \pm 3/2$ levels are split from each other by 11 Gc/sec, which is the Zeeman frequency for spin 1/2 in a field of 4000 gauss. The energy levels of the ground orbital state may be described by the spin Hamiltonian, in which the energy is a function only of S . The zero field splittings are represented by terms in the spin Hamiltonian which contain even powers of S . Neglecting nuclear spins, electron-electron spin interactions, and the diamagnetic term, one has the following form of the spin Hamiltonian for a spin of 3/2 or less

$$\mathcal{H} = \sum 2\beta (\delta_{ij} - \lambda\Lambda_{ij}) H_i S_j - \lambda^2 \Lambda_{ij} S_i S_j - \beta^2 \Lambda_{ij} H_i H_j, \quad (1-11)$$

where

$$\Lambda_{ij} = \sum_{n \neq 0} \frac{\langle 0 | L_i | n \rangle \langle n | L_j | 0 \rangle}{E_n - E_0} . \quad (1-12)$$

The first term in 1-11 is the usual Zeeman energy, and the second, third, and fourth arise from off-diagonal elements of the spin-orbit interaction $\lambda \underline{L} \cdot \underline{S}$, the off-diagonal elements of the orbital Zeeman energy $\beta \underline{L} \cdot \underline{H}$, or both together.

Electric Field Effects in Paramagnetic Resonance

Now consider a sample of material situated in a paramagnetic resonance spectrometer and with electrodes applied for the production of a uniform static electric field across the sample. The construction of two such spectrometers is described in Chapter II. Both were of the magic tee bridge design; one designed to observe the absorption signal and the other the dispersion signal.

The application of an electric field to the sample produces a dielectric polarization of two kinds. [1-3]. If an ionic crystal is considered and if the electronic polarization of the individual ions is ignored, there will remain a polarization resulting from the motion of positive and negative ions with respect to each other. The cation and anion sublattices can be considered to move with respect to each other, each sublattice remaining rigid. This may be termed the ionic polarization, or infrared polarization since it relaxes in the infrared spectral region. From the point of view

of the magnetic cation, its surrounding anions have moved, and the crystalline electric field they produce on the cation has changed. This crystalline field, together with the spin-orbit interaction, gives rise to the zero field splittings, as shown in Eqs. (1-11) and (1-12). The crystalline electric field enters through the energy denominators of Eq. (1-12). Thus, under the application of an electric field to a sample, the crystalline field and, hence, the zero field splittings are altered. This, in turn, results in a shift in magnetic resonance frequency (or field in a constant frequency spectrometer). It is these shifts which constitute the electric field effects in magnetic resonance.

The effect originating as described in the previous paragraph may be termed the ionic electric field effect. There is also an electronic electric field effect originating from the direct action of an applied electric field on the individual ions. In considering this effect, the nuclei are kept fixed and the individual electron clouds are allowed to polarize. This polarization is represented by a mixing of even and odd electronic wave functions (e. g. sp -mixing), and this mixing produces a change in the energy levels of the system. This change in energy levels again is reflected in spectroscopy and, in particular, in microwave spectroscopy primarily through the zero-field splitting. As the electronic electric field effect is associated with the electronic polarization of the ions, so the ionic effect is associated with the ionic polarization.

The electric field effects in paramagnetic resonance are closely related to the effects of pressure on paramagnetic resonance. In both cases an external stress is imposed on the system. In one case the stress is electrical; in the other it is mechanical. The paramagnetic resonance detects an effect of the resultant strain. Walsh [1-4] first observed the effect of applying hydrostatic and uniaxial stress to a crystal in a paramagnetic resonance spectrometer. His experiments were carried out on the paramagnetic resonance of several impurities in MgO and on the resonance of chromium in two salts. Uniaxial strain experiments have been carried out on several ions in MgO by Watkins and Feher [1-5] and on ruby by Donoho and Hemphill [1-6]. Date and Miyako [1-7] have studied the pressure dependence of the cobalt resonance in TiO_2 , and recently other workers have carried out similar experiments in SrTiO_3 and calcite [1-8, 1-9]. Such experiments provided the suggestion that there might also be observable electric field effects in paramagnetic resonance.

The electric field effects described here are in addition to the indirect effect which may exist in a piezoelectric material. In a piezoelectric material there is the effect that the piezoelectric strain also distorts the surroundings of the magnetic ion, and a mechanical strain experiment will separate this effect from the combination of the direct electronic and ionic effects described previously. Such an experimental

separation between ionic and electronic effects can not be made, since it is impossible to produce mechanically the strain associated with the dielectric lattice polarization.

The actual calculation of the electric field effects, direct or indirect, involves the rederivation of the spin Hamiltonian in the presence of the electrical perturbation. This, in turn, leads to the somewhat more general question of the calculation of the entire electronic spectrum of a magnetic ion, a subject which has been treated by many authors [1-1]. The spin Hamiltonian describes the splitting of the optical ground state under the influence of the Zeeman and crystalline fields. The details of this splitting involve high order perturbation theory between the ground and optically excited levels, and this requires a fairly detailed knowledge of the entire optical spectrum. The traditional approach to this problem involves the so-called point-charge crystal field model, in which the effect of the surroundings of the magnetic ion are described by a classical electrostatic crystalline field interaction produced by point charges located at the sites of each of the neighbors. It will be shown in Chapter IV that this approach is inadequate to describe the magnitudes of the observed electric field effects, and a molecular orbital calculation will be presented which does account for the results.

Linear Electric Field Effects

A linear electric field effect can exist only if the magnetic ion is located at a lattice site which is not a center for inversion symmetry [1-10]; if the site has inversion symmetry, there can be only a quadratic

effect. This arises because a linear effect must reverse its sign on reversal of the direction of the applied electric field. If there is inversion symmetry, this is impossible, since there is nothing to distinguish the positive from the negative directions.

The first linear electric field effects in magnetic resonance were observed in nuclear pure quadrupole resonance. Kushida and Saiki [1-11] observed an electrically induced shift in the pure quadrupole resonance of the bromine nuclei in a single crystal of NaBrO_3 , and Armstrong, Bloembergen, and Gill [1-12] observed the electrically induced additional broadening of the resonance line from chlorine nuclei in powdered KClO_3 and NaClO_3 . In all three cases the nuclear site does not have inversion symmetry, allowing the resonance frequency shift to be linear in the applied electric field. The crystal KClO_3 has an inversion center, which means that shifts from two sites related to each other by inversion are in opposite directions. This effect was, however, washed out by the use of a powder sample. NaClO_3 and NaBrO_3 do not have inversion centers, and true shifts should be observable. The use of a powder sample of NaClO_3 , however, again obscured this fact. Armstrong, Bloembergen, and Gill [1-13] have observed electric field broadenings in p-dichlorobenzene, and Dixon [1-14] has observed electrically induced broadenings in several other chlorine compounds. These experiments were all done on the pure quadrupole splitting of the chlorine nuclei in polycrystalline samples. Gill and Bloembergen [1-15] have studied the nuclear magnetic resonance of Ga and As nuclei in GaAs single crystals. Both Ga and As have nuclear spin $I = 3/2$. In GaAs the lattice sites are of cubic symmetry but do

not have inversion symmetry. Since the sites are cubic, there is no initial quadrupole splitting, and a single resonance line is observed in a magnetic field. Under the influence of an applied electric field, an induced quadrupole splitting of the fourfold degenerate spin energy levels occurred. The single resonance line was split into three lines. Because GaAs does not have an inversion center, there is also a piezoelectric strain effect, which was separated out by a pressure experiment.

The first linear electric field effect in paramagnetic resonance was observed by Ludwig and Woodbury for an Fe^0 impurity in silicon. [1-16]. Through the kindness of Dr. Ludwig, a suitable sample of iron doped silicon was obtained, and the effect observed by Ludwig and Woodbury was confirmed qualitatively. Details are presented in Chapter II. More recently, Ludwig and Woodbury have investigated many other ions in the silicon lattice and have found numerous electric field effects. [1-17]. The silicon lattice, of course, contains an inversion center, though the tetrahedral sites themselves do not. As a result of the inversion symmetry of the lattice, one should consider at least two non-equivalent sites which are inversion images of each other. Such sites will be equivalent for ordinary paramagnetic resonance but will have electric field induced shifts which are equal in magnitude but opposite in sign. Thus, while an electric field effect which consists of a shift in resonance frequency or field is calculated for a particular transition of an ion at a single site, in fact

both kinds of sites are observed together. The ground state of the Fe° ion in the cubic environment of silicon is threefold degenerate; the effective spin in the spin Hamiltonian is one. The applied electric field lifts this degeneracy, and the observed paramagnetic resonance line in magnetic field is split into a doublet. The $M_S = 0 \rightarrow +1$ transition and $M_S = 0 \rightarrow -1$ transition shift in opposite directions due to the applied electric field; they are degenerate in the absence of an applied electric field. For one site in the silicon lattice it is the $M_S = 0 \rightarrow +1$ transition which shifts up in field, while for the other site, it is the $M_S = 0 \rightarrow -1$ transition which shifts up, but of course, this cannot be observed because of the initial degeneracy.

Chromium substituted in MgO enters the lattice primarily by substituting for magnesium at sites which have inversion symmetry and are in fact cubic [1-18]. Such ions should not show a linear electric field effect. Some of the ions, however, will have a vacancy at the site of the nearest magnesium neighbor in a 100 direction for purposes of charge compensation. This gives rise to a site which has axial symmetry and which is not an inversion center. Cr^{+3} , with an effective spin of $3/2$ has two Kramers doublets in the optical ground state for the axial site. The application of an electric field should alter the initial splitting between the $M_S = \pm 1/2$ and $M_S = \pm 3/2$ doublets, and should cause a shift of the $M_S = 1/2 \rightarrow 3/2$ transition. Since this transition is non-degenerate for a particular axial site, a shift rather than a splitting of the resonance line should be observed. As in the silicon lattice, however, there is an

inversion center in the MgO lattice, and two sites which are inversion images of each other must be considered. These sites should have electrically induced shifts of opposite sign and a single resonance line should be observed apparently being split into two components moving in opposite directions under the application of the electric field. While one could speak of the electric field splitting, it should be remembered that in this case there would be only an apparent splitting of the observed resonance line arising from all of the spins in the solid. Microscopically, there would be an electrically induced shift in the resonance line and in the energy levels giving rise to it.

An attempt was made to detect an electric field splitting of the resonance line from ions in the axial sites in MgO, but none could be detected, and an upper bound was determined by the experiment. This bound is of some importance to the theory of the electric field effect in ruby, since the point-charge crystal field theory of the electric field effect in ruby, when scaled by the value of D in MgO, predicts an effect in MgO ten times larger than the experimental upper bound. The molecular orbital theory, however, is able to account for the smallness of the electric field effect in MgO as compared to the electric field effect in ruby.

The situation of the chromium ions in ruby [1-19, 1-20] is similar to that in MgO in that, while the crystal has inversion symmetry, the individual sites do not. Thus, electric field induced shifts in the resonance

lines from individual sites combine to produce an observed electrically induced splitting of the line. Details of the symmetry of the sites in ruby are presented in Chapter III. The electric field induced splitting in ruby was first detected by Artman and Murphy [1-21]. These experiments were duplicated, and the angular dependence of the effect was determined. Further details of this work are given in Chapter III and have been reported [1-22] and published elsewhere [1-23].

Second-Order Effects

For sufficiently strong electric fields it should be possible to observe a second-order electric field effect proportional to the square of the applied electric field. In TiO_2 the large dielectric constant would indicate that the indirect electric field effect on magnetic resonance should be large. The second-order ionic effect was calculated for the resonance of Fe^{+3} in TiO_2 [1-24] by the molecular orbital method. Experimentally, the effect could not be found, and an upper bound was set which is an order of magnitude smaller than the calculated effect. This experiment is interpreted in Chapter V to give details about the electrical polarizability of the impurity in the strongly dielectric host lattice.

Recently, Weger and Feher [1-25] have reported second-order electric field effects in the paramagnetic resonance of Cr^{+3} in ruby and of Cr^{+3} and Co^{+2} in MgO . These experiments are discussed in Chapter IV.

Permanent Electric Dipole Moments

The observed electric field effects should not be confused with the possible existence of an intrinsic electric dipole $\underline{P} = 2 \xi \beta \underline{S}$, which would give rise to a term in the Hamiltonian $-2 \xi \beta \underline{S} \cdot \underline{E}$. β is the Bohr magneton; ξ is the pseudo-scalar. A consequence of such a term is that the Kramers degeneracy would be lifted by an applied electric field or by any electrostatic potential of odd symmetry, such as the odd terms in the crystalline potential. The effect of such a term on paramagnetic resonance has been calculated by Sachs and Schwebel [1-26], who predict a line shift of the order

$$\Delta W = \lambda (W_g - W_u)^{-1} 2 \xi \beta |e^{-1} \nabla V_{\text{crystal}}^u - E_{\text{applied}}|. \quad (1-13)$$

Browne [1-27] has experimentally attempted to detect such an effect using an externally applied electric field, with negative results.

The term $e^{-1} \nabla V_{\text{crystal}}^u$, however, is much larger than any applied field, and a scheme was devised to check the existence of a permanent electric dipole using this fact. This experiment on ruby has yielded an upper bound on the electric dipole moment of the electron which is three times lower than the limit, set by the electron beam experiments of Nelson, et. al., [1-28]. Further details are given in Chapters II and VI.

Chapter II

EXPERIMENTAL PROCEDURES, APPARATUS, AND RESULTS

The paramagnetic resonance phenomenon has been described in Chapter I [2-1]. Experimentally, one has a sample of paramagnetic material absorbing power at certain frequencies, which are determined by differences in the eigenvalues of the spin Hamiltonian. These frequencies are a fairly complicated function of the magnitude of the applied magnetic field and of the orientation of the magnetic field with respect to the crystallographic axes. The paramagnetic resonance spectrometer is a device for detecting the absorption of a small amount of power by such a sample. Experimentally, the magnetic field at resonance absorption is measured as a function of the angle of the magnetic field with respect to the crystallographic axes, the microwave frequency being held fixed. In this work, a uniform electric field was applied to the sample as well, and the resultant shifts of the value of the resonance field were studied. Usually, these shifts appeared as splittings of the observed line.

Practical Considerations in Paramagnetic Resonance Experiments

Of considerable practical importance in spectroscopy is the width of the observed resonance line. Not only is the position of a broad resonance line difficult to resolve, but also, the spreading of the absorption over a wide spectral region weakens the intensity of absorption at a particular point.

Spin-spin interactions between the resonant ion and some other like or unlike ion causes an effective local variation of the magnetic field acting on the resonant ion. Random fluctuations in time or space in these local

variations produce a line broadening. Dilution of the magnetic ions in a diamagnetic host lattice will reduce this broadening mechanism as much as desired. There may also be an exchange interaction between the like magnetic ions, which broadens the base of the line but sharpens the peak. It, too, is reduced by dilution.

Nuclei may have small magnetic moments, and the hyperfine interaction between the nuclear moments and the electron moment of the resonant ion may either split the line into a series of lines or may broaden the line. Fortunately, for the materials used in this work, hyperfine splittings and broadenings are of no importance, since most of the nuclei have no magnetic moment.

The lifetime of a state produces an uncertainty in its energy given by the usual quantum mechanical uncertainty relation. In the case of the ions used in this work, the relaxation rates are sufficiently slow so that this is no problem. In some cases lifetime broadening may be fairly serious. The relaxation of spins from one state to another takes place by means of the coupling of the spins to the crystalline lattice through the spin-orbit and possibly the spin-spin interactions. The direct process involves emission of a single phonon of lattice vibration, while the Raman-like process involves two phonons. The direct process is proportional to $1/T$ and dominates at low temperatures, while the Raman process has a faster temperature dependence and dominates at higher temperatures. These simple interactions may be further complicated

by interactions with defect centers or clusters of impurity atoms. A more serious problem arising from the lifetime occurs if the lifetime is too long. In this case, only a small amount of power can be absorbed, and the sensitivity is severely reduced. This problem will be dealt with further.

The dominant line broadening for the ions of interest in this work arises from variations in the crystalline field splitting. Such variations from point to point in the lattice arise from defects in the lattice structure.

The selection rules on the transition probabilities for magnetic dipole transitions require that the radio frequency magnetic field be at right angles to the static magnetic field. In the presence of zero-field splittings, and with the magnetic field not taken along the axis of quantization of the crystalline field, these selection rules break down due to mixing of the wave functions. However, transition probabilities are still favorable with the radio-frequency magnetic field perpendicular to the static magnetic field, except at very low fields.

The Absorption Spectrometer

In order to enhance the interaction of the sample with the microwave field, the sample is placed in a resonant microwave cavity [2-2]. The spectrometers constructed for this work employed a rectangular waveguide cavity operating in the TE_{012} mode (Fig. 2-1). The sample was located at the center of the cavity at a position of the maximum transverse microwave magnetic field. The static magnetic field was applied normal to the broad face of the waveguide, making it perpendicular to the microwave field, in

keeping with selection rules mentioned. In the work on ruby, in order to rotate the magnetic field with respect to the crystallographic axes, the sample was kept fixed in the cavity, and the entire spectrometer was rotated in the magnetic field. Less favorable transition probabilities were then encountered, but this proved not to be disastrous. Provision was made to adjust remotely the resonant frequency of the cavity and the coupling of the cavity to the input waveguide. Adjustment of the coupling was accomplished by moving a teflon wedge in a section of waveguide beyond cutoff. A small tuning adjustment was made by screwing a threaded teflon rod into the cavity. Control rods for both operations were placed inside the waveguide; a waveguide bend at the top of the spectrometer assembly allowed the control rods to leave the waveguide.

Microwave power, generated by a Varian Associates X-12 klystron, was reflected from the cavity and compared to that reflected from a matched load by means of a magic tee bridge. The amount of power reflected is adjusted by adjusting the coupling. This reflected power is proportional to the Q of the cavity and, hence, to any power absorption. When the paramagnetic resonance condition is fulfilled, the sample absorbs a small amount of power, and the power reflected changes accordingly (Fig. 2-2).

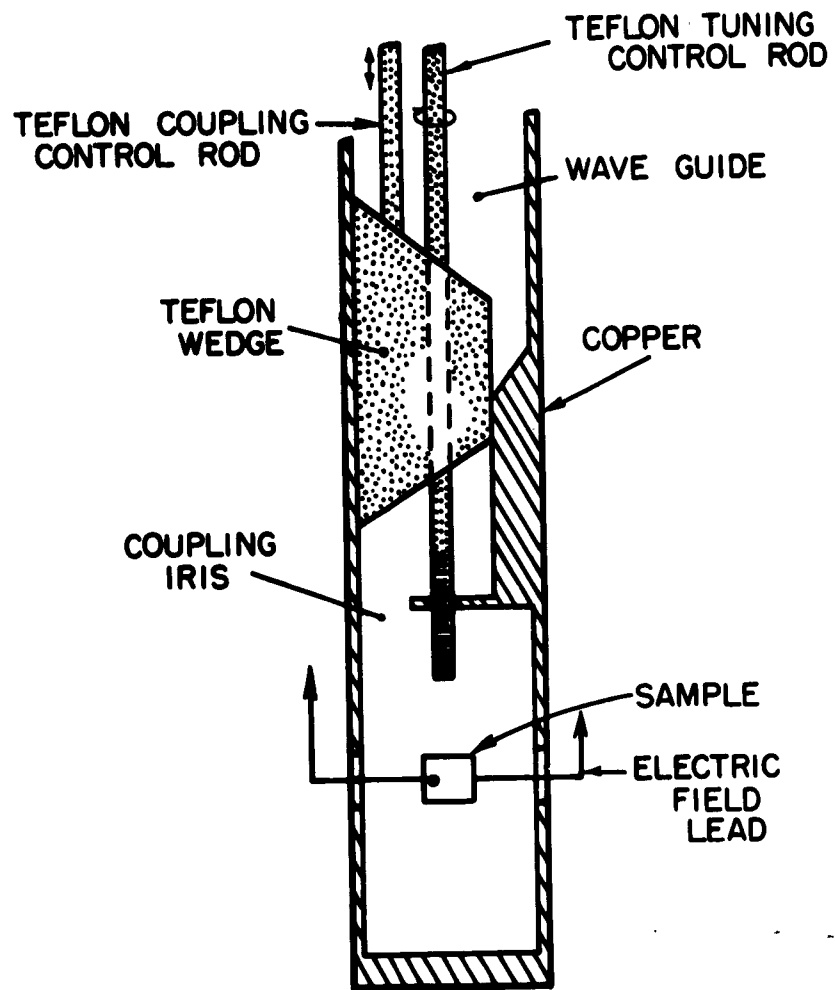


FIG.2-1. DETAIL OF THE MICROWAVE CAVITY.

The magnetic field was modulated by Helmholtz coils at 50 cps, and the output of the microwave detector was fed to a phase detector deriving its reference from the same 50 cps generator. The output of the phase detector is the derivative of the absorption line and was recorded as the magnetic field was slowly swept. A low noise transistorized preamplifier designed by S. C. Prévot was used before the phase detector, and this contributed much to the sensitivity of the apparatus.

The microwave detectors used are square law devices, that is, the output voltage is proportional to the square of the incident microwave signal voltage. A small change in the incident microwave voltage produces a change in the detected output voltage proportional to the product of the change in incident voltage and the average microwave voltage. This means that it is desirable to have as much power incident on the detector as possible subject to certain limitations.

If a crystal detector is used, the signal-to-noise-ratio is limited by the $1/f$ noise of the crystal diode. This noise is proportional to the power incident on the detector and limits the incident power which may be used. A bolometer detector is much less sensitive than a crystal detector but has the advantage that the incident power may be much higher. Because of this, the use of bolometer detection improved the sensitivity of the spectrometer by a factor of three over crystal detection.

A much more serious source of noise results from the FM noise present on the klystron output. This noise is converted to amplitude variations by the dispersion associated with the cavity resonance. An order of magnitude decrease in spectrometer noise resulted from stabilizing the frequency of the klystron to the sample cavity. The response time of the stabilization system was made fast enough to reduce greatly the FM noise in the spectral region below one kilocycle. The stabilization was accomplished by introducing a small 26 kc/sec voltage on the klystron reflector in order to produce a small amount of FM on the klystron. This FM is converted to an AM signal on reflection from the cavity, and the phase of this AM depends on whether the resonant frequency of the cavity is above or below the klystron frequency. Phase detection at 26 kc/sec results in an error signal suitable for correcting the frequency of the klystron, and this voltage is introduced on the reflector of the klystron. This is a conventional system of klystron stabilization.

The trouble with the bolometer detection system arises from the relatively high power level at which it must operate. Some of the magnetic resonance transitions were saturated at this power level, greatly reducing sensitivity. This was particularly a problem where the samples were cooled to liquid nitrogen or liquid helium temperatures. In these cases the crystal detector gave much better results. Most of the work to be reported

was done with these two configurations of the spectrometer. The bolometer used was a Narda 610B; the crystal, a selected Sylvania 1N26.

Frequency measurements were usually made with a commercial wavemeter since there was no need for an accurate absolute frequency measurement. However, provision was made to check occasionally the klystron frequency against harmonics of a Gertsch FM-4A UHF generator phase locked to a Gertsch FM-6 precision VHF generator. The stability of the klystron frequency when locked to the sample cavity was verified in this way.

The sensitivity of the spectrometer at room temperature, using bolometer detection, and in the absence of saturation, was roughly estimated at $4 \times 10^{12} \Delta H$ spins for unity signal-to-noise ratio and for an integration time of 0.5 sec. Samples were prepared in the form of plates usually one half or one fourth millimeter in thickness. The sample cutting and grinding were skillfully done by S. Maurici. X-ray orientation was done when necessary. Silver electrodes were evaporated on the two sides of the sample to provide an electric field, and 0.005 inch copper wires were ultrasonically soldered to the sample with indium to provide leads to the electrodes. Other methods of attaching electrodes to the sample were tried but proved unreliable. The sample was then entirely coated with an insulating material to prevent electrical arcing from one electrode to the other around the edge of the sample. Voltages up to six times the breakdown voltage of an uninsulated sample were used. For room temperature measurements polystyrene

Q-dope* was found to be a good insulating material for this application. At liquid nitrogen and liquid helium temperatures Flexrock #80 cement** was found to hold its strength, not to crack, and to provide adequate electrical insulation. The sample was supported in the microwave cavity by the two high voltage leads, which were brought into the cavity through large holes in the sides.

It was found that the presence of heavy silver electrodes on the sample greatly perturbed the cavity in two ways. First, the microwave field was shielded from the sample, so that interaction with the sample was weaker than with an unplated sample. Second, the cavity Q was greatly lowered, presumably due to losses in the silver. These effects were minimized by making the evaporated silver electrodes much less than a microwave skin-depth in thickness. Such a coating is partially transparent optically but still has sufficient direct current conductivity to provide an electric field on the sample.

The magnetic field was measured by monitoring the proton nuclear magnetic resonance in a sample of water containing a small amount of ferric nitrate. A modified Pound-Watkins [2-3] marginal oscillator was used in the

*General Cement Mfg. Co., Rockford, Illinois

**Flexrock Co., Philadelphia 1, Pennsylvania

spectrometer; the circuit was designed by J. Jeener. For magnetic fields low enough so that the proton resonance frequency was below 10 Mc/sec, the frequency of the spectrometer was counted on an LFE counter after suitable buffering. For frequencies above 10 Mc/sec, the beat was obtained between the Pound box and the harmonics of a war surplus frequency meter of fundamental frequency between two and four Mc/sec. The frequency meter was then counted on the LFE counter. An oscilloscope presentation of the NMR signal was used.

The Dispersion Spectrometer

The second spectrometer built was similar to the first except that the frequency of the microwave source was locked to a second cavity rather than to the sample cavity. By introducing a ninety degree phase shift in the microwave signal from the reference arm of the magic tee, the spectrometer can be made sensitive to the dispersion component of the magnetic resonance rather than to the absorption component.

Portis [2-4] has shown that for an inhomogeneously broadened line, such as those dealt with in this work, saturation of the resonance is not as severe if one looks at the dispersion signal rather than at the absorption signal. In addition, when tuned to the dispersion mode, one may obtain adiabatic rapid or fast passage signals as discussed by Portis and by Weger [2-5]. These, also, give a usable signal under saturation conditions. Such was indeed found to be the case, and this spectrometer was used in the experiments which attempted to detect an electric dipole moment of the electron.

Experimental Work

The chromium impurity in magnesium oxide [2-6] enters the lattice predominantly at sites which have a cubic environment as evidenced from the magnetic resonance spectrum. Such a site should be an inversion center and, hence, cannot show a linear electric field effect. A few percent of the chromium ions are found at sites such as to yield a spectrum of axial symmetry. It is thought that in this site there is a magnesium vacancy at a magnesium site along a 100 direction. The spectrum is described by the following spin Hamiltonian

$$\mathcal{H} = g\beta\mathbf{H} \cdot \mathbf{S} + D [S_z^2 - (1/3) S(S+1)] \quad , \quad (2-1)$$

where $D = 2.5$ Gc/sec, $g = 2.00$, with the z-axis along a 100 direction. Thus, if the magnetic field is applied along a 100 direction, it will be in the x-, y-, or z-direction for each third of the sites. The sites where the field is perpendicular to the z-axis give one spectrum, and the sites where the field is parallel to the z-axis give another spectrum.

We assume that any electric field effect will result from moving the magnetic ion nearer to or farther from the vacancy, and this will result only if the electric field is also along the z-axis of the site. Thus, by taking both \mathbf{E} and \mathbf{H} parallel to each other and along a 100 direction, the z-axis spectrum should show an electric field effect but the x- and y-axis spectra should not.

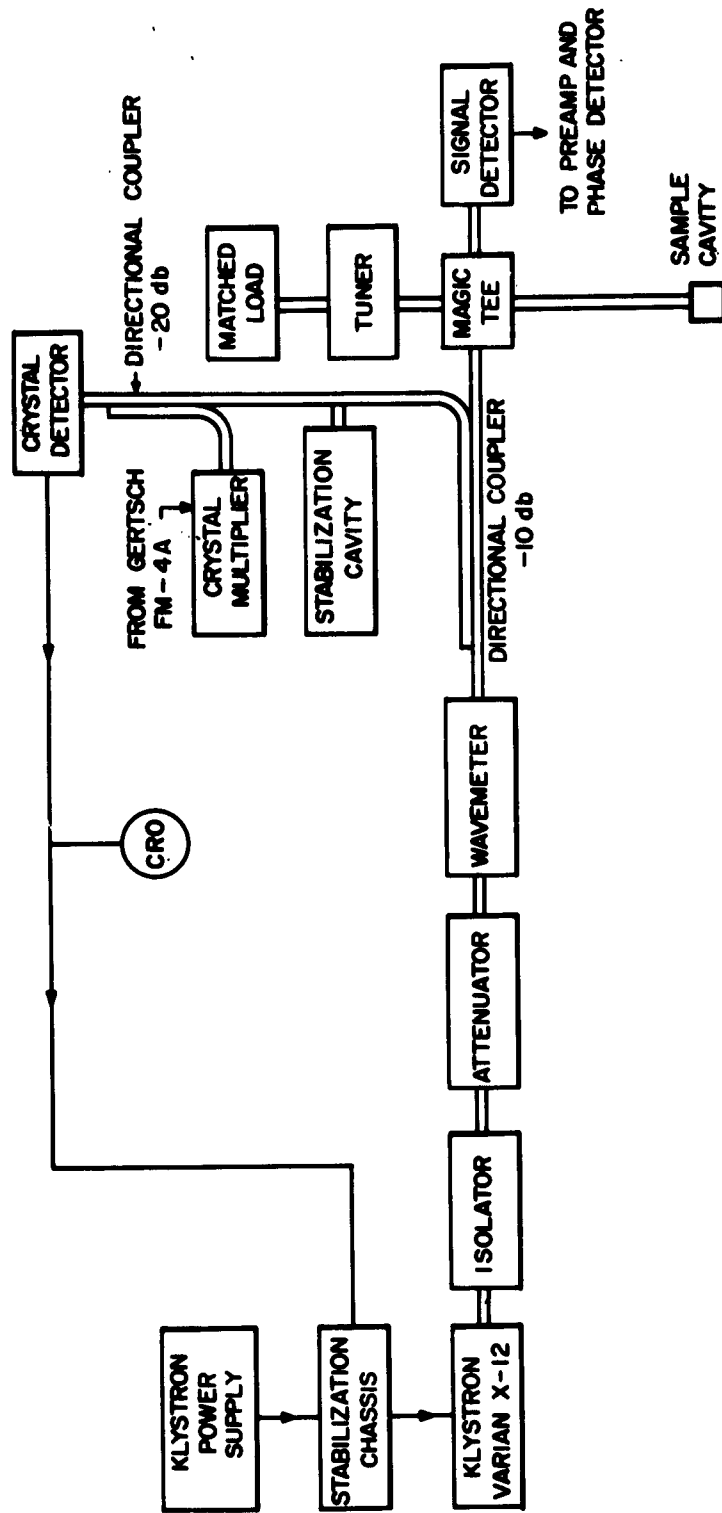


FIG. 2-3. BLOCK DIAGRAM OF THE PARAMAGNETIC RESONANCE DISPERSION SPECTROMETER. COMPONENTS COMMON TO BOTH SPECTROMETERS ARE NOT SHOWN.

Cr^{+++} in MgO was the first material studied for a possible electric field effect, and most of the techniques were perfected on this material. Single crystals were obtained from the Norton Co. via W. M. Walsh, Jr., of the Bell Telephone Laboratories and M. Cohen of this laboratory. Initial measurements were made on a sample with silver painted electrodes at a field of 20 kv/cm. The presence of the electrodes reduced the signal-to-noise ratio for the axial site line from 100 to 10 and significantly lowered the Q of the cavity. Only a fairly small sample could be used in order to prevent the electrodes from extending significantly into the E-field region of the cavity. An upper bound of 0.3 gauss was set for the electrically induced line broadening; the line width was 8 gauss. Since the fractional broadening of the line is proportional to the square of the fractional splitting, this implies that the splitting induced by the electric field was less than 2 gauss, or 0.3 Mc per kv/cm. Better techniques for insulating the sample lowered this bound to 0.15 Mc per kv/cm.

By going to liquid helium temperature, the signal-to-noise ratio was increased by an order of magnitude. Heavy silver-plated electrodes were introduced at this time. In order to take advantage of this enhanced signal-to-noise ratio, it was decided to modulate with the electric field and to phase detect. An electric field of 18 kv/cm rms was applied to the sample at 60 cps, and the magnetic field was strongly modulated at 170 cps. Since the electric field broadening goes through a maximum twice for each cycle

of the electric field modulation, the combined electric and magnetic modulation should produce a signal at 50 cps. The large 170 cps signal was eliminated with a tuned filter, and the remaining signal was fed to a 50 cps phase detector, whose reference signal was synthesized from the two modulating signals. It was found that there was some 120 cps signal present, but this was presumably due to vibrations produced by electrostatic forces; it was eliminated by the phase detector. A signal was indeed detected at 50 cps using the phase detector, but this signal was present on both the spectra for which the fields were parallel to the z-axis and for which the fields were perpendicular to the z-axis. Since only one of these spectra should show an electric field effect, it was concluded that the signal was spurious. It is not difficult to think of mechanisms by which such a signal could be produced. Because of this spurious signal, it was not possible to take advantage of the enhanced signal-to-noise ratio, and the upper bound on the effect determined by this experiment was actually worse than previously obtained.

Considerably better techniques for insulating the sample were evolved during the work on the ruby, and following this work, the experiments on MgO were repeated. With the sample at liquid helium temperatures, a signal-to-noise ratio of 200 was attained on a thin sample with semi-transparent evaporated silver electrodes. Whereas previously, contact to the evaporated electrodes had been a pressure contact, leads were now soldered to the sample. Higher fields were attained by the use of a thin sample, but at a corresponding loss in signal strength. With the samples used previously, a signal-to-noise

ratio of 1000 should have been possible in this arrangement. Alternately, a DC electric field of 170 kv/cm and an AC field of 80 kv/cm rms were used, the phase detection scheme being employed in the latter case. Again a stray signal prevented the theoretical sensitivity of the modulation system from being attained, and the upper bounds as determined from the AC and DC experiments were essentially identical. The sensitivity to the electric field broadening was increased over previous measurements by an order of magnitude, and the upper bound on the electrically induced splitting was determined as 0.05 Mc per kv/cm, which corresponds to a shift in D of 0.01 Mc per kv/cm or $4 \times 10^{-7} \text{ cm}^{-1}$ per kv/cm. The molecular orbital theory predicts a shift in D of $3 \times 10^{-7} \text{ cm}^{-1}$ per kv/cm; while scaling the Artman theory of ruby by $D^{1/2}$ gives a shift of $4 \times 10^{-6} \text{ cm}^{-1}$ per kv/cm (see Chapter IV).

Iron enters the TiO_2 lattice [2-7] substitutionally for the titanium, the local environment being orthorhombic. There are two kinds of sites, both with their y -axes along the c -axis of the crystal. The x -axis of one site and the z -axis of the other are along a 110 direction. The spin Hamiltonian is

$$\begin{aligned} \mathcal{H} = & g\beta\mathbf{H} \cdot \mathbf{S} + D [S_z^2 - (1/3)S(S+1)] \\ & + (1/6)a [S_x^4 + S_y^4 + S_z^4 - (1/5)S(S+1)(3S^2 + 3S + 1)] \\ & + (7/36)F \{ S_z^4 + [5/7 - (6/7)S(S+1)] S_z^2 \\ & - (6/35)S(S+1) + (3/35)S^2(S+1)^2 \} + E (S_x^2 - S_y^2), \end{aligned} \quad (2-2)$$

where $D = 20.4 \text{ Gc/sec}$, $E = 2.2 \text{ Gc/sec}$, $a = 1.1 \text{ Gc/sec}$, $F = -0.5 \text{ Gc/sec}$, $g = 2.000$. The dominant terms aside from the Zeeman term, are the D - and E - terms. The terms quartic in the effective spin will be ignored since they are small and rather more difficult to calculate. Samples of iron doped TiO_2 were

obtained from the National Lead Company, South Amboy, New Jersey, but were found to be unusable because of DC conductivity. Apparently, this conductivity is due to a non-stoichiometric titanium oxygen ratio. Stoichiometric samples were grown by Solid State Materials Company, East Natick, Massachusetts, and these samples were used in this work.

First experiments done on Fe^{+++} in TiO_2 were at room temperature using a fairly large sample, which yielded a signal-to-noise ratio of 500. The applied electric and magnetic fields were taken along the c-axis of the crystal, which is the y-axis of the magnetic site. The $\pm 1/2$ transition was observed. Electrodes were heavy silver plate with pressure contacts for the leads. Working at an applied field of 60 kv/cm, an upper bound was placed on the second-order electrically induced shift in resonance frequency. This bound on the shift is 1×10^{-4} of the resonant frequency, which is just the effect predicted for this field and orientation (see Chapter V).

Attempting to increase sensitivity, the resonance was examined at liquid helium temperature, where a comparable signal-to-noise-ratio was observed for a sample some ten times smaller. The absorption signal was totally saturated, and the dispersion signal was observed [2-4]. In order to tune the absorption spectrometer for dispersion, the reflection from the "matched" arm of the magic tee bridge was made larger than the reflection from the cavity arm and was tuned 90 degrees out-of-phase with the signal from the cavity arm. To minimize the effects

of FM klystron noise, the klystron was stabilized on the resultant total response of the bridge. It is estimated that this tuning yielded some 10 % of the dispersion signal. The dispersion spectrometer was not constructed until some time later; it would have greatly helped in this work. The signal observed [2-4, 5] was a mixture of an adiabatic rapid passage signal, with the shape of the absorption line (Portis case II A, Weger case 2), and the slow passage signal, having the shape of the derivative of the dispersion (Portis case I, Weger case 1). These signals can be separated, since the former occurs 90 degrees out-of-phase with respect to the field modulation.

An electric field effect was observed using 44 kv/cm rms electric field modulation and the phase detection scheme described for the MgO experiment. The magnitude of the effect was comparable with that predicted by the theory, but there was no way of knowing that the effect was not spurious.

If the magnetic field is taken along a 110 axis, it will be oriented along the z-axis for one site and the x-axis for the other. Whereas for the z-axis spectrum, the $\pm 1/2$ line will not show an electric field effect, this transition in the x-axis spectrum should show an effect 2.5 times that for the same transition in the y-axis spectrum previously observed. Unfortunately, this orientation of the sample required placing the sample with the microwave electric field lying in the plane of the electrodes rather than normal to them as previously. While the sample was in a low E-field region of the cavity, the field was not zero, and this resulted in more than an order

of magnitude reduction in cavity Q and sensitivity. A somewhat larger sample was used, and a signal-to-noise ratio of 100 was attained at liquid helium temperature on the dispersion signal. A field of 44 kv/cm rms was applied, phase detection was used, and no effect could be detected on any transition. An upper bound on the electrically induced shift in the resonance of 1×10^{-5} times the resonance frequency was set, whereas the calculations predict 2×10^{-4} for this field and orientation. Ultrasonically soldered high voltage leads to the electrodes were used in place of pressure contact leads, increasing the reliability of this measurement over previous ones.

Experiments were also tried using carbon electrodes similar to those used in the silicon experiments, but the results were no better than the best results using silver electrodes.

Ludwig and Woodbury [2-8] observed the first linear electric field effect in paramagnetic resonance by studying the Fe^0 impurity in silicon. Through the kindness of Dr. Ludwig, a suitable sample of doped silicon was obtained and the effect was qualitatively confirmed. Because of the temperature sensitivity of the impurity centers, the high temperatures required for the production of evaporated silver electrodes prohibited their use. Electrodes were formed from carbon paper by painting paper with a thin coating of Aquadag. These electrodes were sufficiently resistive not to perturb seriously the microwave cavity. Subsequently, in the work on the ruby resonance, such electrodes were found to be unreliable, and this may explain some of the difficulty experienced.

The experiments were done at liquid helium temperature in order to have sufficient sensitivity for the small spin concentration present. Unfortunately, as was pointed out above, the spectrometer used was only sensitive to about 10% of the dispersion signal, and since the spins were totally saturated at any usable power levels, the signal-to-noise ratio was rather bad. A chromium doped sample of silicon gave a similarly poor signal-to-noise ratio, and work on these materials was dropped at this point.

The experimental results of the electric field effect in ruby are the subject of Chapter III. The experiments on ruby were done on small plates 1/4 mm thick with thin evaporated silver electrodes. Leads to the electrodes were ultrasonically soldered to the sample prior to the evaporation of the electrodes. The electrodes were much thinner than one microwave skin depth and did not produce a serious perturbation of the cavity. Fields up to 200 kv/cm were applied to suitably insulated samples. The work on the angular dependence of the effect was all done at room temperature, where a signal-to-noise ratio of 100 was obtained.

In cutting the plates, x-ray orientation to $\pm 1/2^\circ$ was done. The orientation of the samples with respect to the magnetic field was determined from the angular dependence of the magnetic resonance spectrum. This gives the polar angle from the c-axis, but unfortunately the spectrum is insensitive to the azimuthal angle. Samples were prepared in which a second plate was cemented to the first, the c-axis of the samples being

orthogonal. Observing the dependence of the spectrum from this composite sample on the orientation of the magnetic field allowed one to determine both the polar and azimuthal angles of the magnetic field.

In ruby, an apparent splitting of the resonance line is produced by the sum of the ordinary electric field effect discussed previously and the possible effect of a permanent electric dipole moment acted on by the crystalline field. In Chapter VI it is shown that if either the applied electric or magnetic field is reversed, the relative signs of these two terms change, allowing them to be separated.

Experiments were made on ruby to attempt to detect the possible existence of an electronic electric dipole moment using this fact. In an attempt to increase sensitivity, the experiment was tried at liquid helium temperature. The dispersion spectrometer was constructed for this experiment in order to observe the dispersion signal, the absorption being totally saturated. Unfortunately, the signal observed was a mixture of two signals [2-4, 5]: a signal having the shape of the usual dispersion derivative, and a signal with the shape of the absorption line. The latter is an adiabatic rapid fast passage signal (Portis case IIIB, Weger case 7), and has been further discussed by Feher [2-9]. The addition of the dispersion derivative signal probably comes from a partial breakdown of the adiabatic condition (Weger case 10) or of the rapid passage condition (Weger case 1, Portis case I). The lines are similar in shape to those observed by

Solomon and Ezratty [2-10] in nuclear magnetic resonance. The two components are 180 degrees out-of-phase so that they essentially cancel in the central region of the line. Thus, the resultant line was much weaker than predicted and also much broader in appearance. This precluded doing the experiment at helium temperature, and the work was done at liquid nitrogen temperature.

Previous work on the electric field effect in ruby had used Linde ruby of 0.05% Cr^{+3} concentrations. In this work searching for a possible dipole moment, a stronger signal was obtained from 0.17% Cr^{+3} ruby from the Adolf Meller Company, Providence, Rhode Island. At higher concentrations than 0.17% the line is wider than the 17 gauss which seems to be the minimum line width obtainable. Somewhat heavier silver electrodes were used for greater reliability. As a result, the signal-to-noise ratio was only slightly better than that obtained in earlier work with a more dilute but larger sample at room temperature.

Eight runs were made in which the electrically induced splitting of the $-1/2$ to $-3/2$ transition was observed for varying polarities of the applied electric and magnetic fields. The applied electric field was 175 kv/cm. The change in the observed splitting on reversing either the electric or the magnetic field was found from these runs to be 0.025 ± 0.125 gauss. The

2-20

uncertainty arises primarily from instabilities in the electronics associated with the experiment. Improved electronics would probably allow a better upper bound to be placed on this quantity.

Chapter III

EXPERIMENTAL RESULTS, RUBY ELECTRIC FIELD EXPERIMENT

The electric field effect in ruby was first detected by Artman and Murphy [3-1]. These experiments were duplicated, and the angular dependence of the electric field effect was measured. The results have been reported [3-2] and are to be published [3-3].

Figure 3-1 shows the apparent splitting of the paramagnetic resonance line of chromium in ruby [3-4] under the influence of a uniform applied electric field. Both electric and magnetic fields were taken parallel to the c-axis of the ruby, the orientation which gives the largest effect. This is the orientation used by Artman and Murphy. Examination of such absorption curves shows that there is no residual unsplit line at the center of the pattern, that neither split component is appreciably broader than the original resonance line, and that the center of the unsplit line is midway between the centers of the two components.

Figure 3-2 shows the dependence of this splitting on the strength of the applied electric field for several samples. The effect is linear in the applied electric field for splittings greater than one linewidth. Data for individual samples shows a scatter of 1% from linearity, though different samples differ by as much as 10% from one to the other. This difference is due to variations in the preparation of the electrodes on the samples, such as, for example, the closeness of the plated area to the edge of the sample. The two boules were both from the Linde Company. The first was a slow grown boule produced in 1960; the second was a somewhat older

standard ruby boule (probably produced in 1958). The Cr^{3+} concentration in both boules was 0.05%. The electric field splitting was also observed in a 0.17% Cr^{3+} sample from the Adolf Meller Company, Providence, Rhode Island. No effect of concentration was observed, nor was there any change in going from room temperature to liquid nitrogen temperature. Unless otherwise indicated, all measurements reported were made at room temperature.

For small electric fields one, of course, observes only an apparent additional broadening of the resonance line over the initial linewidth rather than a splitting. As one can calculate, this additional broadening is proportional to the square of the splitting and, hence, is proportional to the square of the applied electric field.

$$\frac{\text{Change in linewidth}}{\text{Linewidth}} = k \left(\frac{\text{Splitting}}{\text{Linewidth}} \right)^2 \quad (3-1)$$

Figure 3-3 shows the experimental confirmation of this fact. Surprisingly, the square law seems to be valid for additional broadenings up to 75% of one linewidth. Linewidths were taken as the distance between points of maximum slope of the absorption. Comparing this figure with Fig. 3-2 gives an experimental evaluation of the constant $k = 0.90 \pm 0.05$.

Equation 3-1, together with this value of k , is then used to evaluate the splitting for orientations where the electric field effect is too small to give more than an apparent broadening of the line. When the splitting is calculated in this way from a line broadening, it is called the effective splitting.

SPLITTING OF Cr^{3+} PARAMAGNETIC RESONANCE IN Al_2O_3 DUE TO
THE APPLICATION OF AN ELECTRIC FIELD

E AND H PARALLEL TO C-AXIS
 $\nu = 13.9$ GC/SEC
H = 900 GAUSS

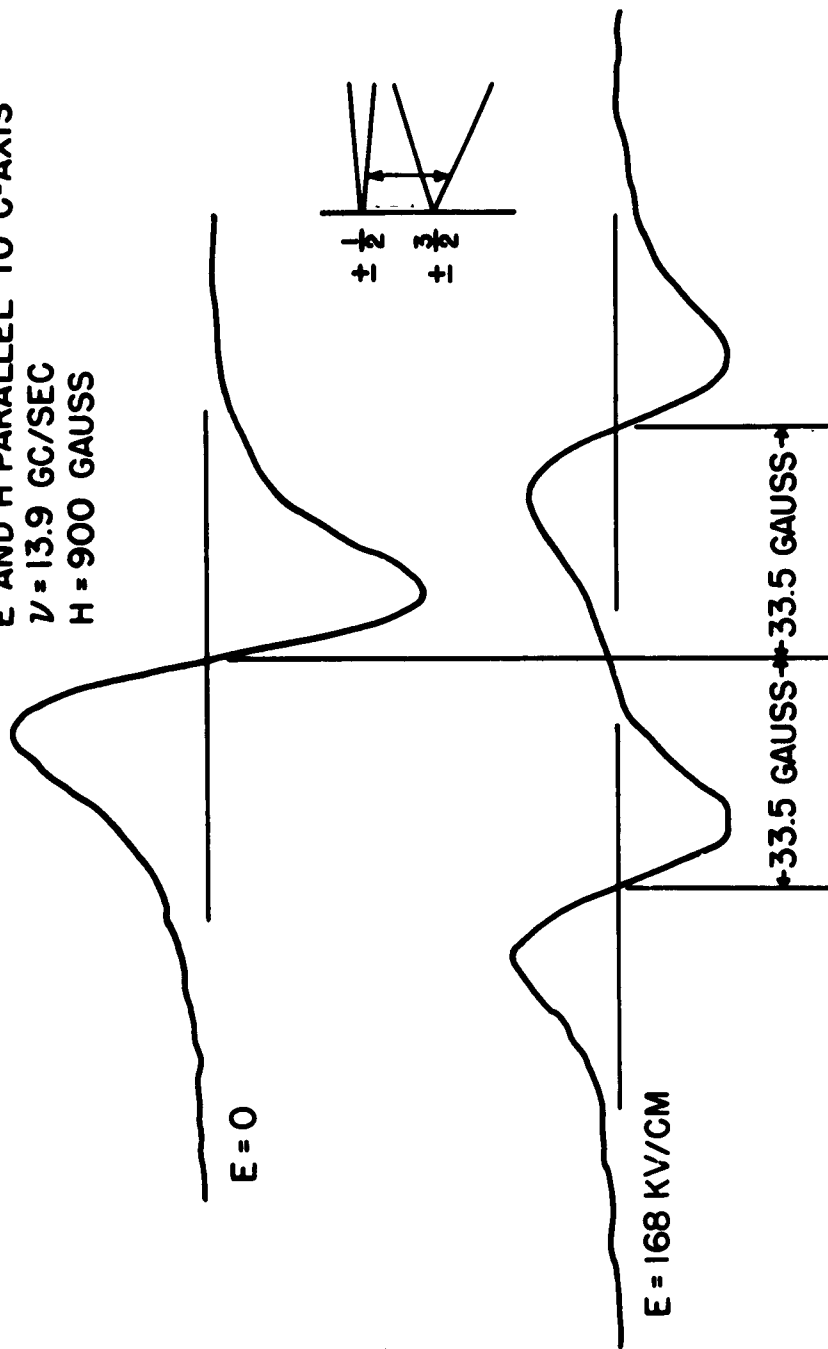


FIG. 3-1. EXPERIMENTAL ABSORPTION DERIVATIVE CURVE SHOWING ELECTRIC
FIELD INDUCED SPLITTING OF $Cr^{+3} 1/2 \rightarrow 3/2$ RESONANCE LINE.

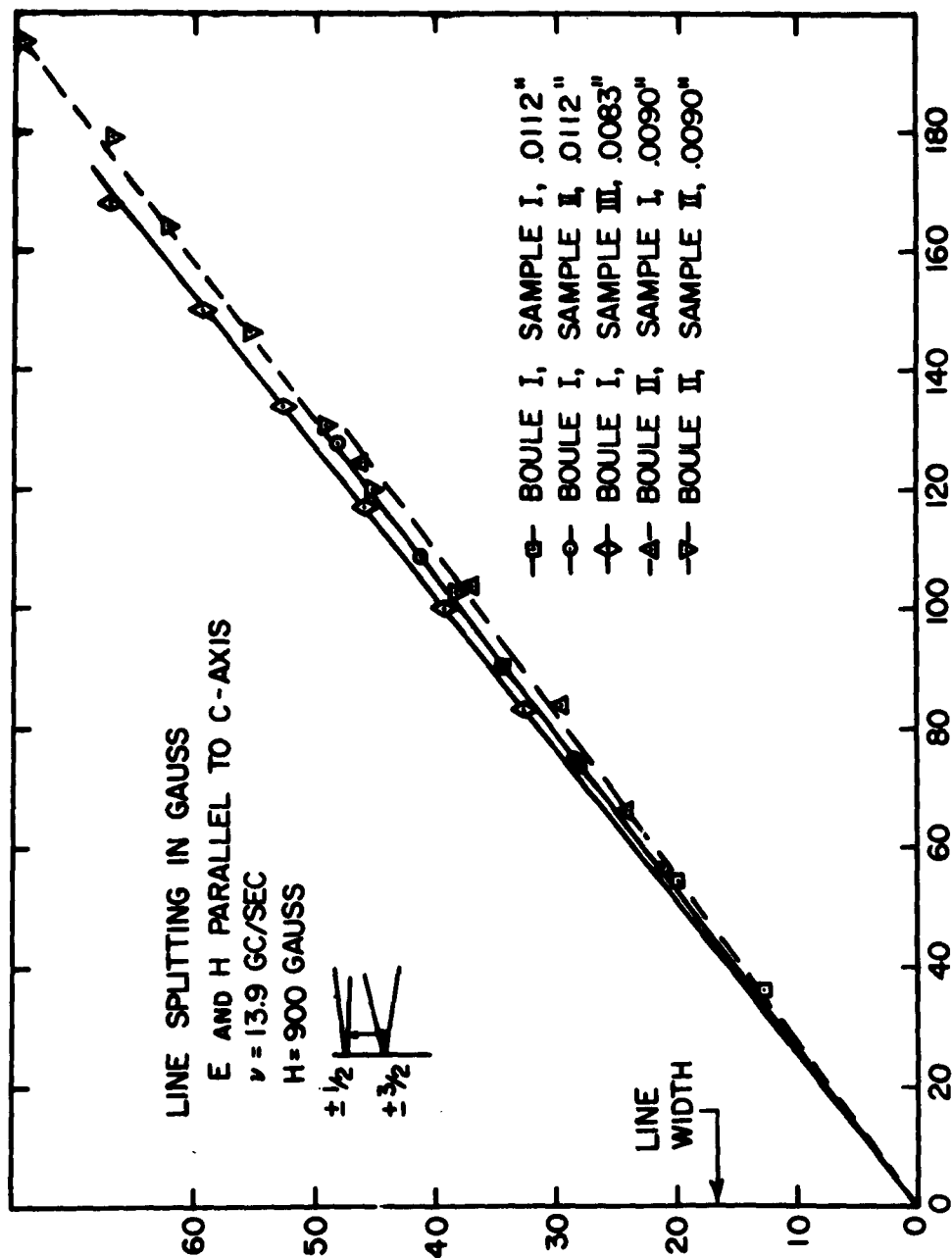


FIG.3-2. LINEAR VARIATION OF ELECTRIC FIELD INDUCED LINE SPLITTING.

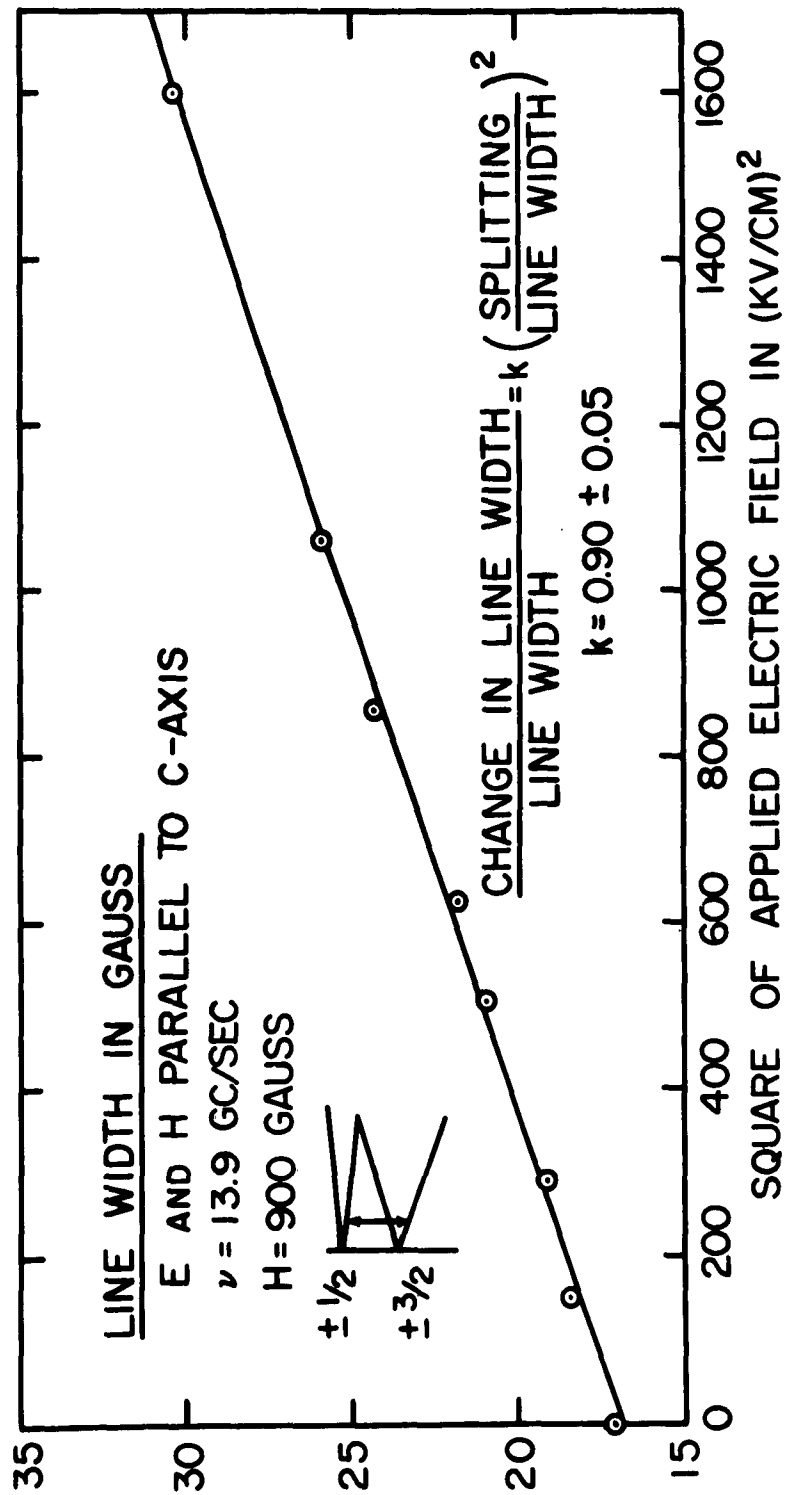


FIG. 3-3. QUADRATIC VARIATION OF THE ELECTRIC FIELD INDUCED LINE BROADENING FOR SPLITTINGS LESS THAN ONE LINE WIDTH.

Figure 3-4 shows a portion of the structure of ruby and is taken from a paper by Geschwind and Remeika [3-5]. Note that there are four distinct, non-equivalent sites for the chromium to substitute for aluminum. As far as the magnetic resonance spectrum is concerned, these sites are all equivalent for chromium, but under the influence of an applied uniform electric field, each site behaves differently. Sites b and c in the figure are related to each other by the symmetry operation of inversion through the metal atom, as are f and a. c and a are related by reflection in a vertical mirror plane normal to the y- or A-axis, as are b and f. The difference between b and c on the one hand and f and a on the other hand is the result of a 4.3° rotation of one half of the oxygen triangles forming the environment of the metal atom, as the figure shows. Since none of the sites is an inversion center, the application of a uniform electric field produces a linear shift in the resonance value of the magnetic field for each particular site, and an equal but oppositely directed shift of the resonance field for the site related to the first by inversion symmetry. These opposite shifts of the resonance lines from the two sites produce an apparent splitting of the resonance line. In the optical case, Kaiser, Sugano, and Wood [3-6] have termed this kind of effect a pseudo-Stark splitting.

The angular dependence of this electric field effect was measured by varying the directions of the applied electric and magnetic fields. There is an electric field induced shift of the energy levels giving rise to the paramagnetic resonance transitions, and this shift may be described formally by additional terms in the usual spin Hamiltonian describing these levels:

$$\mathcal{H}_S = g_{||} \beta H_z S_z + g_{\perp} \beta (H_x S_x + H_y S_y) + D [S_z^2 - (1/3)S(S+1)]$$

$$+ \sum_i \sum_{j \leq k} (1/2) R_{ijk} E_i (S_j S_k + S_k S_j) + \sum_{ijk} T_{ijk} E_i H_j S_k. \quad (3-2)$$

The first three terms are the usual spin Hamiltonian with $g = 1.98$, $D = -0.112 \text{ cm}^{-1}$, $S = 3/2$. The term containing the R-tensor is a perturbation of D, while the T-tensor term is a perturbation of g. Making use of the C_3 symmetry of the chromium site, these tensors take the forms below, where 1, 2, 3, refer to x, y, z, respectively.

	S_1^2	S_2^2	S_3^2	$(\frac{1}{2})(S_2 S_3 + S_3 S_2)$	$(\frac{1}{2})(S_1 S_3 + S_3 S_1)$	$(\frac{1}{2})(S_1 S_2 + S_2 S_1)$
E_1	R_{111}	$-R_{111}$	0	R_{123}	R_{113}	$-2R_{222}$
E_2	$-R_{222}$	R_{222}	0	R_{113}	$-R_{123}$	$-2R_{111}$
E_3	R_{311}	R_{311}	R_{333}	0	0	0

(3-3)

	$S_1 H_1$	$S_2 H_2$	$S_3 H_3$	$S_2 H_3$	$S_1 H_3$	$S_1 H_2$	$S_3 H_2$	$S_3 H_1$	$S_2 H_1$
E_1	T_{111}	$-T_{111}$	0	T_{123}	T_{113}	$-T_{222}$	T_{132}	T_{131}	$-T_{222}$
E_2	$-T_{222}$	T_{222}	0	T_{113}	$-T_{123}$	$-T_{111}$	T_{131}	$-T_{132}$	$-T_{111}$
E_3	T_{311}	T_{311}	T_{333}	0	0	0	0	0	0

(3-4)

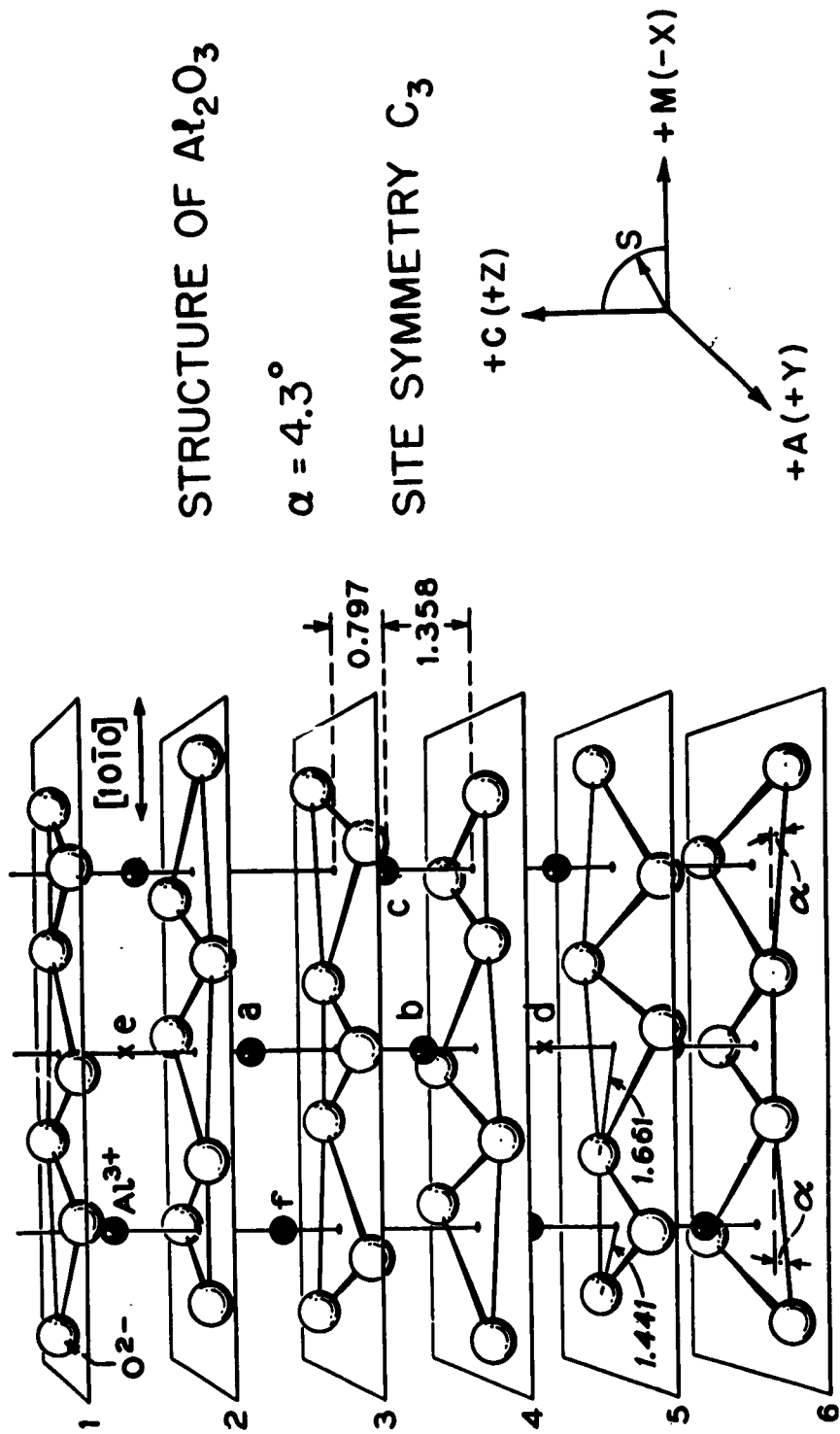


FIG. 3-4. PORTION OF THE Al_2O_3 LATTICE SHOWING THE COORDINATE SYSTEM USED IN THIS WORK. (AFTER GESCHWIND AND REMEIK)

The trace of the perturbation $\sum_j R_{ijj}$ may be taken equal to zero, in which case one has $R_{311} = -(1/2)R_{333}$. This gives five independent components in the R-tensor. If the trace of the perturbation is not taken equal to zero, there would be six independent components, but one of them could not be evaluated experimentally. The terms may be grouped into three groups, one longitudinal term, two transverse, and two skew terms, according to the orientation of the magnetic field with respect to the c-axis of the crystal. The longitudinal term appears with the applied electric and magnetic fields parallel to the c-axis as was the case for the previously quoted results, and is described by R_{333} . This is the term evaluated by Artman and Murphy. The transverse terms involving R_{111} and R_{222} and the skew terms involving R_{113} and R_{123} come from a transverse electric field with the magnetic field transverse or skew to the c-axis, respectively. All but the longitudinal term give no first-order contribution to the energy if the states are unmixed, as is the case if the magnetic field is parallel to the c-axis. A transverse component of the magnetic field is required to mix the states and thus to bring in the transverse and skew terms linearly in the perturbation.

With the magnetic field parallel to the c-axis, there may, however, be a quadratic electric field effect from the transverse and skew components of the R-tensor, as can be calculated from the second-order perturbation theory on the pure state wave functions. This would be in addition to the linear effect from R_{333} except for certain transitions.

It was found possible to fit all of the experimental results using only the R-tensor, and for this reason only the R-tensor is considered in the following analysis. Limits on the values of the components of the T-tensor may be estimated from the experimental uncertainties quoted on the values of the components of the R-tensor. It is not surprising that the T-tensor may be ignored since g is close to the free spin value. The crystalline field effects on g are hence small, and one should not expect a detectable electric field effect.

The usual spin Hamiltonian has been diagonalized by Chang and Siegman [3-7] for arbitrary angles of the magnetic field with respect to the z-axis, and their wave functions were used as a basis set for evaluating the electric field perturbation. The effect of the electric field terms was evaluated in first-order perturbation theory by taking diagonal elements between these wave functions. The wave functions calculated by Chang and Siegman may be written

$$|> = a |3/2> + b |1/2> + c |-1/2> + d |-3/2>. \quad (3-5)$$

Writing out the perturbation of the energy gives the following additional term in the spin Hamiltonian

$$\begin{aligned} \mathcal{H}' = & (R_{111} E_1 - R_{222} E_2)(S_1^2 - S_2^2) - (R_{222} E_1 + R_{111} E_2) \\ & (S_1 S_2 + S_2 S_1) + (R_{123} E_1 + R_{113} E_2)(1/2) (S_2 S_3 + S_3 S_2) + \\ & + (R_{113} E_1 - R_{123} E_2) (1/2) (S_1 S_3 + S_3 S_1) + \\ & + (3/2) R_{333} E_3 [S_3^2 - (1/3)S(S+1)]. \end{aligned} \quad (3-6)$$

Taking diagonal elements of this perturbation between the wave functions given by Chang and Siegman yields

$$\begin{aligned} \mathcal{H}^0 = & [(R_{111} E_1 - R_{222} E_2) \cos 2\phi - (R_{222} E_1 + R_{111} E_2) \\ & \sin 2\phi] A(\theta) + [(R_{113} E_1 - R_{123} E_2) \cos \phi + \\ & + (R_{123} E_1 + R_{113} E_2) \sin \phi] B(\theta) + \\ & + (3/2) R_{333} E_3 C(\theta) , \end{aligned} \quad (3-7)$$

$$\text{where } A(\theta) = 2\sqrt{3} (bd + ac)$$

$$B(\theta) = \sqrt{3} (ab - cd)$$

$$C(\theta) = (a^2 - b^2 - c^2 + d^2). \quad (3-8)$$

The dependence of these diagonal elements on the orientation of the electric field is given by the components E_1 , E_2 , E_3 . The Chang and Siegman wave functions assume the magnetic field to lie in the xz -plane; ϕ is the azimuthal angle about the z -axis of the magnetic field out of this plane. The dependence on the polar angle of the magnetic field from the z -axis is contained in the coefficients a , b , c , d , and is not given explicitly. From formulas (3-8), it is clear that in the case where the applied magnetic field is along the c -axis, the pure state wave functions have only the R_{333} term in first-order perturbation theory, as was pointed out earlier.

Orienting the electric and magnetic fields along certain selected directions, it was possible to evaluate each component of the R-tensor. The linearity with electric field for the effect depending on each component of the R-tensor was verified at these orientations.

In addition to this work, the electric field splitting was measured as a function of the angle of the magnetic field for several directions of the applied electric field. Figure 3-5 shows the dependence of the electric field splitting on polar angle of the magnetic field for an azimuthal angle $\phi = 0^\circ$. The electric field was along the x-axis. The curves drawn are the evaluation of the perturbation on the spin Hamiltonian (Eq. 3-7). Values of the components of the R-tensor were selected to fit the experimental data. In the particular case shown, the effect comes from mixing the skew component R_{113} and the transverse component R_{111} of the R-tensor. The line splits into two rather than four components since for these orientations the four sites are grouped into two sets of equivalent pairs of sites.

Figure 3-6 shows the dependence on polar angle again for an azimuthal angle $\phi = 0^\circ$, but with the electric field along the y-axis. The effect here comes from a mixing of the transverse component R_{222} and the skew component R_{123} and is again a splitting into two rather than four components. Relative signs as well as magnitudes of the skew and transverse components were evaluated from such measurements.

Figure 3-7 shows the dependence on azimuthal angle of the magnetic field with a polar angle of 90° . Two transverse orientations of the electric field were taken. Only the transverse components of the R-tensor R_{111} and R_{222} enter, and this allows their relative signs to be determined. In this case, there is no equivalence of the two kinds of sites which are mirror

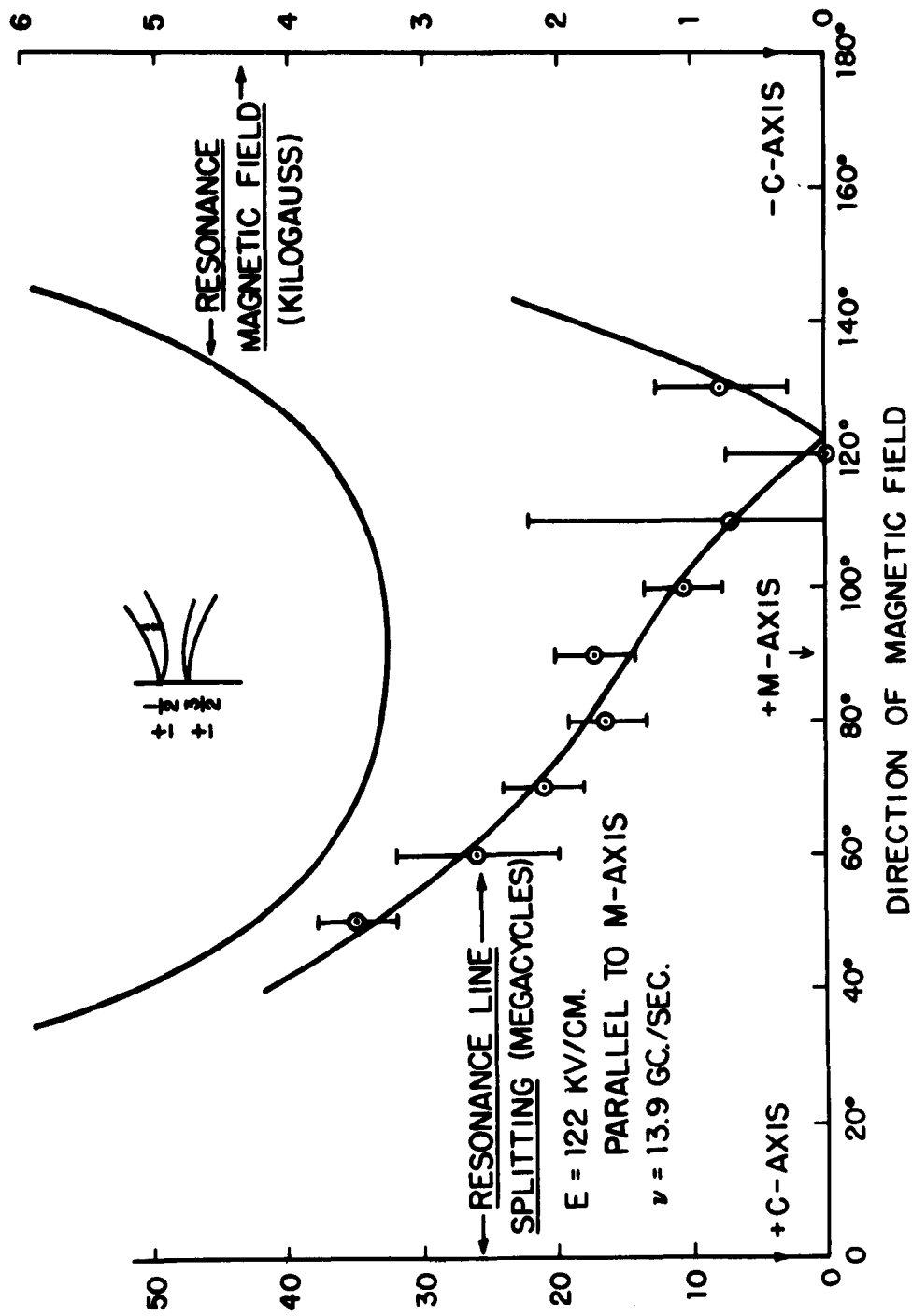


FIG. 3-5. ANGULAR DEPENDENCE OF ELECTRIC FIELD INDUCED SPLITTING WHERE THE
 MAGNETIC FIELD IS ROTATED ABOUT THE Y-AXIS. E PARALLEL TO THE X-AXIS.

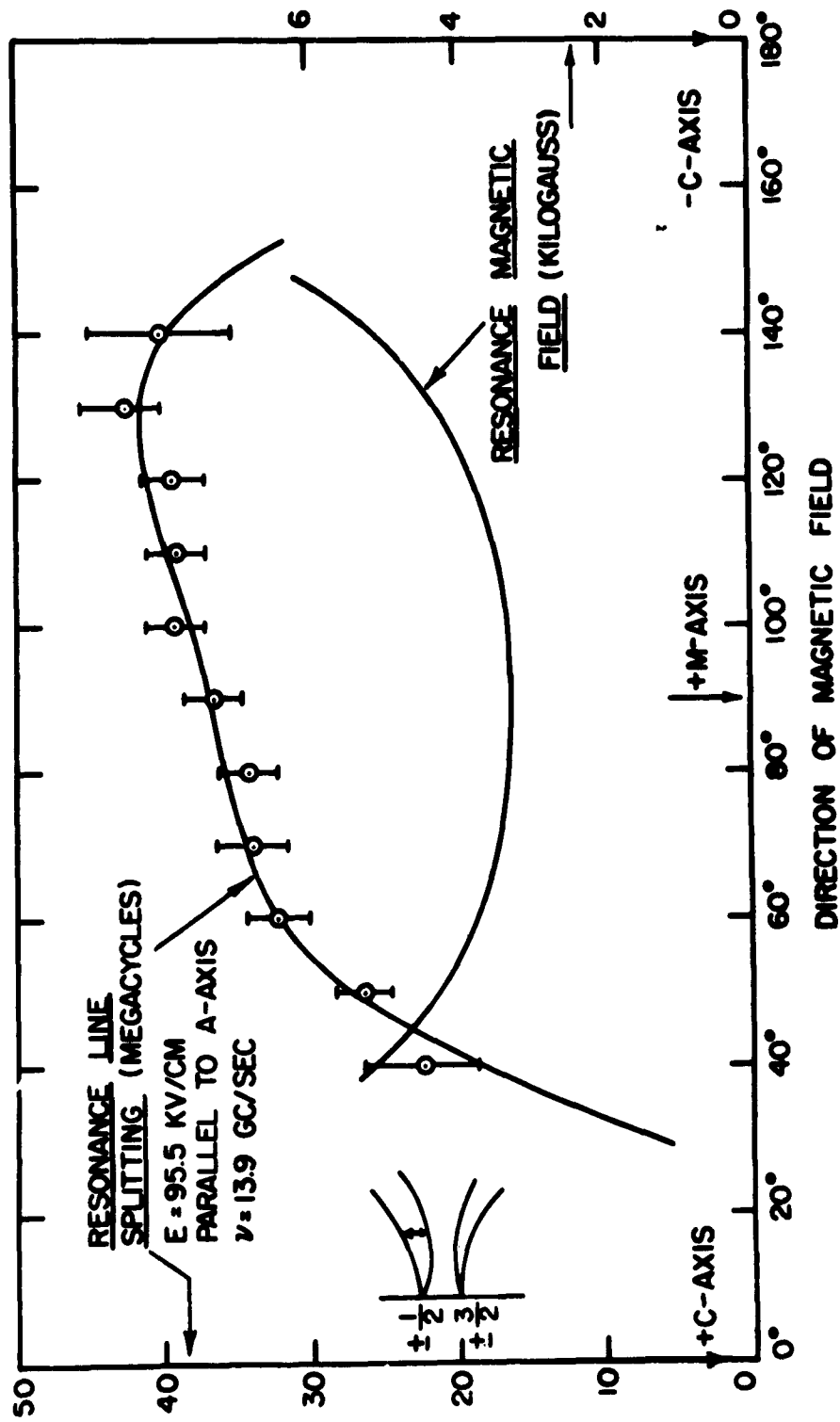


FIG. 3-6. ANGULAR DEPENDENCE OF THE ELECTRIC FIELD INDUCED SPLITTING WHERE THE MAGNETIC FIELD IS ROTATED ABOUT THE Y-AXIS. E PARALLEL TO THE Y-AXIS.

EFFECTIVE SPLITTING OF LINE IN MC/SEC

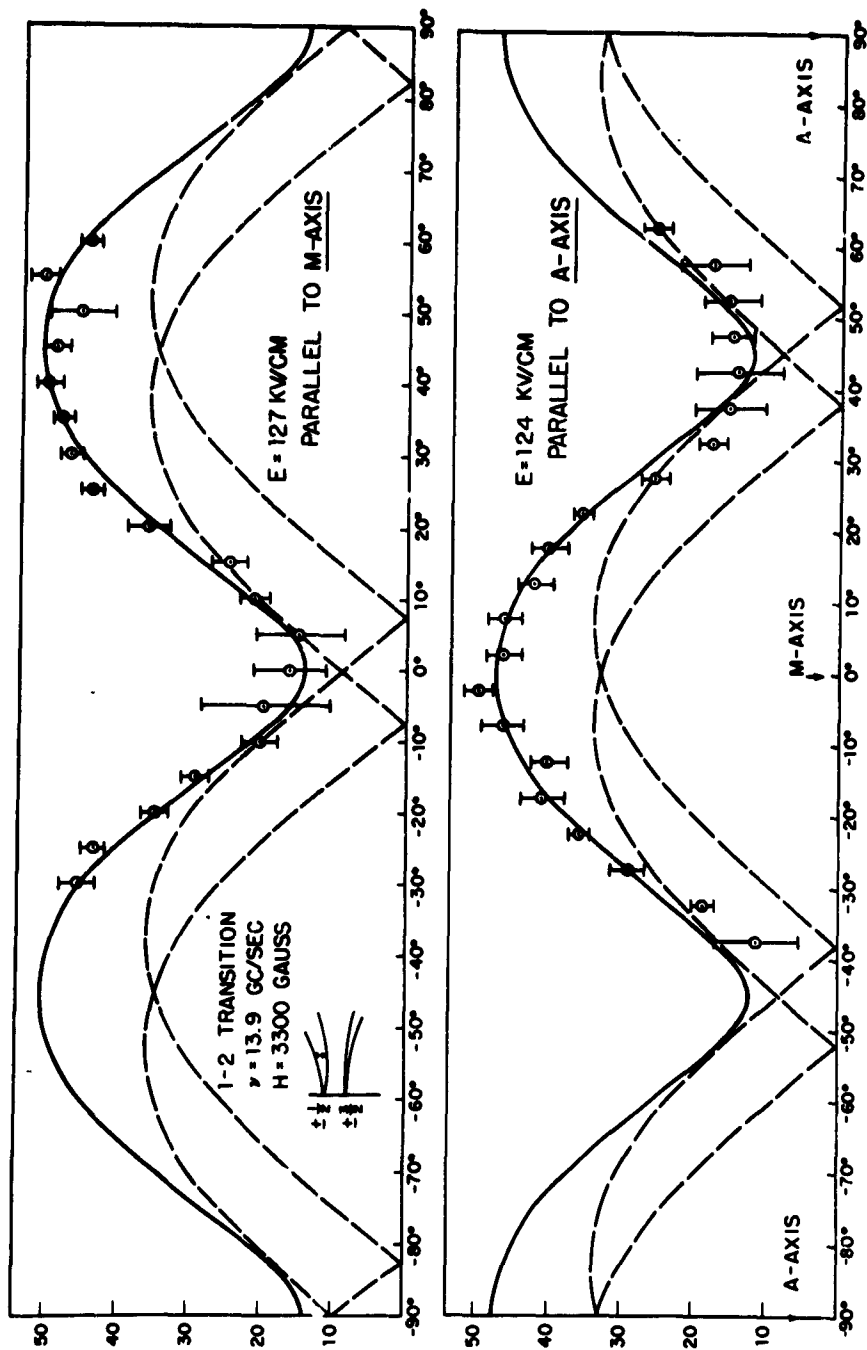


FIG. 3-7. ANGULAR DEPENDENCE OF THE ELECTRIC FIELD INDUCED SPLITTING WHERE THE MAGNETIC FIELD IS ROTATED ABOUT THE Z-AXIS. ELECTRIC FIELD ALONG THE X- AND Y-AXES, RESPECTIVELY.

images of each other in the y-plane. The effect is never zero, since the zeros for the effective splitting for these two sites occur at different angles. The effective splitting of each kind of site is shown as a dashed line and the total effective splitting as a solid line. The latter can be shown to be the square root of the sum of the squares of the individual effective splittings of the two kinds of sites. The contributions from each site were determined by selecting values of the components of the R-tensor for each site to best fit the total effective splitting to the experimental points. The relative signs of R_{111} and R_{333} were determined in a measurement on a separate sample, where the electric field was taken at an angle to the z-axis.

From the position of the minimum splitting at zero degrees we can say that each site contributes equally and, hence, that the population of the sites related to each other by reflection symmetry is the same to one part in seven. From the fact that we never see a shift of the total line, and the fact that the intensities of the split components are equal, we can say that the populations of the sites related to each other by inversion are equal to one part in 200. We can also say that sites such as d in Fig. 3-4, which have inversion symmetry, are not populated. This is in contrast to the results of Geschwind and Remeika [3-8] for gadolinium in Al_2O_3 , where strong site preferences were found between the sites related to each other by reflection. These results could be obtained by magnetic resonance without an applied electric field because Gd^{+3} has such a high spin that its

resonance shows a variation with the azimuthal direction of the magnetic field. Two differences between these cases should be noted, however. First, gadolinium is a much worse fit than chromium in the Al_2O_3 lattice due to its larger ionic radius; and second, the chromium doped samples were flame grown whereas the gadolinium doped samples were grown from a flux. In addition, it should be noted that Geschwind and Remeika did not observe site selectivity for iron in Al_2O_3 , and iron has an ionic radius more comparable to chromium.

Table 3-I gives the final best fit for the components of the R-tensor taking all kinds of data into account. Units are Mc/sec per kv/cm. Relative signs of the various components are significant. The first two sets of data refer to the two kinds of sites related to each other by reflection; the sites related by inversion have all signs reversed.

If the coordinate system is rotated by 5° about the c-axis, R_{111} can be made zero, which would be the case for C_{3v} symmetry. The effect is somewhat spoiled by the fact that R_{123} , which should then also be zero, is, in fact, small but not equal to zero. Thus, we see that the local symmetry of the chromium site is truly C_3 . More important is the fact that while one of the two oxygen triangles which make up the local environment of the magnetic ion is aligned with an edge parallel to the original coordinate system, the second triangle is rotated by 4.3° . This shows that the effect arises predominantly from the second triangle rather than from both equally.

Table 3-1

Values of R-Tensor for Two Types of Sites in Ruby
in Mc/sec per Kv/cm

R_{111}	$-(.020 \pm .003)$	$-(.020 \pm .003)$
R_{222}	$(.073 \pm .003)$	$-(.073 \pm .003)$
R_{333}	$(.179 \pm .003)$	$(.179 \pm .003)$
R_{123}	$(.04 \pm .02)$	$-(.04 \pm .02)$
R_{113}	$(.09 \pm .02)$	$(.09 \pm .02)$

Sites related to these by inversion have all signs reversed.

In a Coordinate System Rotated $5^\circ \pm 1^\circ$

R_{111}	0
R_{222}	$(.076 \pm .003)$
R_{333}	$(.179 \pm .003)$
R_{123}	$\pm (.04 \pm .02)$
R_{113}	$(.09 \pm .02)$

This work has shown that the use of the electric field effect in paramagnetic resonance gives very detailed information about the local symmetry of the paramagnetic site, particularly for sites of low symmetry. Further, the electric field effect gives information about the odd-parity terms in the crystal field.

Chapter IV
 THEORY OF THE ELECTRIC FIELD EFFECT IN
 MgO; Cr AND Al₂O₃; Cr

The observed electric field effect in the paramagnetic resonance of Cr⁺³ is essentially a perturbation of the term DS_z^2 in the spin Hamiltonian describing the optical ground state of the chromium ion. Thus, before it is possible to make a theory of the electric field effect, it will be necessary to review the theory of the origin of the term DS_z^2 in the spin Hamiltonian. This, in turn, requires a review of the optical spectrum of the magnetic chromium ion, since the ground state splitting comes from high order perturbation theory using off-diagonal matrix elements of the spin-orbit interaction and the axial part of the crystalline field between the ground state and the optically excited states.

The Hamiltonian [4-1] of a paramagnetic ion such as chromium is of the form

$$\mathcal{H} = \sum_n \frac{p_n^2}{2m} + V_{\text{nuc}} + V_{\text{el}} + V_{\text{cr}} + \sum_n \zeta_n \ell_n \cdot s_n - \sum_n \beta (\ell_n + 2s_n) \cdot H. \quad (4-1)$$

The first term is the kinetic energy of the electrons, and the second is the potential energy of the electrons in the electrostatic field of the nucleus, given by

$$V_{\text{nuc}} = \sum_n \frac{Ze^2}{r_n}. \quad (4-2)$$

V_{el} is the electrostatic repulsion between electrons, given by

$$V_{el} = \sum_{nn'} \frac{e^2}{r_{nn'}} \quad (4-3)$$

The largest part of V_{el} may be represented as a spherically symmetric potential acting on a single electron and may be grouped with V_{nuc} . The second part of V_{el} is inherently a two particle operator and gives rise to the Russell-Saunders coupling of the l_n 's into L and the s_n 's into S . V_{cr} is the interaction energy of the magnetic ion with its surrounding ligands, and for the 3d transition group it is comparable to the non-spherical part of V_{el} . This results in a partial destruction of the Russell-Saunders coupling, making L no longer a good quantum number. The last two terms in (4-1) are the spin-orbit and Zeeman energy, respectively. They are much smaller than the previous terms and will be treated by perturbation theory on the eigenfunctions of the Hamiltonian which does not contain them.

Part of the difficulty in the crystal field theory of the 3d group arises from the fact that V_{cr} and the non-spherical part of V_{el} are comparable and should be treated together. Because this program is rather difficult, it has been common to work in one of two approximations. In the weak field approximation one considers L to remain a good quantum number and ignores mixing of the various terms. This corresponds to assuming the Russell-Saunders coupling to dominate the crystal field. The crystal field is then introduced as a perturbation on a basis set made up of the M_L

eigenfunctions for the lowest L term. In the strong field approximation, on the other hand, one applies the crystal field perturbation to a basis set made up of the elements of the f^n configuration. Tanabe and Sugano [4-2] have worked out the intermediate cases for the 3d group starting from a strong field basis; Finkelstein and Van Vleck [4-3] have solved the Cr^{+3} problem starting with the ionic terms as a basis.

In the point-charge crystal field theory it is assumed the V_{cr} is given by the electrostatic field produced by point charges located at the centers of each of the ions surrounding the magnetic ion. It is convenient to expand the crystal field in terms of spherical harmonics.

$$V_{\text{cr}} = \sum_n \sum_{l=0}^{\infty} \sum_{m=-l}^l -Ze^2 \frac{4\pi}{2l+1} Y_l^m(0, \phi_n) Y_l^m(0, \phi) \frac{r^l}{r_n^{l+1}}. \quad (4-4)$$

Unfortunately, the crystalline fields so calculated are usually too small by a factor of four or so, and this is compensated for by either expanding the metal ion wave functions [4-4] or by bringing the point charges closer to the metal ion. [4-5] The most successful form [4-1] of the crystal field theory is one in which the strength of the crystal field is taken as an adjustable parameter but where the symmetry of the crystal field is given by the point-charge field. In other words, the group theoretical part of the point-charge theory, which is based on symmetry and which has been outstandingly successful in analyzing optical spectra, is retained. The part of the point-charge theory which has given trouble is the calculation of magnitudes,

and this part of the theory is thrown away in favor of an adjustable parameter. Tanabe and Sugano's work extended this approach to the inclusion of the non-spherical part of V_{el} , the electrostatic repulsion between electrons, by the addition of further adjustable parameters. The work of Finkelstein and Van Vleck is also in terms of an adjustable parameter.

Kleiner [4-6] has attempted to improve on the magnitudes calculated in the point-charge model by replacing the ligand point charge by a charge distributed over the ligand electronic wave functions. The interaction with the metal ion was calculated by classical electrostatics. Unfortunately, this calculation gave the wrong sign of the cubic splitting. Tanabe and Sugano [4-7], however, have shown that a molecular orbital calculation on the complex of the metal ion and its surrounding ligands yields the correct sign of the cubic field splitting.

The first application of the molecular orbital approach to magnetism in solids was made by Van Vleck [4-8] in treating the problem of the cyanide complexes. More recently the molecular orbital approach has been used successfully in accounting for the hyperfine interaction in the paramagnetic resonance of magnetic electrons with a neighboring nucleus. The irridium halide complexes [4-9] and 3d transition group fluorides [4-10] diluted in ZnF_2 have been studied. The hyperfine interaction of fluorine in several 3d group fluorides has also been studied by fluorine nuclear magnetic resonance[4-11]. Shulman and Sugano [4-12] have used the NMR data on the

hyperfine interaction in KNiF_3 as a starting point and have been able to calculate from this the cubic field splitting in a molecular orbital formulation.

It has been assumed that the crystal field is predominantly cubic in symmetry, i. e., that it is invariant under the symmetry elements of the cube. The departures from cubic symmetry in the field are reflections of the departure of the ligand surroundings from a perfect cubic, octahedral, or tetrahedral arrangement. The non-cubic parts of the crystal field V'_{cr} are treated by perturbation theory on the wave functions which result from diagonalizing the Hamiltonian including only the cubic field. Quite commonly for 3d group ions, the non-cubic part of the crystal field is comparable to the spin-orbit energy and is treated at the same time as the spin-orbit interaction.

If V_{cr}^g and V_{cr}^u are the even and odd parts of the crystal field for cubic or octahedral coordination, normally only V_{cr}^g is considered, since matrix elements are taken only within a manifold of wave functions which are purely even or odd in parity. In applying the non-cubic part of the crystal field together with the spin-orbit interaction by perturbation theory, elements such as $\langle g | V'_{\text{cr}}^g | g' \rangle$ and $\langle u | V'_{\text{cr}}^g | u' \rangle$ occur. It is through such perturbation calculations that the ground state splitting occurs. If now one wants to consider also an applied electric field, these elements should be replaced by $\langle g | V'_{\text{cr}}^u | u \rangle \langle u | eEr | g' \rangle (W_g - W_u)^{-1}$ or $\langle u | V'_{\text{cr}}^u | g \rangle \langle g | eEr | u' \rangle (W_u - W_g)^{-1}$.

The splitting of the ground state of Cr^{+3} first appeared in low temperature specific heat measurements on chrome alum. An approximate magnitude for this splitting as well as the magnitude of the susceptibility was calculated by Van Vleck [4-13]. Earlier calculations of the crystal field in chrome alum by Schlapp and Penney [4-14] and by Siegert [4-15] were made in calculating magnetic susceptibilities. The optical line spectrum was calculated in greater detail by Finkelstein and Van Vleck, [4-3], again using a crystal field approach. Similar but more extended calculations have been made by Sugano and Tanabe [4-16], Sugano and Peter [4-17], and McClure [4-18] for chromium in the ruby lattice ($\text{Al}_2\text{O}_3:\text{Cr}$).

The crystal field theory has been quite successful in treating the optical spectrum of Cr^{+3} in ruby. The splitting of the optical ground state is then obtained by a perturbation calculation using off-diagonal elements of the spin-orbit interaction and the low symmetry part of the crystalline field. Unfortunately, these calculations have yielded a value of the splitting of the optical ground state which is smaller than that observed. This ground state splitting is just the D-term in the spin Hamiltonian, the term which is altered by an applied electric field. Nevertheless, it is possible to construct a theory of the electric field effect using the crystal field formulation. In the perturbation calculation, replace elements such as $\langle g | V'_{\text{cr}}^g | g \rangle$ by $\langle g | V'_{\text{cr}}^u | u \rangle \langle u | eEr | g \rangle (W_g - W_u)^{-1}$ as outlined previously. The results

of such a calculation, as might be expected, are in on y fair agreement with experiment. Artman and Murphy [4-19] have called attention to the importance of the odd terms in the crystalline potential $V'_{cr}{}^u$ and have noted that in the original calculations, terms such as $\langle g | V'_{cr}{}^u | u \rangle \langle u | V'_{cr}{}^u | g \rangle (W_g - W_u)^{-1}$ should have been included. They have carried out the perturbation theory in detail including such terms, and they find fair agreement with experiment, both for the microwave and optical electric field effects and for the value of D in the spin Hamiltonian. However, their numerical values assumed for some of the parameters, particularly the spin-orbit parameter, seem unreasonable. This theory will be reviewed after a similar but more primitive calculation is performed for MgO:Cr by way of example.

The calculation of Artman and Murphy is contradicted by experiment on two points. Firstly, on the basis of a point-charge model, it is difficult to understand why, of the two oxygen triangles surrounding the metal ion, one should be so dominant in producing the odd terms in the crystal field, as evidenced by the angular dependence of the electric field effect. The aluminum or chromium-oxygen distances differ by only 10% in the two triangles. A covalent interaction, on the other hand, could be more sensitive to distance, and this indicates that covalency effects should be taken into account more explicitly in the theory.

Secondly, the axial site for Cr^{+3} in MgO consists of a sixfold coordination of nearest neighbor oxygen ions in an octahedral arrangement.

The axial field arises from a next nearest neighbor magnesium vacancy in a 100 direction, whereas in ruby it originates in the distortion of the nearest neighbor oxygen octahedron. If it is assumed that the theory of Artman and Murphy accounts for the D-term in both cases, an electric field effect an order of magnitude larger than experiment is predicted for MgO simply by scaling the ruby theory by $D^{1/2}$. On the other hand, there can be only small covalent bonding to a next nearest neighbor, so again, the assumption that the electric field effect arises from covalent effects will explain the negative results for the electric field experiment in MgO and the positive results in ruby. Actually, the theory in MgO:Cr is somewhat more complicated than presented here but still strongly rules against a theory such as that of Artman and Murphy.

Because of the inadequacy of the point-charge crystal field model in dealing with the electric field effect in the two cases mentioned above, a semi-empirical molecular orbital calculation was performed on the complex CrO_6^{-9} . The calculation was performed by L. Lohr[4-20]. The geometrical arrangement of the complex was taken to be the same as the arrangement of the ions in ruby from X-ray data. It was hoped that such an approach would take covalent effects into account, although the model is surely crude. The rather surprising success of the calculation in accounting for both the D-term in the spin Hamiltonian and the electric field effects will be described.

Before entering into these matters, however, it will be necessary to make a digression on the subject of the dielectric properties of matter.

Digression on the Theory of Dielectrics

Consider a dielectric medium in which the usual relations hold [4-21].

$$\underline{D} = \underline{E} + 4\pi \underline{P} = \epsilon \underline{E} \quad (4-5)$$

The induced dipole moment on each atom is given by

$$\underline{p}_i = \alpha_i (\underline{E}_{\text{eff}})_i \quad (4-6)$$

where $(\underline{E}_{\text{eff}})_i$ is the effective field acting on an atom and is produced by the applied field and the polarization of the surroundings. The average polarization is given by

$$\underline{P} = \frac{\sum_i \underline{p}_i}{\sum_i v_i} = \frac{\sum_i \alpha_i (\underline{E}_{\text{eff}})_i}{\sum_i v_i} \quad (4-7)$$

where v_i is an atomic volume.

Now for the moment consider a solid containing only one atomic species. The applied field \underline{E} is equal to the local field averaged over the volume of one atom. In calculating $\underline{E}_{\text{eff}}$, note that the difference between $\underline{E}_{\text{eff}}$ and \underline{E} is the field produced by the polarization of the atom in question averaged over the atomic volume. This field is

$$\frac{1}{\Delta V} \int_{\Delta V} d\underline{r}' \int_{\Delta V} \rho(\underline{r}) \frac{(\underline{r}' - \underline{r})}{|\underline{r}' - \underline{r}|^3} d\underline{r}$$

$$\begin{aligned}
&= \frac{1}{\Delta V} \int_{\Delta V} d\mathbf{r} \rho(\mathbf{r}) \int_{\Delta V} d\mathbf{r}' \frac{(\mathbf{r}' - \mathbf{r})}{|\mathbf{r}' - \mathbf{r}|^3} \\
&= \frac{1}{\Delta V} \int_{\Delta V} d\mathbf{r} \rho(\mathbf{r}) \left(-\frac{4\pi}{3} \mathbf{r} \right) \\
&= -\frac{4\pi}{3} \mathbf{P} .
\end{aligned} \tag{4-8}$$

Hence the relation

$$\mathbf{E}_{\text{eff}} = \mathbf{E} + \frac{4\pi}{3} \mathbf{P} \tag{4-9}$$

holds. In evaluating the first integral evaluated, it has been assumed that the volume ΔV is spherical. This effective field is, also, the field calculated inside a hollow sphere in a uniform dielectric, and this is an equivalent way of looking at the problem. Equation 4-9 may be termed the Lorentz effective field and leads immediately to the Clausius-Mossotti equation

$$\frac{\alpha}{V} = \frac{3}{4\pi} \frac{(\epsilon - 1)}{(\epsilon + 2)} \tag{4-10}$$

A susceptibility may be defined by the relation

$$\mathbf{P} = \frac{(\epsilon - 1)}{4\pi} \mathbf{E} \equiv \chi \mathbf{E} , \tag{4-11}$$

in which case there results immediately by definition

$$\chi = \frac{(\alpha/V)}{\left(1 - \frac{4\pi}{3} \frac{\alpha}{V}\right)} \tag{4-12}$$

When the polarizability arises from only one source, and when the lattice symmetry is cubic, the treatment above is adequate, but when the polarization arises from several mechanisms, the problem becomes much more complicated. In general, the effective field will be different for each polarization mechanism.

As one limiting case, consider two polarization mechanisms which have similar (assumed identical) spatial distributions but which are associated with different electrons. Assume these different mechanisms depend on the same averages of the local field. One such case would be the polarization of different electronic shells of an atom. If \underline{P}_1 and \underline{P}_2 are the polarizations resulting from each mechanism,

$$\underline{P} = \underline{P}_1 + \underline{P}_2 = a_1 (\underline{E}_{\text{eff}})_1 + a_2 (\underline{E}_{\text{eff}})_2 \quad (4-13)$$

The atomic volume v has been suppressed in the definition of a for the moment. $(\underline{E}_{\text{eff}})_1$ is the effective field producing polarization \underline{P}_1 , and is equal to the effective field on the atom given by Eq. 4-9 plus the field produced by \underline{P}_2 in the region of the polarization. Hence, the relation

$$\begin{aligned} (\underline{E}_{\text{eff}})_1 &= \underline{E} + \frac{4\pi}{3} \frac{\underline{P}}{v} - \frac{4\pi}{3} \frac{\underline{P}_2}{v} \\ &= \underline{E} + \frac{4\pi}{3} \frac{\underline{P}_1}{v} \end{aligned} \quad (4-14)$$

Equation 4-14 could also be obtained by noting that the difference between $(\underline{E}_{\text{eff}})_1$ and \underline{E} is just $(4\pi/3) \underline{P}_1$ (Eq. 4-8). This is a reflection of the fact that the need for an effective field arises because one wishes to write the polarization as a function of the field existing before the polarization takes place rather than as a function of the field existing after the polarization. Adler [4-22] has worked out a quantum mechanical theory of the dielectric constant in which the polarization is written as a function of the field existing after

polarization, and he obtains rather complicated correction terms in this formulation.

Note from Fig. 4-14, that if the polarization due to a particular mechanism, such as the polarization of one electronic shell of an atom, is small, the effective field to be used in calculating this polarization is just the macroscopic applied field. This assumption has been made by Sternheimer [4-23] in calculating electronic polarizabilities of free ions and atoms. Most of the contribution comes from the outermost electrons, but even so, the polarization of one individual electronic orbit is small, and the effective field may be taken equal to the applied field. Havinga [4-24] has used a similar approximation.

Brodky and Burstein [4-25] have found that in calculating the dielectric constants in III - V compounds with non-localized valence band wave functions, the appropriate effective field is the macroscopic field. In calculating the electric field effect in nuclear magnetic resonance, Gill and Bloembergen [4-26], also, found it necessary in GaAs to assume the effective field equal to the macroscopic field. These findings are reasonable in light of the previous paragraph when it is noted that the contribution of each itinerant electron to the total polarization is small. A similar assumption has been used in interpreting Dixon's [4-27] data on electric field effects in the pure quadrupole resonance of Cl^{35} in several organic solids, where the electrons in question itinerate over a large molecule.

Now from Eqs. (4-11, 12, 13, 14)

$$\begin{aligned} \chi &= \frac{a}{1 - \frac{4\pi}{3} a} \\ &= \frac{a_1}{1 - \frac{4\pi}{3} a_1} + \frac{a_2}{1 - \frac{4\pi}{3} a_2} \end{aligned} \quad (4-15)$$

It is easy to show that

$$a = \frac{(a_1 + a_2) - 2(4\pi/3)(a_1 a_2)}{1 - (4\pi/3)^2 a_1 a_2} \quad (4-16)$$

Note that while $a \neq a_1 + a_2$, $\chi = \chi_1 + \chi_2$. This is because the effective field for one polarization is independent of the second polarization as long as the problem is written in terms of internal fields.

Now consider as a second limiting case, two polarization mechanisms which are separated in space. One example would be the electronic polarization of the two ions in an alkali halide crystal. Define fields and polarizations averaged over the areas occupied by the cations (E_1 , P_1) and the anions (E_2 , P_2). Then there are relations for the macroscopic field.

$$\begin{aligned} (v_1 + v_2) \underline{\underline{E}} &= v_1 \underline{\underline{E}}_1 + v_2 \underline{\underline{E}}_2 \\ (v_1 + v_2) \underline{\underline{P}} &= v_1 \underline{\underline{P}}_1 + v_2 \underline{\underline{P}}_2 \end{aligned} \quad (4-17)$$

Also,

$$\begin{aligned} (\underline{E}_{\text{eff}})_1 &= \underline{E}_1 + \frac{4\pi}{3} \underline{P}_1 \\ (\underline{E}_{\text{eff}})_2 &= \underline{E}_2 + \frac{4\pi}{3} \underline{P}_2, \end{aligned} \quad (4-18)$$

and

$$\begin{aligned} v_1 \underline{P}_1 &= a_1 (\underline{E}_{\text{eff}})_1 \\ v_2 \underline{P}_2 &= a_2 (\underline{E}_{\text{eff}})_2. \end{aligned} \quad (4-19)$$

The problem is to find a relation between \underline{E}_1 and \underline{E}_2 in view of the fact that only the total dielectric constant can be measured. One possible approximation is to assume

$$(\underline{E}_{\text{eff}})_1 = (\underline{E}_{\text{eff}})_2 = \underline{E} + \frac{L}{\underline{m}} \underline{P}, \quad (4-20)$$

with $L = 4\pi/3$, in which case the simple relation results,

$$\underline{P} = \frac{(a_1 + a_2)}{(v_1 + v_2)} \left[\underline{E} + \frac{4\pi}{3} \frac{\underline{P}}{\underline{m}} \right], \quad (4-21)$$

$$\text{or} \quad a = a_1 + a_2. \quad (4-22)$$

An alternative approach is to calculate the effective field from its sources. Following Lorentz, take a large spherical cavity centered on one atom. The effective field produced by the applied voltage plus the polarization outside the sphere is then $\underline{E} + \frac{4\pi}{3} \frac{\underline{P}}{\underline{m}}$. It is necessary to take the sphere large so that the surrounding dielectric may be treated as being continuous and uniform. The contribution from the atoms inside the cavity is

evaluated by replacing each atom by a point dipole. The resultant field is then evaluated at the nucleus of the atom being polarized.

This procedure may be criticized on two grounds. Firstly, one is interested in the value of the field at all points where there are polarizable electrons of the atom, not just at the nucleus. Since such dipole sums are rather violent functions of the position where the field is being evaluated, the poor-ness of this approximation becomes apparent. To get a reasonable result, one would have to evaluate the field given by the dipole sum at many places, then average this result over the space occupied by the electronic orbits. Experimental evidence that this is so comes from Dixon's [4-27] results on the electric field effect on the Cl^{35} pure quadrupole resonance in a series of substituted methanes and benzenes. He finds about the same electric field effect in all compounds in spite of the fact that the effective field at the chlorine nucleus calculated by dipole sums is very different for the different materials. This is because the effects of the nearest dipoles should be very different in different molecular structures. One explanation of this result is to note that the chlorine electrons experience not only the effective field at the nucleus, but also the effective field all over their orbit. (It is the electrons which actually sense the applied field, not the nuclei.) Presumably, in this averaging, the variations in effective field are washed out. In dealing with ionic crystals, the electrons are more localized than

in the covalently bonded materials of Dixon's experiments, but a similar washing out of sharp variations in the dipole sums should still occur. Of course, in ionic crystals the localization is sufficient that the effective field is not the same as the macroscopic field.

Secondly, the major contribution to this dipole sum will be from the close dipoles, and for these dipoles the approximation of a point dipole is rather bad. One should probably include quadrupole and possibly higher fields from these atoms. Belford, Bernheim, and Gutowsky [4-28] have attempted to calculate by the method of lattice sums the asymmetry parameter η in nuclear pure quadrupole resonance for crystals far from cubic in symmetry. They find very poor agreement with experiment, and this tends to confirm the objections raised to the dipole sum method.

Note, however, that for a cubic lattice, such as the alkali halides, the dipole sum is zero when evaluated at the nucleus. In this case Eq. 4-21 immediately results, and the question of reliability of the dipole sum procedure does not arise. For simplicity, in this work Eq. 4-21 will be assumed valid for non-cubic lattices, also. Tessman, Kahn, and Shockley (TKS) [4-29] have used Eq. 4-21 (based on approximation 4-20) to evaluate the electronic polarizabilities α_i for the individual alkali metal and halogen ions from the index of refraction of the various alkali halides. Roberts [4-30] has treated the static polarization in a similar manner. The success of these evaluations shows that, indeed, one has a linear addition of the separate polarizabilities, as given by Eq. 4-21 or 4-22. TKS have also varied L in Eq. 4-20, getting a new set of α_i 's each time. They found that the α_i 's were most consistent for $L = 4\pi/3$, as one might expect.

Two limiting cases have been discussed here. In the first case (Eqs. 4-13 to 4-16) two polarization mechanisms associated with different electrons were assumed to be superimposed in space. In this case the local field contains a Lorentz correction only for the polarization being considered; the rest of the polarization is considered uniform throughout the medium. In the second case (Eqs. 4-17 to 4-22), one considers the two components of the polarization to be separated in space, so that the effective field producing either polarization is the same. Throughout this discussion, the assumption has been made that the polarization may be written as a function of the effective field averaged over some region, thus enabling one to avoid consideration of rapidly varying local fields. For a more exact treatment, see the work of Adler.

In calculating the electronic part of the electric field effect in magnetic resonance, the perturbation of the chromium wave functions will be calculated under the influence of the applied electric field. To verify that the perturbation is being calculated correctly, the calculation is extended to calculating the index of refraction. Denoting the electronic polarizability by α^{el} and noting that the polarization on the two atoms is distinctly separated in space,

$$\alpha_{tot}^{el} = \alpha_1^{el} + \alpha_2^{el} . \quad (4-23)$$

Since from 4-12, one has

$$n^2 - 1 = 4\pi \chi_{\text{tot}}^{\text{el}} = [a_{\text{tot}}^{\text{el}} / (v_1 + v_2)] \times \left\{ 1 - \left[\frac{4\pi}{3} a_{\text{tot}}^{\text{el}} / (v_1 + v_2) \right] \right\}^{-1}, \quad (4-24)$$

one, hence, obtains

$$\frac{(a_1^{\text{el}} + a_2^{\text{el}})}{(v_1 + v_2)} = \frac{3(n^2 - 1)}{4\pi(n^2 + 2)} \quad (4-25)$$

(see Eq. 4-10). Electronic polarizabilities are given by TKS for aluminum magnesium and oxygen, but unfortunately not for chromium. Assume that electronic polarizabilities of all ions (Al, Mg, O, Cr) are proportional to the atomic volume. This approximation should be good within a factor of two. This yields the simple relation

$$a_i^{\text{el}} = \frac{3(n^2 - 1)}{4\pi(n^2 + 2)} v_i \quad (4-26)$$

\underline{P} is the same on all ions, the dipole moment per ion being given by

$$\underline{p}_i^{\text{el}} = \underline{P}^{\text{el}} v_i = [(n^2 - 1)/4\pi] v_i \underline{E}. \quad (4-27)$$

Turning to the static dielectric constant, consider the combined effects of the electronic polarization of the individual ions together with the ionic polarization corresponding to a movement of the positive and negative sublattices with respect to each other. Because the polarization motion involves, in part, the motion of the same electrons for both components

of the polarization, and because it is not correct to consider the two polarizations to be superimposed in space, neither of the cases previously described is appropriate for the effective field problem for the electronic and ionic effects. For simplicity, the effective field will be assumed identical for the ionic and electronic effects, namely that given for this problem by Szigeti [4-21].

$$\underline{E}_{\text{eff}} = \underline{E} + \frac{4\pi}{3} \underline{P} \quad (4-28)$$

In this approximation, one has

$$\underline{P} = \alpha \left(\underline{E} + \frac{4\pi}{3} \underline{P} \right) = \left(\frac{\epsilon - 1}{4\pi} \right) \underline{E} \quad (4-29)$$

From Eq. 4-12

$$\alpha = \frac{(\epsilon - 1)/4\pi}{1 + \frac{(\epsilon - 1)}{3}} = \frac{3}{4\pi} \frac{(\epsilon - 1)}{(\epsilon + 2)} \quad (4-30)$$

Also

$$\alpha_{\text{el}} = \frac{3}{4\pi} \frac{(n^2 - 1)}{(n^2 + 2)} \quad (4-31)$$

at optical frequencies. At low frequencies, one has

$$\begin{aligned} \underline{P}_{\text{el}} &= \alpha_{\text{el}} \left(\underline{E} + \frac{4\pi}{3} \underline{P} \right) \\ &= \frac{3}{4\pi} \frac{(n^2 - 1)}{(n^2 + 2)} \left(\underline{E} + \frac{4\pi}{3} \underline{P} \right). \end{aligned} \quad (4-32)$$

Therefore, using 4-29, 30, 32

$$\begin{aligned} \underline{P}_{\text{ion}} &= \underline{P} - \underline{P}_{\text{el}} \\ &= \frac{3}{4\pi} \left[\frac{(\epsilon - 1)}{(\epsilon + 2)} - \frac{(n^2 - 1)}{(n^2 + 2)} \right] \left(\underline{E} + \frac{4\pi}{3} \underline{P} \right). \end{aligned} \quad (4-33)$$

Using 4-29 yields

$$P_{\text{ion}} = \frac{3}{4\pi} \frac{(\epsilon - n^2)}{(n^2 + 2)} \frac{E}{m} \quad (4-34)$$

Finally, there is the relation

$$P_{\text{ion}} = e^* N_0 \delta x \quad (4-35)$$

where N_0 is the number of charges per unit volume, and where e^* is an effective charge. The effective charge will be taken equal to 0.8 times the ionic charge [4-24, 4-31]. Table 4-I lists pertinent quantities [4-32] for the materials of interest in this work.

Table 4-I, Dielectric parameters

	<u>Al₂O₃</u>	<u>MgO</u>	<u>TiO₂</u>
e^* (cation)	$3e^\dagger$	$2e^\dagger$	$4e^\dagger$
N_0 (cation)	$4.7 \times 10^{22}/\text{cc}$	$5.6 \times 10^{22}/\text{cc}$	$3.2 \times 10^{22}/\text{cc}$
ϵ	$8.6 - 10.55^{\dagger\dagger}$	9.65	$89 - 173^{\dagger\dagger}$
n	1.77	1.74	2.6 - 2.9
$n^2 - 1$	2.1	2.0	5.8 - 8.4
$\epsilon - n^2$	5.5 - 7.45	6.65	82 - 164
$(\delta x)_{\text{ion}}$ for 10^5 v/cm (Eqs. 4-34, 4-35).			
	(1.78 - 2.18) $\times 10^{-12}$ cm	2.43×10^{-12} cm	(1.5 - 2.3) $\times 10^{-11}$ cm

† also, times 0.8, see above

†† perpendicular and parallel to the c-axis.

Primitive Crystal Field Theory for MgO: Cr

Cr^{+3} substituting for magnesium in MgO enters an octahedral site surrounded by a sixfold coordination of oxygen ions. Some of the sites have a magnesium vacancy at the nearest site in an (001) direction for charge compensation, and it is the magnetic spectrum of this Cr^{+3} site which is of interest. Assume that the cubic part of the crystalline field is the same for both the compensated and non-compensated sites. Cr^{+3} ($3d^3$) has a 4F term lowest in the free ion spectrum. The cubic field

$$V_{\text{cubic}} = C_c [Y_4^0 + \sqrt{\frac{5}{14}} (Y_4^4 + Y_4^{-4})] \quad (4-36)$$

splits the sevenfold orbitally degenerate 4F term into two orbital triplets 4T_1 and 4T_2 and an orbital singlet 4A_2 . The resulting wave functions are

$$\begin{aligned} T_1 & - \left\{ \begin{array}{l} \sqrt{5/8} Y_3^{-3} + \sqrt{3/8} Y_3^1 \\ \sqrt{5/8} Y_3^3 + \sqrt{3/8} Y_3^{-1} \\ Y_3^0 \end{array} \right\} - \begin{array}{l} E' \\ \\ A_2' \end{array} \\ T_2 & - \left\{ \begin{array}{l} \sqrt{5/8} Y_3^1 - \sqrt{3/8} Y_3^{-3} \\ \sqrt{5/8} Y_3^{-1} - \sqrt{3/8} Y_3^3 \\ \sqrt{1/2} Y_3^2 + \sqrt{1/2} Y_3^{-2} \end{array} \right\} - \begin{array}{l} E \\ \\ B_2 \end{array} \\ A_2 & - \sqrt{1/2} Y_3^2 - \sqrt{1/2} Y_3^{-2} - B_1 \end{aligned} \quad (4-37)$$

The energies for 4A_2 , 4T_2 , and 4T_1 levels are $-12Dq$, $-2Dq$, and $6Dq$, respectively, where $10Dq = 75\sqrt{2} C_c$. Actually a 4T_1 (4P) multiplet mixes with the 4T_1 (4F) multiplet, producing two 4T_1 multiplets whose energies do not follow the results of the calculation above. We will be interested only in the 4T_2 orbital multiplet, however, and this is well accounted for in our weak field scheme.

Note the additional tetragonal crystal field is

$$V' = C_6 Y_6^0 + C_6' Y_6^{\pm 4} + C_4 Y_4^0 + C_2 Y_2^0 \quad (4-38)$$

an orthorhombic field would also include Y_2^{+2} , Y_4^{+2} , and Y_6^{+2} terms. Any $Y_4^{\pm 4}$ terms are lumped with the cubic field by adding and subtracting a suitable amount of Y_4^0 . The tetragonal field splits 4T_2 into a 4E and 4B_2 and the 4T_1 into a 4E and 4A_2 . An orthorhombic field would split the 4E orbital doublets.

The spin-orbit energy $\lambda L \cdot S$ connects the 4A_2 , 4B_1 ground state only to the 4T_2 levels. The required matrix elements of L are

$$\begin{aligned} \langle {}^4A_2, {}^4B_1 | L_z | {}^4T_2, {}^4B_2 \rangle &= 2 \\ \langle {}^4A_2, {}^4B_1 | L_x | {}^4T_2, {}^4E^{(1)} \rangle &= 2 \\ \langle {}^4A_2, {}^4B_1 | L_y | {}^4T_2, {}^4E^{(2)} \rangle &= \pm 2i \end{aligned} \quad (4-39)$$

In second-order perturbation theory, consider

$$\Delta W = \frac{\langle {}^4A_2 | \lambda L \cdot S | {}^4T_2 \rangle \langle {}^4T_2 | \lambda L \cdot S | {}^4A_2 \rangle}{W({}^4A_2) - W({}^4T_2)} \quad (4-40)$$

This expression gives the energy perturbation of the ${}^4A_2, {}^4B_1$ level.

Expansion yields

$$\Delta W = -4\lambda^2 \left\{ \frac{S_z^2}{W({}^4T_2, {}^4B_2)} + \frac{S_x^2}{W({}^4T_2, {}^4E^{(1)})} + \frac{S_y^2}{W({}^4T_2, {}^4E^{(2)})} \right\} \quad (4-41)$$

where $W({}^4A_2, {}^4B_1)$ was taken as zero. Rearranging (4-41) into the usual spin Hamiltonian form yields

$$\mathcal{H}' = D[S_z^2 - \frac{1}{3} S(S+1)] + E(S_x^2 - S_y^2), \quad (4-42)$$

where

$$D = \frac{2\lambda^2}{[W({}^4T_2)]^2} \left[W({}^4T_2, {}^4E^{(1)}) + W({}^4T_2, {}^4E^{(2)}) - 2W({}^4T_2, {}^4B_2) \right]$$

$$E = \frac{2\lambda^2}{[W({}^4T_2)]^2} \left[W({}^4T_2, {}^4E^{(1)}) - W({}^4T_2, {}^4E^{(2)}) \right]. \quad (4-43)$$

If $W({}^4T_2) - W({}^4A_2) = 10Dq$, and $W({}^4T_2, {}^4E) - W({}^4T_2, {}^4B_2) = -3K_1$, then

$$D = -\frac{4\lambda^2}{(10Dq)^2} (3K_1). \quad (4-44)$$

Similarly, the departure of g from 2.0023 may be obtained by the perturbation

$$\Delta W = \frac{\langle {}^4A_2 | \lambda L \cdot S | {}^4T_2 \rangle \langle {}^4T_2 | \beta L \cdot H | {}^4A_2 \rangle}{W({}^4A_2) - W({}^4T_2)}, \quad (4-45)$$

whence

$$\Delta g = \frac{4\lambda}{10Dq}. \quad (4-46)$$

From the optical spectrum $10Dq \approx 15,000 \text{ cm}^{-1}$. The value $\lambda = 70 \text{ cm}^{-1}$ will be justified when the spectrum of ruby is discussed. This conveniently leaves $3K_1$ as a parameter to be adjusted to yield the observed value of D . It should be emphasized that so far nothing has been calculated, since there have been as many adjustable parameters as there are observed quantities.

The application of an electric field will change $10Dq$ and, hence, Δg only in second order, which may be presumed unobservable. Similarly by symmetry, a field applied transverse to the chrome-vacancy axis can cause only a second-order effect. Only an applied field along the axis should produce a first-order effect by changing the chrome-vacancy interaction. From Eqs. 4-38 and 4-4, note that $3K_1$ is proportional to $(1/r_0^n)$, where n is 3, 5 or 7 depending on which term in (4-38) dominates, and where r_0 is the spacing between the vacancy and the magnetic ion. Hence, if δ represents the perturbation on the application of an electric field, one has

$$\frac{\delta D}{D} = -n \frac{\delta r_0}{r_0}. \quad (4-47)$$

In calculating δr_o , note first that if the chromium ion had the same charge as the magnesium it replaces, both the chromium and the neighboring vacancy in the magnesium sublattice would move with the magnesium sublattice, and δr_o would be zero. Because of the excess charge on the chromium, however, it moves $3/2$ times farther than the magnesium sublattice (assuming the oxygen sublattice fixed). Hence, δr_o is one half the motion of the magnesium sublattice due to ionic polarization. From the constants in Table 4-I, Eq. 4-47 with $n = 5$ yields $\delta D/D = 2 \times 10^{-4}$ for a field of 10^5 v/cm, or $\delta D = 0.5$ Mc/sec, which is conveniently smaller than the experimental upper bound of 1 Mc/sec set for this quantity.

The assumption has been made that the ionic electric field effect will dominate the electronic electric field effect associated with the electronic polarization of the chromium ion. This would appear to be a fairly good assumption, since the static dielectric constant is much larger than the optical constant. To calculate the electronic effect, replace matrix elements of $(V'_{cr}{}^g)_{ax}$ by $\langle g | (V'_{cr}{}^u)_{ax} | u \rangle \langle u | eEz | g \rangle (W_g - W_u)^{-1}$ as previously outlined. This introduces a new parameter, the strength of $(V'_{cr}{}^u)_{ax}$, which would require experimental determination.

From Eq. 4-44, $3K_1 = 960 \text{ cm}^{-1}$ since $D = 2.5 \text{ Gc/sec}$ or 0.083 cm^{-1} . But

$$K = \langle g | (V'_{cr}{}^g)_{ax} | g \rangle \quad (4-48)$$

If all of D or K is attributed to $(V'_{cr^u})_{ax}$, then

$$K = \frac{\langle g|(V'_{cr^u})_{ax}|u\rangle \langle u|(V'_{cr^u})_{ax}|g\rangle}{W_g - W_u} \quad (4-49)$$

If $g = 3d$ and $u = 4p$, and $W_g - W_u = -40,000 \text{ cm}^{-1}$, then $\langle g|(V'_{cr^u})_{ax}|u\rangle = 5000 \text{ cm}^{-1}$. This is an upper bound on the quantity in order that D shall not be too large. But if all of D or K is attributed to $(V'_{cr^u})_{ax}$, then

$$\frac{\delta D}{D} = \frac{\langle g|eEz|u\rangle}{\langle g|(V'_{cr^u})_{ax}|u\rangle} \quad (4-50)$$

and if $\langle g|eE_{eff}z|u\rangle = 2 \text{ cm}^{-1}$, for $E = 10^5 \text{ v/cm}$, $\delta D/D = 10 \times 10^{-4}$. In other words, at most the electronic contribution to D may be five times greater than the ionic contribution. The effective field used in calculating the electronic effect was taken as $E_{eff} = [(\epsilon + 2)/3]E$.

After discussing the much better understood case of ruby it will be possible to return to the problem of MgO:Cr .

Crystal Field Theory of $\text{Al}_2\text{O}_3 : \text{Cr}$

The structure of the Cr^{+3} site in Al_2O_3 (ruby) has been discussed in detail in Chapter III, and the reader is referred to that chapter and, in particular, to Fig. 3-4 for details. Briefly, the chromium site is between two non-equivalent oxygen triangles and has C_3 symmetry.

The preceding theory for MgO:Cr was worked out in the weak field limit. It will now be convenient to work in the strong field limit, allowing

the addition of configuration mixing at the cost of considerable increase in the complexity of the theory. The increased complexity arises because there are much more experimental data to be accounted for on $\text{Al}_2\text{O}_3:\text{Cr}$ than on $\text{MgO}:\text{Cr}$. The splitting of the 3d single electron wave functions under the action of the cubic and trigonal field is shown in Fig. 4-1 .

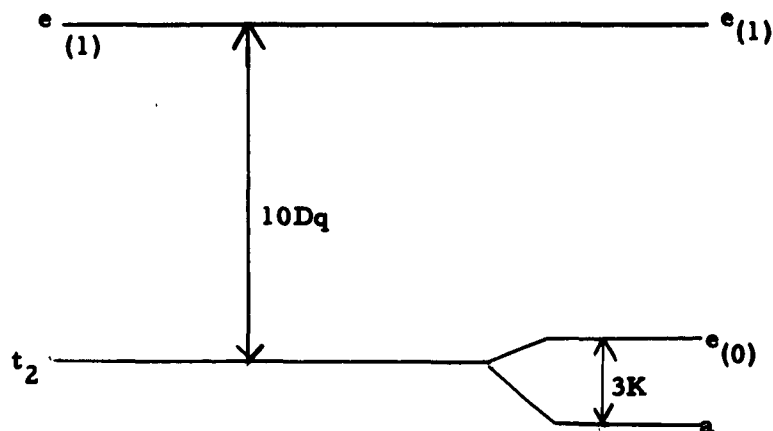


Figure 4-1, One-electron crystal field splitting in ruby for cubic and trigonal fields.

Sugano and Tanabe [4-16] and Sugano and Peter [4-17] have worked out the three-electron problem in the strong field limit including the electron-electron repulsions assuming a cubic crystal field. The resultant energy level diagram is given in Fig. 4-2 , where only the important, low-lying levels are shown. Strong field notation is used, though it is easy to identify the spin quartets occurring in the weak field theory of $\text{MgO}:\text{Cr}$ presented earlier.

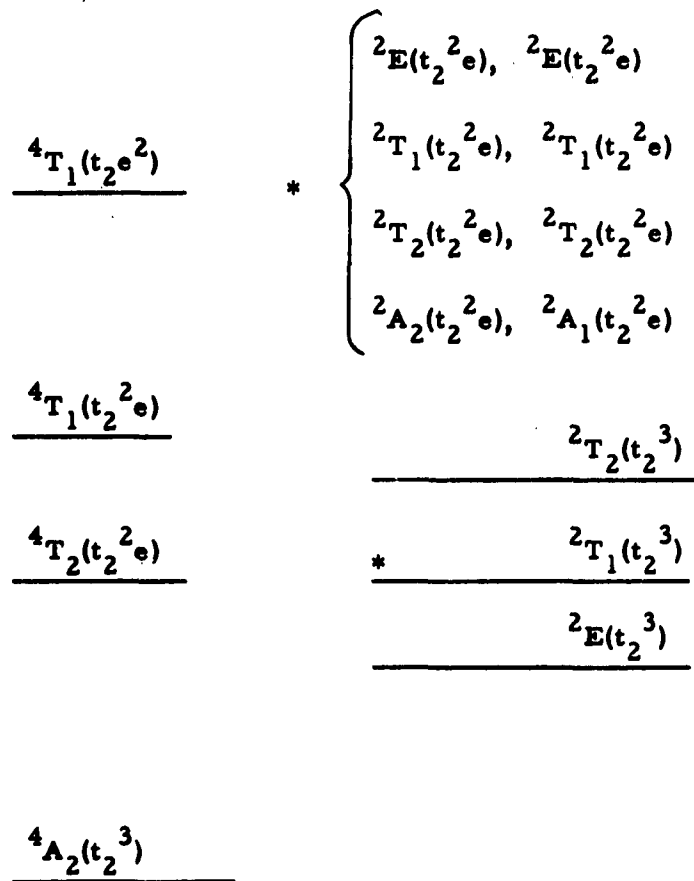


Figure 4-2, Energy levels for d^3 in a cubic field.

(* Positions uncertain)

These calculations of Sugano, et. al., have been outstandingly successful in accounting for the optical spectrum of $Al_2O_3:Cr$. The non-cubic part of the crystal field together with the spin-orbit interaction

is then treated by perturbation theory using the cubic field wave functions as a basis set. Define a trigonal field parameter K by the relations

$$2K = - \langle a | V_{\text{trig}}^g | a \rangle$$

$$K = \langle e_{(0)} | V_{\text{trig}}^g | e_{(0)} \rangle \quad (4-51)$$

The trigonal splitting of t_2 is then $3K$, and the trigonal splitting of ${}^4T_2(t_2^2 e)$ is $(3/2)K$. K is determined experimentally from optical data, whereas for MgO:Cr , K_1 was retained as an adjustable parameter to fit D. Note also that $W({}^4T_2) - W({}^4A_2) \approx 10Dq$. Now introduce the spin-orbit energy

$$V_{\text{so}} = \lambda \underline{L} \cdot \underline{S} = \sum_{i=1}^3 \zeta_{2i} \underline{L}_i \cdot \underline{S}_i \quad (4-52)$$

using Eqs. (4-39) to evaluate the matrix elements of L . For $3d^3$, $3\lambda = \zeta$.

In analogy with Eqs. (4-40 to (4-44), write the perturbation of 4A_2 ($= DS_z^2$) as

$$W({}^4A_2) = \frac{\langle {}^4A_2 | V_{\text{so}} | {}^4T_2 \rangle \langle {}^4T_2 | V_{\text{trig}}^g | {}^4T_2 \rangle \langle {}^4T_2 | V_{\text{so}} | {}^4A_2 \rangle}{[W({}^4A_2) - W({}^4T_2)]^2} \quad (4-53)$$

This term, however, is almost cancelled by the term

$$W({}^4A_2) = \frac{\langle {}^4A_2 | V_{\text{trig}}^g | {}^4T_1 \rangle \langle {}^4T_1 | V_{\text{so}} | {}^4T_2 \rangle \langle {}^4T_2 | V_{\text{so}} | {}^4A_2 \rangle}{[W({}^4A_2) - W({}^4T_1)] [W({}^4A_2) - W({}^4T_2)]} \quad (4-54)$$

as was pointed out by Sugano and Tanabe. Even without this cancellation, however, the calculated value of D is an order of magnitude smaller than experiment and of the wrong sign, if one uses $K = -350 \text{ cm}^{-1}$, $\lambda = 70 \text{ cm}^{-1}$, $10Dq = 18,000 \text{ cm}^{-1}$ from optical data. This led Sugano and Tanabe to suggest correctly that D originated in an anisotropic spin-orbit interaction. This is another story, to be presented later.

Artman and Murphy [4-19] have noted that the usual calculations are done within the $3d^3$ configuration, in which case one uses only $V'_{cr}{}^g$, the even part of the crystalline field. However, $V'_{cr}{}^g$ may be replaced by $(V'_{cr}{}^u)^2$ in the perturbation calculation involving the non-cubic field. This gives an additional term

$$W({}^4A_2) = \frac{\langle {}^4A_2 | V_{so} | {}^4T_2 \rangle \langle {}^4T_2 | V'_{cr}{}^u | u \rangle \langle u | V'_{cr}{}^u | {}^4T_2 \rangle \langle {}^4T_2 | V_{so} | {}^4A_2 \rangle}{\Delta_1 \Delta_2 \Delta_3}, \quad (4-55)$$

Note that this is exactly what was done in the MgO:Cr calculation. However, if such a term as (4-55) is larger than (4-53), there would be an additional splitting of 4T_2 given by

$$W({}^4T_2) = \frac{\langle {}^4T_2 | V'_{cr}{}^u | u \rangle \langle u | V'_{cr}{}^u | {}^4T_2 \rangle}{W({}^4T_2) - W(u)}, \quad (4-56)$$

and this is not observed. Artman and Murphy have also included energy perturbations such as

$$W({}^4A) = \frac{\langle {}^4A_2 | V'_{cr}{}^u | u \rangle \langle u | V'_{so} | u' \rangle \langle u' | V'_{so} | u'' \rangle \langle u'' | V'_{cr}{}^u | {}^4A_2 \rangle}{\Delta_1 \Delta_2 \Delta_3}, \quad (4-57)$$

and by taking V'_{so} , the spin-orbit energy in the excited odd state, to be some ten times that in the 3d states, they get satisfactory agreement with the experimental D. Replacing $\langle g | V'_{cr}{}^u | u \rangle$ by $\langle g | eEz | u \rangle$, and by multiplying the matrix element by ~ 4 , they are also able to calculate the R_{333} component of the electric field effect in agreement with experiment, as well as the optical electric field effect observed by Kaiser, Sugano, and Wood[4-33]. Their justification for multiplying by four is that all electrostatic matrix elements are multiplied by such a factor in the point-charge crystal field theory in order to get agreement with the observed optical spectrum. However, a study of Moore's Atomic Energy Levels [4-34] reveals from multiplet splittings that $\lambda(u)$ is only two or at the most three times $\lambda(3d)$, making the results of the calculations of D by the mechanism of Artman and Murphy an order of magnitude too small as compared with experiment.

It was concluded from these considerations that if one allows sufficient number of adjustable parameters in the crystal field theory, all data can be accounted for. The parameters which Artman has added to the usual ruby crystal field theory are $V'_{cr}{}^u$ and the excited state spin-orbit parameter $\lambda(u)$. Actually, $V'_{cr}{}^u$ was estimated from a point-charge model and gave the value required to fit the experiments when scaled by the usual factor of four. If, however, these parameters are determined from outside evidence, particularly $\lambda(u)$, the crystal field

theory fails to yield the experimentally observed magnitudes. The way out of this dilemma was suggested by Sugano and Tanabe, who pointed out that one could add an additional adjustable parameter by considering the spin-orbit interaction to be anisotropic. The spin-orbit anisotropy parameter has the virtue that it cannot be determined from optical data, allowing it to be fitted to the microwave spin Hamiltonian. The spin-orbit perturbation of 4A_2 is then

$$\begin{aligned} \Delta W &= DS_z^2 \\ &= \sum_i \frac{\langle {}^4A_2 | \lambda_i L_i S_i | {}^4T_2 \rangle \langle {}^4T_2 | \lambda_i L_i S_i | {}^4A_2 \rangle}{W({}^4A_2) - W({}^4T_2)} \\ &= \frac{4}{W({}^4A_2) - W({}^4T_2)} \left\{ \lambda_{\parallel}^2 S_z^2 + \lambda_{\perp}^2 (S_x^2 + S_y^2) \right\}. \end{aligned} \quad (4-58)$$

The summation runs over $i = x, y, z$. This yields

$$D = \frac{4(\lambda_{\parallel}^2 - \lambda_{\perp}^2)}{W({}^4A_2) - W({}^4T_2)}. \quad (4-59)$$

If the anisotropy $(\lambda_{\parallel}^2 - \lambda_{\perp}^2)$ is dependent on an applied electric field, the D-term and the electric field effects have been successfully accounted for. In the following section, covalent effects are shown to account for the observed effects by just this mechanism, and the anisotropy is explicitly calculated.

Semi-Empirical Molecular Orbital Theory of $\text{Al}_2\text{O}_3:\text{Cr}$

In the molecular orbital (MO) procedure the complex CrO_6^{-9} was considered, and the MO wave functions for the complex were written as a linear combination of the atomic wave functions centered on the various atoms of the complex. Coordinates of the atoms in the complex were taken as those in the Al_2O_3 crystal structure. The mixing of the atomic wave functions on different centers in the LCAO-MO procedure arises from the exchange energy

$$V_{\text{exchange}} = \int \psi_1^*(1) \psi_2^*(2) \frac{1}{r_{12}} \psi_1(2) \psi_2(1) d\tau. \quad (4-60)$$

This term should be added to the single atom Hamiltonian, and the total Hamiltonian then diagonalized.

The semi-empirical method used here [4-20] is one in which an approximation to the Hamiltonian of the problem is made, after which the Hamiltonian is diagonalized numerically. The whole procedure is done in a machine calculation once certain starting parameters are specified. The off-diagonal elements of the effective Hamiltonian between the AO basis functions were specified by the relation:

$$\mathcal{H}_{ij} = -2 (\mathcal{H}_{ii} \mathcal{H}_{jj}) \frac{1}{2} S_{ij}, \quad i \neq j, \quad (4-61)$$

where S_{ij} is the atomic orbital overlap matrix. The diagonal elements \mathcal{H}_{ii} were estimated from the ionization potentials of the free ion [4-34]

after reduction due to screening effects in the solid. The atomic wave function basis set was taken to be of the Slater form

$$\psi = Y_l^m(\theta, \phi) R(r)$$

$$R(r) = N r^{n-1} e^{-\kappa r} \quad (4-62)$$

The constant κ was chosen so that the wave function would approximate as closely as possible the analytic SCF wave function on its outer extremities. This means that the wave functions are fairly good for calculating properties which depend on the outer part of the electron distribution, such as ligand overlap, but very bad for calculating properties which depend on the wave function close to the nucleus, such as the spin-orbit parameter λ . For this reason, it was impossible to calculate λ , and λ was taken as an adjustable parameter. The strength of the "crystal field" was fitted to the optical spectrum by slightly adjusting κ to give the proper "cubic splitting," but no other crystal field parameter was adjusted. In the usual crystal field theory, one has in addition to the cubic field parameter $10 Dq$, also a trigonal parameter K and perhaps parameters for the odd components of the field. Of course, these parameters may be related to each other by a point-charge model including the specific geometry of the site, in which case there is only one field strength parameter, namely the constant by which all calculated crystal field quantities are to be multiplied. In the molecular orbital formulation the non-cubic parts of the crystalline field are taken into account automatically by the geometry of the problem.

The atomic orbital (AO) basis set used included 2s and 2p orbitals on each of the oxygen ions and 3d, 4s and 4p orbitals on the chromium. The one-electron MO's which result from the procedure when applied to ruby include at the lowest energies MO's which are made up primarily of ligand AO's. These MO's make contributions to the spectroscopic problem only in the charge transfer spectra since they are occupied by two electrons. At higher energies there are five MO's of primarily 3d composition, which are to contain the remaining three electrons. These MO's are split as shown in Fig. 4-1. Placing the three electrons in various of the one-electron MO's yields a series of three-electron primitive wave functions (e. g. $a e_{(0)}^2$, $a e_{(0)} e_{(1)}$, $e_{(0)}^2 e_{(1)}$), and suitable linear combinations of these wave functions have the transformation properties of the states given in Fig. 4-2. Unfortunately, the non-spherical part of the electron-electron repulsion energy

$$V_{\text{correlation}} = \int \psi_1^*(1) \psi_2^*(2) \frac{1}{r_{12}} \psi_1(1) \psi_2(2) d\tau \quad (4-63)$$

has not been completely included in this problem, which means that the resulting energy levels are still quite different from those in Fig. 4-2. Only the cubic field splitting $10Dq = W(^4T_2) - W(^4A) = W(e_{(1)}) - W(t_2)$ and the trigonal splitting $3K = W(e_{(0)}) - W(a)$ have been accounted for so far. Correlation effects were taken into account approximately as follows. Note that the predominantly 3d MO's are not very different from the pure 3d AO's,

where the problem has been treated by Sugano, et. al., in terms of several adjustable parameters. It was assumed that the solution of the correlation problem in the MO's would be essentially the same as in the pure 3d case, in which case the energy levels of Fig. 4-2 result for suitable values of the parameters, in agreement with experiment.

Stevens [4-35] first pointed out that in a molecular orbital formulation, the spin-orbit energy $\lambda L \cdot S$ would be reduced because matrix elements of L would be non-zero from the 3d part of the MO but would be zero from the ligand part. This served to define an orbital angular momentum reduction parameter k , which would be one for a pure 3d orbital. Koide and Price [4-36] introduced the additional covalency parameter ϵ to take into account the fact that the e orbitals are more covalent than the t_2 orbitals. The orbital angular momentum reduction factor for t_2 orbitals is k , while for e orbitals, it is $k(1-\epsilon)^{1/2}$. This formulation has been used successfully in analyzing spectra by Stout [4-37], Pappalardo [4-38], and Sugano and Peter [4-17]. However, Zahner and Drickamer [4-39] had only poor success in fitting pressure data on a nickel spectrum.

A more serious objection to the orbital reduction picture has been raised by Marshall and Stuart [4-40], who point out that when the non-orthogonality of the AO basis set is properly taken into account, the orbital angular momentum is no longer reduced. This is in agreement with the results of the calculations performed here. The spin-orbit energy reduction

observed in fitting optical spectra, as in ruby, probably comes from the slight expansion of the chromium wave function in the solid due to shielding from the ligand electrons. The spin-orbit parameter in the solid is obtained from the optical spectrum by the relation (Ref. 16, Eq. 5.6)

$$\delta(^2E) = 4K \zeta / [W(^2E) - W(^2T_2)], \quad (4-64)$$

where $\delta(^2E)$ is the 2E level splitting of the R-lines and $(3/2)K$ is the trigonal splitting of the 4T_2 levels. Experimentally, $K = -350 \text{ cm}^{-1}$, whereas the MO program yields $K = -250 \text{ cm}^{-1}$. Using experimental (spectroscopic) values of K , $\delta(^2E)$, and $W(^2E) - W(^2T_2)$ yields $\lambda = \zeta/3 = 50 \text{ cm}^{-1}$ [4-16] as compared with 90 cm^{-1} in the free ion. However, configuration mixing alters the formula for $\delta(^2E)$, resulting in an estimate of $\lambda = 70 \text{ cm}^{-1}$ [4-17], the value used in this work. A slightly smaller value of λ would have yielded better agreement with experiment for the ground state splitting $2D$ and for the electric field effect but did not seem justified.

Matrix elements of the spin-orbit interaction connect the $^4A_2(t_2^3)$ ground state to the levels of $^4T_2(t_2^2e)$, $^2T_2(t_2^3)$ and $^2T_2(t_2^2e)$ [4-41]. Using the methods of irreducible tensorial operators, one obtains the splitting of the 4A_2 ground state as

$$2D = 8\lambda^2 \left[\left(\frac{\lambda'_{||}}{\lambda} \right)^2 - \left(\frac{\lambda'_{\perp}}{\lambda} \right)^2 \right] \times \left[\frac{1}{W(^4A) - W(^4T_2, t_2^2e)} \right]$$

(over)

$$\begin{aligned}
 & - \frac{1}{W(^4A) - W(^2T_2, t_2^2e)} \Bigg] - 6\lambda^2 \left[\left(\frac{\lambda_{\parallel}}{\lambda} \right)^2 - \left(\frac{\lambda_{\perp}}{\lambda} \right)^2 \right] \times \\
 & \left[\frac{1}{W(^4A) - W(^2T_2, t_2^3)} \right]. \tag{4-65}
 \end{aligned}$$

λ_{\parallel} , λ_{\perp} , λ'_{\parallel} , and λ'_{\perp} are defined in terms of the one-electron MO's by the relations

$$\begin{aligned}
 & 4 \left[\left(\frac{\lambda'_{\parallel}}{\lambda} \right)^2 - \left(\frac{\lambda'_{\perp}}{\lambda} \right)^2 \right] \\
 & = \sum_{\alpha, \beta} [\langle e\alpha | l_z | t_2\beta \rangle^2 - \langle e\alpha | l_x | t_2\beta \rangle^2] , \tag{4-66}
 \end{aligned}$$

$$\begin{aligned}
 & \left[\left(\frac{\lambda_{\parallel}}{\lambda} \right)^2 - \left(\frac{\lambda_{\perp}}{\lambda} \right)^2 \right] \\
 & = \sum_{\beta > \gamma} [\langle t_2\beta | l_z | t_2\gamma \rangle^2 - \langle t_2\beta | l_x | t_2\gamma \rangle^2] . \tag{4-67}
 \end{aligned}$$

In evaluating the matrix elements on the right in Eqs. 4-66 and 4-67, only matrix elements between the 3d components of the MO's were used. Small coefficients (entering squared) make the 4p contributions negligible (<1 %). The ligand AO's have no spin-orbit interaction about the chromium center. Surprisingly, the dominant contribution to 2D comes from the levels of $^2T_2(t_2^3)$, whereas previous calculations have emphasized the levels of $^4T_2(t_2^2e)$ [4-16] or of $^2T_2(t_2^2e)$ [4-17]. The

energy denominators used were the experimental values $W(^4A) - W(^4T_2, t_2^2e) = -18,000 \text{ cm}^{-1}$, $W(^4A) - W(^2T_2, t_2^3) = -21,000 \text{ cm}^{-1}$, and $W(^4A) - W(^2T_2, t_2^2e) \approx -50,000 \text{ cm}^{-1}$. The splittings of these levels were ignored in the energy denominators.

The anisotropy of λ , which produced ΔD in this formulation, is a manifestation of the fact that the a MO (x_0 of ref. 16) has a different degree of covalency from the $e_{(0)}$ MO's (x_{\pm} of ref. 16). Undoubtedly, this could be described in terms of an additional covalency parameter, though such has not been done here. It should be mentioned that Lacroix [4-42] and Kamimura [4-43] have also suggested that covalency would produce the observed value of ΔD in this manner.

Table 4-II gives the results of these calculations for several cases. On some of the runs the site symmetry was distorted to C_{3V} from the true C_3 symmetry by rotating the larger oxygen triangle, with no significant effect on the spectrum. The omission of the 4s and 4p chromium AO's produced only a moderate increase in the trigonal optical and microwave splittings, an indication that these orbitals are not particularly important. Because of the form of the interaction (Eq. 4-61), however, the matrix element of the approximate Hamiltonian between 4p and 3d is zero, whereas this is clearly not the case in the true Hamiltonian

Table 4-II, Crystal field splittings in the molecular orbital
formulation (in cm^{-1})

	10Dq	-3K	-D	δD^{**}	δD^{***}
C_3 (4s 4p)	21.1*	420	0.37	77 [†]	10 [†]
+0.1 \AA	18.5	580	0.78		
-0.1 \AA	23.5	260	0.09		
C_{3V}	21.2	450	0.39		
C_3 (no 4s 4p)	21.5	850	0.47	70	20
C_{3V}	21.6	900	0.48		
C_3 (4s 4p) + 4Al	20.2	400	0.36	80	10
Experiment	18.0	1050 1425	0.18		90 ^{††}

* $\times 10^3$ all entries for 10Dq

** ionic effect for 10^5 v/cm

*** electronic effect for 10^5 v/cm

† $\times 10^{-5}$ all entries for δD

†† electronic and ionic effects combined

simply from electrostatic considerations. It is estimated that the admixture of 4p is too small by a factor of two or so, and this should not seriously affect the result.

Displacement of the chromium atom along the c-axis has a strong effect on the microwave trigonal splitting but only a weaker effect on the optical splitting. Since Cr^{+3} is somewhat larger than the Al^{+3} it replaces, such a displacement probably exists and is most likely in the positive direction, which is towards the large, open triangle. Because of the uncertainty in the position of the chromium, not too much significance should be attached to exact agreement or disagreement of the calculated D-value with experiment. It can be said, however, that the molecular orbital formulation gives satisfactory agreement with experiment as regards the signs and magnitudes of the optical and microwave spectral splittings.

Sugano and Peter [4-17] have pointed out that configuration mixing will increase the value of D even in the usual electrostatic crystal field picture. Presumably, this occurs here as well, though not necessarily to the largest extent calculated by Sugano and Peter. Because of the arguments about displacements presented above, agreement or disagreement with the observed value of D is probably not too significant.

Turning to the electric field effects, both the effects of ionic and electronic polarization must be calculated. In principle, it would be possible to calculate the ionic effect by finding the shift in the equilibrium position of the chromium ion under an electrostatic perturbation. From this calculation the ionic component of the dielectric constant could be

calculated as a check on the accuracy of the method. The perturbation should also yield the electric field induced shift in the spectral lines, the electric field effects. Unfortunately, the equilibrium position of the chromium calculated in the distorted oxygen octahedron alone is far from the equilibrium position of aluminum in the solid as determined by X-ray diffraction. From the displacement effects on the spectrum as given in Table 4-II, however, the position of the chromium can not be far from the aluminum position in the solid. Apparently, the equilibrium position is determined by more than just the nearest neighbor oxygen ions. Since the MO program is limited in the number of atoms which can be considered, it was concluded that it is not possible to calculate a meaningful equilibrium configuration for complexes of such a low symmetry without the influence of the surrounding crystal.

The ionic electric field effect was calculated by noting that the ionic dielectric displacement may be calculated from the dielectric constant, as given in Table 4-I. The perturbation of D due to such a displacement was calculated simply by repeating the MO program with displaced coordinates. The results are given in Table 4-II and are in good agreement with the experimental results. Note that while the value of D calculated is sensitive to displacement of the initial position of the chromium along the z -axis, the electric field effect δD is not.

Thus, the agreement of the electric field effect with experiment is much stronger evidence for the validity of the molecular orbital method.

The electronic effect proved somewhat more tedious to calculate, because the effects of $V'' = eE_{\text{eff}}z$ had to be evaluated between all of the MO's calculated with fixed coordinates. It proved more convenient to use the AO's as a basis set but to include a crystal field whose magnitude was such as to produce the observed mixing of the AO's in the MO's. Second-order perturbation theory on the AO basis set was done using V'_{cr}^u and V'' once each. The results were $\delta D = -10 \times 10^{-5} \text{ cm}^{-1}$ for 10^5 v/cm as compared with a calculated ionic effect of $+77 \times 10^{-5} \text{ cm}^{-1}$. The electronic effect so calculated corresponds essentially to the theory of Artman and Murphy but without the exceptionally large spin-orbit parameter and without the scaling by a factor of four on the applied field matrix elements as introduced in their theory. These terms represent a direct effect of the applied field in mixing the AO's. These calculations also yielded the electronic polarization of each of the ions and, hence, the index of refraction $n^2 - 1 = 3.8$. The major contribution comes from the oxygen ion, which means that a comparison with the experimental index of refraction of Al_2O_3 , $n^2 - 1 = 2.1$, shows the validity, but relatively poor accuracy, of the method.

However, going to higher order in V'_{cr}^u in the perturbation theory yielded additional terms in the electric field effect, which made

the total electronic effect $\delta D = +10 \times 10^{-5} \text{ cm}^{-1}$. These higher terms were not evaluated by the usual methods but rather by noting that they correspond to the fact that the two ions polarize their electron clouds by different amounts and that this relative displacement alters the overlap interaction between the ions. The effect of this electronic motion of the two ions is the same as that which occurs for the ionic polarization, and the displacement results were used to evaluate this part of the electronic effect. As can be seen from Table 4-II, the ionic effect dominates the electronic effect, even allowing for the fact that the electronic effect was only crudely evaluated, probably with an uncertainty of a factor of two or so. Because of the dominance of the ionic effect, the electronic effect in ruby will be neglected henceforth. The effective field used in these calculations of the electronic effect was

$$\underline{E}_{\text{eff}} = \frac{\epsilon + 2}{3} \underline{E} \quad (4-68)$$

This is in line with Eqs. 4-28 and 4-29 .

The remaining terms of the R-tensor for the ionic effect were calculated by the molecular orbital method by introducing displacements in the x- and y- directions. In analogy with Eq. 4-65, it can be shown by the method of irreducible tensor operators that the elements of the R-tensor are given by the following relations.

$$\begin{aligned}
 R_{ijk} = & 4R_{ijk}(\lambda') \left\{ [W({}^4A) - W({}^4T_2, t_2^2 e)]^{-1} \right. \\
 & \left. - [W({}^4A) - W({}^2T_2, t_2^2 e)]^{-1} \right\} \\
 & - 3R_{ijk}(\lambda) [W({}^4A) - W({}^2T_2, t_2^3)]^{-1}. \quad (4-69)
 \end{aligned}$$

$R_{ijk}(\lambda)$ is given in Table 4-III.

Table 4-III, $R_{ijk}(\lambda)$ in Eq. (4-69).

Displacement along	<u>x</u>	<u>y</u>	<u>z</u>
$R_{111}(\lambda)$	$\frac{1}{2}(\lambda_x^2 - \lambda_y^2)$		
$R_{222}(\lambda)$		$-\frac{1}{2}(\lambda_x^2 - \lambda_y^2)$	
$R_{123}(\lambda)$	$2\lambda_y \lambda_z$		
$R_{113}(\lambda)$	$2\lambda_x \lambda_z$		
$R_{333}(\lambda)$			$\frac{2}{3}(\lambda_{\parallel}^2 - \lambda_{\perp}^2)^*$
$R_{112}(\lambda) (= -2R_{222})$	$2\lambda_x \lambda_y$		
$R_{212}(\lambda) (= -2R_{111})$		$2\lambda_x \lambda_y$	
$R_{223}(\lambda) (= R_{113})$		$2\lambda_y \lambda_z$	
$R_{213}(\lambda) (= -R_{123})$		$2\lambda_x \lambda_z$	

* also, subtract $\frac{2}{3} D$ (undisplaced).

Signs are correct for an a-site in Fig. 3-4. Furthermore, in analogy with (4-66, 4-67, the products in Table 4-III are calculated according to

$$\lambda'_i \lambda'_j = \frac{\lambda^2}{4} \sum_{\alpha, \beta} \langle e\alpha | l_i | t_2 \beta \rangle \langle t_2 \beta | l_j | e\alpha \rangle, \quad (4-70)$$

$$\lambda_i \lambda_j = \lambda^2 \sum_{\beta > \gamma} \langle t_2 \beta | l_i | t_2 \gamma \rangle \langle t_2 \gamma | l_j | t_2 \beta \rangle. \quad (4-71)$$

Results of such calculations are shown in Table 4-IV.

Table 4-IV, Calculated values of the elements of the R-tensor
(ionic effect only).

	Experiment	C_3 (4s 4p)	C_3 (4s 4p) + 4A1
R_{111}	$-.020 \pm .003$	$-.017$	$-.017$
R_{222}	$+.073 \pm .003$	$.053$	$.049$
R_{333}	$.179 \pm .003$	$.154$	$.160$
R_{123}	$+.04 \pm .02$	$.008$	$.010$
R_{113}	$.09 \pm .02$	$.092$	$.101$

Units are Mc/sec per kv/cm.

The agreement with experiment is better than there is good reason to expect, the only significant discrepancy being R_{123} . The electronic effect probably adds 5% to 10% to these values (see Table 4-II).

Note that all signs are in agreement with experiment, both for D and for components of the R-tensor.

In an attempt to get better agreement with experiment the calculation was extended to include four additional aluminum next nearest neighbors. Aluminum 3s and 3p electrons were included in the MO basis set. The results are shown in Tables 4-II and 4-IV. In general, there is little change over previous calculations, although the agreement on R_{123} is slightly improved. Note that R_{123} would be zero if the local site symmetry were C_{3V} . The fact that R_{123} is experimentally larger than the value calculated using Al_2O_3 coordinates may be an indication that the insertion of the Cr^{+3} ion in the lattice in place of the smaller Al^{+3} ion causes a distortion of the site which makes the C_3 site symmetry less like a C_{3V} symmetry. Presumably, remaining discrepancies arise from more fundamental limitations of the method.

In the calculations which included aluminum ions it was necessary to adjust the aluminum-oxygen interaction by adjusting the diagonal elements of the aluminum AO's in the approximate Hamiltonian. The contact hyperfine interaction of the predominantly 3d MO's on the aluminum nuclei is given by

$$\mathcal{H} = \langle A \rangle I \cdot S, \quad (4-72)$$

where

$$A = \frac{8\pi}{3} g\beta \frac{\mu}{I} \delta(r). \quad (4-73)$$

If the density of the 3s aluminum AO at the aluminum nucleus is taken as $15 \times 10^{24}/\text{cc}$, $\langle \delta(r) \rangle$ is simply this number times the square of the 3s coefficient in the predominantly 3d MO. With a suitable aluminum-oxygen interaction, A for the aluminum nucleus in the same plane as the chromium was calculated as 3.7 Mc/sec, in good agreement with the observed value [4-44] of 3.24 Mc/sec obtained in an ENDOR experiment. This agreement assures that the aluminum-oxygen interaction is of a reasonable value.

In discussing the ionic electric field effect, it has been assumed that the ionic polarizability of chromium in the Al_2O_3 lattice is the same as that of aluminum in the same lattice. Recently, the dielectric constants of Cr_2O_3 (having the same structure as Al_2O_3) have been measured [4-45] as 13.3 and 11.9, compared to 8.6 and 10.55 for Al_2O_3 . If the polarizability of chromium in the Al_2O_3 lattice is the same as in the Cr_2O_3 lattice, the ionic polarizabilities and, hence, the calculated ionic electric field effects would increase by 86% and 18% perpendicular and parallel to the c-axis, respectively. However, the interatomic Cr - O spacing in the Al_2O_3 lattice is probably nearer to the Al - O spacing in Al_2O_3 than to the Cr - O spacing in Cr_2O_3 , and this would tend to make the chromium polarizability closer to that for aluminum. The agreement with experiment of the originally calculated electric field effect (calculated using the Al_2O_3 dielectric constants) is not close enough to shed much light on this question. The proper polarizability to use in these calculations is probably an intermediate value.

Improved Theory of MgO:Cr

Following the method used in the successful calculations for the optical spectrum of ruby by Sugano and Tanabe [4-16], we now consider MgO:Cr in the strong field approximation. This will allow extension to the semi-empirical molecular orbital formulation. The one-electron wave functions in the strong field limit are split as shown in Fig. 4-3 (see also Fig. 4-1 for ruby).

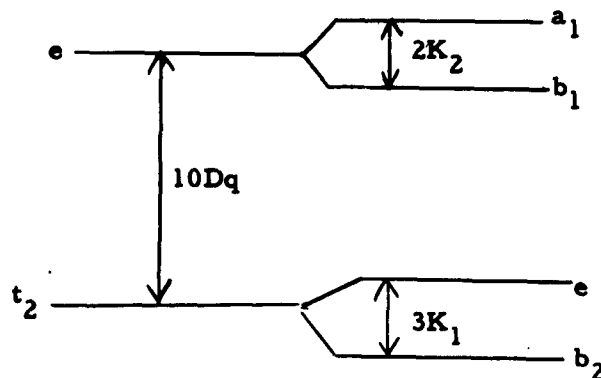


Figure 4-3, One-electron splittings in MgO:Cr in cubic and tetragonal fields.

Three-electron states have an energy level diagram similar to Fig. 4-2 for ruby, if it is assumed that the electron repulsion terms are similar to those in ruby.

If the cubic crystal field splitting is calculated by a point-charge model, $10Dq$ is almost an order of magnitude too small to account for the optical splitting of $15,000 \text{ cm}^{-1}$ obtained by noting that the crystals are

green. The magnitude of the cubic field splitting $10Dq$ may be accounted for on a covalent model, however, as was done for ruby. From the preceding discussion of ruby in the molecular orbital formulation, it appears that D should arise mainly from the anisotropic spin-orbit interaction due to covalent effects. To test these ideas, molecular orbital calculations were performed on a CrO_6^{-9} complex with coordinates taken from MgO. The complex was stretched 0.1 \AA along the Cr-vacancy axis to simulate the tetragonal distortion of the octahedron which might exist due to the charge compensating vacancy on the far side of one oxygen. $10Dq$ was calculated as $10,500 \text{ cm}^{-1}$ in fair agreement with a probable true value of less than $15,000 \text{ cm}^{-1}$. No adjustment of parameters was made in this calculation, the wave functions being identical to those used in the ruby calculation. The discrepancy probably reflects the fact that the ionic radius of the chromium is smaller than that of the magnesium it replaces. This should cause the oxygen ions to move closer to the chromium than the coordinates used would indicate.

The tetragonal splitting of the ground state $2D$ was calculated by Eq. 4-65 and came to only $1/10$ of the observed value! It seems unreasonable to assume a large covalent effect from a next nearest neighbor vacancy, especially since next neighbor effects in ruby were found to be so small. Thus, the molecular orbital theory accounts nicely for the cubic splitting of MgO:Cr but fails completely in accounting for the tetragonal splitting. Apparently the axial splitting is due almost completely to the electrostatic field from the charged vacancy.

A purely electrostatic calculation of the matrix elements of the field from a point charge located at the site of the vacancy gives $3K_1$ as 390 cm^{-1} , while Eq. 4-44 requires $3K_1 = 960 \text{ cm}^{-1}$ to account for ground state splitting of 5.0 Gc/sec. Equation 4-44 is based on second-order perturbation loops to only the ${}^4T_2(t_2^2e)$ levels; whereas for ruby, Sugano and Peter [4-17] have shown that configuration mixing introduced effects of the ${}^2T_2(t_2^2e)$ levels and may make D much larger without any increase in $3K_1$. An increase in the calculated value of D by a factor 2.5 would account for the observed value and is within the range of effects predicted by Sugano and Peter for ruby.

Turn now to the electric field effect. The ionic effect may be calculated by an equation of the form of 4-47, except that working with the one electron functions, one has $K \propto r_0^{-3}$, other terms being much smaller. Hence, one has in Eq. 4-47, $n = 3$ and $\delta D = 0.3 \text{ Mc/sec}$.

In evaluating the electronic effect, $V'_{cr}{}^u$ was estimated from the point-charge model. Using Eqs. 4-44 and 4-49 yields $\delta D = 0.6 \text{ Mc/sec}$. The contribution of $V'_{cr}{}^u$ to D through Eq. 4-49 has already been included in the value of D previously quoted; this contribution is about 25 % of the total. The total calculated value of the electric field effect is 0.9 Mc/sec for 10^5 v/cm , which is conveniently not larger than the experimental upper bound of 1 Mc/sec at 10^5 v/cm .

Quadratic Electric Field Effects in Ruby and MgO

Weger and Feher [4-46] have observed quadratic electric field effects in the Cr^{+3} EPR in ruby and MgO:Cr . In order to observe small effects, they used a modulation technique similar to those described in Chapter II. AC fields of 10^5 v/cm were used. Phase detection at twice the modulation frequency gave an absorption derivative shaped line for a quadratically shifted resonance and a dispersion derivative shaped line for a quadratically broadened line.

It has been previously noted that in systems such as $\text{Al}_2\text{O}_3:\text{Cr}$ and MgO:Cr , the total lattice has an inversion center, though the individual sites do not. This means that if one site exhibits a linear shift in resonance frequency, the other site must exhibit a similar shift in the opposite direction. If the resultant splitting is less than one line width, there will be observed only a broadening of the line proportional to the square of the applied field. This quadratic broadening was frequently observed in determining the transverse and skew components of the R-tensor for ruby, as described in Chapter III. Taking the applied electric and magnetic fields along the c- or z-axis, the $1/2 \rightarrow 3/2$ transition will show a quadratic broadening (and eventually a linear splitting) from a term in the spin Hamiltonian $R_{ijk} E_i S_j S_k$. The T-tensor described in Chapter III is associated with terms of the form $T_{ijk} E_i S_j H_k$ and might also contribute to the quadratic

broadening of the $1/2 \rightarrow 3/2$ transition. In addition, it should also produce a quadratic broadening of the $1/2 \rightarrow -1/2$ transition.

Weger and Feher observed no quadratic broadening of the $1/2 \rightarrow -1/2$ transition but did observe a quadratic shift of 0.1 gauss for 10^5 v/cm. They attribute this shift of the $1/2 \rightarrow -1/2$ transition to strains in the crystal which produce terms in the spin Hamiltonian having only off-diagonal elements. In second order, these terms then produce a shift proportional to E^2 . Such a quadratic shift of the $1/2 \rightarrow -1/2$ transition was observed by Weger and Feher for Cr^{+3} , Fe^{+3} and Mn^{+2} in MgO, also, and in all cases attributed to strains.

Co^{+2} in MgO has an effective spin of $1/2$ and may not show the strain effects exhibited by the other ions. For a field of 18,000 v/cm, Weger and Feher observed a shift of $1/2$ milligauss for Co^{+2} and attribute this to a true quadratic effect.

Weger and Feher have also observed a linear splitting (actually a quadratic broadening) in MgO for a line 13 gauss above the Cr^{+3} $1/2 \rightarrow -1/2$ transition. They have attributed this line to a defect center similar to that studied in the present work. Presumably, the charge compensating vacancy is much farther removed from the site in order to reduce the zero-field splitting to the observed value. However, if this were the case, there should be a second line at 13 gauss on the other side of the Cr^{+3} $1/2 \rightarrow -1/2$ line, and this does not appear. Apparently, in this case, Weger and Feher have observed an electric field effect on a line originating from some unknown impurity.

Quadratic electric field effects in $\text{TiO}_2:\text{Cr}$ and $\text{TiO}_2:\text{Fe}$ are discussed in Chapter V.

Discussion and Conclusions

The use of a molecular orbital approach in the ligand field problem does not imply that binding in the material is entirely covalent. Van Vleck [4-8] has pointed out that the molecular orbital method is a general one, and that the purely ionic crystal field scheme and the purely covalent valence bond scheme are the two limiting cases included in a molecular orbital calculation. In the molecular orbital method, the expansion of the molecular orbital in terms of an atomic orbital basis set is in terms of coefficients which may take on any values from zero to one (subject to the normalization condition), and these variable values of the coefficients may represent any "degree of covalency" one wishes. Actually, the bonding of the chromium in the Al_2O_3 oxygen sublattice is primarily ionic since the coefficients of ligand AO's in the predominantly 3d MO's are typically of the order 0.05.

What is suggested by the calculations which have been exhibited here, as well as by earlier molecular orbital calculations, [4-7, 42, 43] is first, the incompleteness of the concept of the "crystal field" arising from the classical electrostatic field of the ligands interacting on the

chromophoric electrons. The work of Kleiner [4-6] already showed that this was the case. As a result of these difficulties, there arose a crystal field method [4-1] in which the strength of the crystal field was taken as an adjustable parameter, and this, together with symmetry arguments, allowed an explanation of the origin of spectra in solids. In general, fields were calculated by a point-charge model and then scaled upwards by a factor of the order four or so. A more complete picture of the ligand field, suggested by this work, has the ligand field arising primarily from the repulsive covalent interaction of the ligand electrons on the chromophoric electrons; the attractive force holding the supposedly ionic crystal together is still the electrostatic attraction of the charged ions. (We are not speaking here of truly covalent solids, such as GaAs, but only of solids which are normally considered primarily ionic, such as NaCl or Al_2O_3 .) The adjustable magnitude in the crystal field theory presumably takes this effect into account, though a molecular orbital calculation would obviously be a better way to handle the problem.

However, when the electric field effect is considered, even this modified form of the crystal field theory is in trouble. The electric field effect is accounted for [4-19] in the crystal field scheme only at the sacrifice of reasonableness of the spin-orbit parameter. While it is true that such a theory is internally self consistent, it is far from being in

agreement with external data. The second suggestion arising from the calculations made here is that the splitting of the 4A ground state of Cr^{+3} in ruby and the electric field effects on this splitting are due primarily to covalent effects producing an anisotropic spin-orbit interaction. In this calculation the modified crystal field theory is quite inadequate, unless an artificial spin-orbit anisotropy parameter is introduced.

It should be emphasized that the calculations done here are semi-empirical in nature; the correct molecular orbital problem has not been solved. The success of these calculations is taken to reflect the closeness of the semi-empirical approximation to the correct molecular orbital formulation and to reflect the correctness of the molecular orbital approach.

Note added: N. Wiser [Phys. Rev. 129, 62 (1963)] has considered the problem of local fields in the calculation of dielectric constants. His conclusions are in agreement with those presented here, but his arguments are much more explicit. He shows that for solids where the weak binding approximation is valid (covalent solids), the appropriate local field is just the macroscopic field, while for solids where the tight binding approximation is valid (ionic solids), the Lorentz effective field is correct. For the contribution to the dielectric constant of conduction electrons, he shows that the correct effective field is the macroscopic field. Finally, Wiser points out that the appropriate average of the microscopic field used to obtain the effective field is an average weighted by the local electronic polarizability. This is not the same as the average appropriate for calculating the force on an electron. In this work, the distinction between these averages is not made.

Chapter V

THEORY OF THE QUADRATIC ELECTRIC FIELD EFFECT

IN $\text{TiO}_2\text{:Cr}$ AND $\text{TiO}_2\text{:Fe}$

Titanium dioxide has an unusually large dielectric constant, though the material is not ferroelectric [5-1]. The large dielectric constant suggested that this material should exhibit a large electric field effect on the paramagnetic resonance of impurities.

Fe^{+3} and Cr^{+3} substitute for titanium in TiO_2 at a site which is a center of inversion symmetry. Such a site may not show a linear electric field effect but may show a quadratic effect. There are two magnetic sites per unit cell, each with its y-axis along the crystallographic tetragonal c-axis. The sites themselves are of orthorhombic symmetry [5-2], with the z-axis of one and the x-axis of the other parallel and along a 110 direction. Figure 5-1 shows the local geometry of the site and the coordinate system used in this work. The y- or c-axis is normal to the x- and z- axes as shown, and displacements δ along the c-axis will be considered. Four oxygen ligands are at a distance b , and two are at a distance a . Let $\Delta = a - b$. The four oxygen ions equidistant from the metal are in a rectangular rather than a square arrangement.

eliminates three components leaving six independent components. In this work, only the case where the applied electric field is parallel to the y-axis will be considered. Only two independent components are then involved and are redefined as follows,

$$\delta D = R_{2233} - \frac{1}{2} (R_{2211} + R_{2222}), \quad (5-3)$$

$$\delta E = \frac{1}{2} (R_{2211} - R_{2222}). \quad (5-4)$$

Molecular Orbital Theory for $\text{TiO}_2:\text{Cr}$

A crystal field theory of $\text{TiO}_2:\text{Cr}$ would be similar to that presented in Chapter IV for ruby. In view of the difficulties encountered by this theory in accounting for the crystal field splittings and the electric field effect in ruby, the theory has not been worked out for $\text{TiO}_2:\text{Cr}$.

A semi-empirical molecular orbital theory for $\text{TiO}_2:\text{Cr}$ was worked out by Lohr [5-3] along the lines of the theory for ruby. These calculations are here extended to include the electric field effect. The spin Hamiltonian for $\text{TiO}_2:\text{Cr}$ is of the following form [5-4], where the effective spin is $3/2$.

$$\mathcal{K} = g\beta H \cdot S + D \left[S_z^2 - \frac{1}{3} S(S+1) \right] + E(S_x^2 - S_y^2) \quad (5-5)$$

$D = 0.68 \text{ cm}^{-1}$ and $E = 0.14 \text{ cm}^{-1}$. In analogy with Eq. 4-65, D and E are given by the relations below, where the usual irreducible tensorial method has been used [5-5].

$$\begin{aligned}
D = & 4 [(\lambda_z')^2 - \frac{1}{2}(\lambda_x')^2 - \frac{1}{2}(\lambda_y')^2] \times \\
& \left\{ [W(^4A_2) - W(^4T_2, t_2^2e)]^{-1} - [W(^4A_2) - W(^2T_2, t_2^2e)]^{-1} \right\} \\
& - 3 [(\lambda_z')^2 - \frac{1}{2}(\lambda_x')^2 - \frac{1}{2}(\lambda_y')^2] \times \\
& [W(^4A_2) - W(^2T_2, t_2^3)]^{-1} , \tag{5-6}
\end{aligned}$$

$$\begin{aligned}
E = & 2 [(\lambda_x')^2 - (\lambda_y')^2] \times \\
& \left\{ [W(^4A_2) - W(^4T_2, t_2^2e)]^{-1} - [W(^4A_2) - W(^2T_2, t_2^2e)]^{-1} \right\} \\
& - \frac{3}{2} [(\lambda_x')^2 - (\lambda_y')^2] [W(^4A_2) - W(^2T_2, t_2^3)]^{-1} . \tag{5-7}
\end{aligned}$$

$\lambda_i'^2 = \lambda_i \lambda_i$ and $(\lambda_i')^2 = \lambda_i' \lambda_i'$ are given by Eqs. 4-70 and 4-71 .

The results of such a calculation are $D = 0.45 \text{ cm}^{-1}$ and $E = 0.16 \text{ cm}^{-1}$, in satisfactory agreement with experiment. The same parameters and wave functions as for ruby were used; only the site geometry was changed.

The ionic electric field effect was calculated as $\delta D = 1.1 \times 10^{-4} \text{ cm}^{-1}$, and $\delta E = 0.03 \times 10^{-4} \text{ cm}^{-1}$ for an applied field of 50 kv/cm. Dielectric parameters for TiO_2 from Table 4-I were used in the calculation, which is equivalent to assuming that the ionic polarizability of chromium in the TiO_2 lattice is the same as that of titanium. This may well overestimate the dielectric displacement by as much as a factor of ten, and hence, the electric field effect by a factor of 100.

Crystal Field Theory for $\text{TiO}_2:\text{Fe}$

The spin Hamiltonian for $\text{TiO}_2:\text{Fe}$ is of the form [5-6] below, where the effective spin is $5/2$.

$$\begin{aligned} \mathcal{H} = & g\beta H \cdot S + D[S_z^2 - \frac{1}{3}S(S+1)] + E(S_x^2 - S_y^2) \\ & + \frac{1}{6}a[S_x^4 + S_y^4 + S_z^4 - \frac{1}{5}S(S+1)(3S^2 + 3S - 1)] \\ & + \frac{7}{36}F\left\{S_z^4 + \left[\frac{5}{7} - \frac{6}{7}S(S+1)\right]S_z^2 \right. \\ & \left. - \frac{6}{35}S(S+1) + \frac{3}{35}S^2(S+1)^2\right\}. \end{aligned} \quad (5-8)$$

$D = 0.69 \text{ cm}^{-1}$, $E = 0.073 \text{ cm}^{-1}$, $a = 0.036 \text{ cm}^{-1}$, $F = 0.017 \text{ cm}^{-1}$. In this work only the terms quadratic in S will be considered as these are the largest terms.

Now according to Watanabe [5-7], the second-order spin terms in the spin Hamiltonian arise from the fourth-order perturbation expression

$$\begin{aligned} \Delta W_{M, M'} = & \frac{1}{P^2 D} \sum_{J''M''} \langle {}^6S_{5/2} M | \lambda L \cdot S | {}^4P_{5/2} M \rangle \times \\ & \langle {}^4P_{5/2} M | V' | {}^4D J'' M'' \rangle \langle {}^4D J'' M'' | V' | {}^4P_{5/2} M' \rangle \times \\ & \langle {}^4P_{5/2} M' | \lambda L \cdot S | {}^6S_{5/2} M' \rangle, \end{aligned} \quad (5-9)$$

where the tables of Racah [5-8] have been used. Further, by the use of Racah's tables and the irreducible tensorial method [5-5], the following expressions may be obtained. Differences in the energy denominators in the sum have been ignored.

$$D = K [- 2 |A_2^2|^2 + |A_2^1|^2 + |A_2^0|^2], \quad (5-10)$$

$$E = -(K/3) [2\sqrt{6} \operatorname{Re} A_2^2 A_2^0 + 3 |A_2^1|^2] \quad (5-11)$$

Equation 4-4 has been rewritten in the form

$$V_{cr} = -Ze^2 \sum_{l,m} \sqrt{\frac{4\pi}{2l+1}} A_l^m Y_l^m(0\phi) \langle r^l \rangle, \quad (5-12)$$

$$A_l^m = \sum_n \sqrt{\frac{4\pi}{2l+1}} Y_l^m(0\phi_n) r_n^{-l-1}. \quad (5-13)$$

Only the $l = 2$ terms have been considered under the assumption that $l = 4$ and higher terms will be smaller because of the factor $\langle r^l \rangle / r_n^{l+1}$. The constant K was not evaluated because of uncertainties in energy denominators, spin-orbit energies, and above all, because from previous experience an arbitrary constant is needed to get good results from a point-charge model. Keeping only terms quadratic in δ , one obtains the following expressions.

$$A_2^0 = \frac{1}{a^3} \left[3 \left(\frac{\Delta}{a} \right) + 6a + \frac{51}{4} \left(\frac{\delta}{a} \right)^2 + \frac{27}{2} a \left(\frac{\delta}{a} \right)^2 \right]$$

$$A_2^{\pm 1} = 0$$

$$A_2^{\pm 2} = -\frac{1}{a^3} \left[\frac{3\sqrt{6}}{2} \left(\frac{\Delta}{a} \right) - \sqrt{6}a - \frac{9\sqrt{6}}{4} a \left(\frac{\delta}{a} \right)^2 + \frac{11\sqrt{6}}{8} \left(\frac{\delta}{a} \right)^2 \right] \quad (5-14)$$

Substituting in Eqs. 5-10 and 5-11 yields

$$D = Ka^{-6} \left\{ -18 \left(\frac{\Delta}{a} \right)^2 + 24a^2 + 72 \left(\frac{\Delta}{a} \right) a + \left(\frac{\delta}{a} \right)^2 \left[27 \left(\frac{\Delta}{a} \right) + 186a + 162 \left(\frac{\Delta}{a} \right) a + 108a^2 \right] \right\}, \quad (5-15)$$

$$E = Ka^{-6} \left\{ 18 \left(\frac{\Delta}{a} \right)^2 - 24a^2 + 24 \left(\frac{\Delta}{a} \right) a + \left(\frac{\delta}{a} \right)^2 \left[93 \left(\frac{\Delta}{a} \right) - 18a + 54 \left(\frac{\Delta}{a} \right) a - 108a^2 \right] \right\}. \quad (5-16)$$

Now approximately [5-2] $(\Delta/a) = 0.05$ and $a = 0.09$, which yields the result

$$D = Ka^{-6} \left[0.48 + 19.7 \left(\frac{\delta}{a} \right)^2 \right], \quad (5-17)$$

$$E = Ka^{-6} \left[0.04 - 2.3 \left(\frac{\delta}{a} \right)^2 \right]. \quad (5-18)$$

Experimentally, $D = 0.68 \text{ cm}^{-1}$ and $E = 0.073 \text{ cm}^{-1}$. Fitting Ka^{-6} to D gives $Ka^{-6} = 1.42 \text{ cm}^{-1}$ from 5-17. Then from 5-18 one obtains $E_{\text{exp}} = 0.057 \text{ cm}^{-1}$, which is in adequate agreement with experiment considering uncertainties in the unit cell parameters.

Now consider a field of 50 kv/cm. From Table 4-I it is easy to obtain $(\delta/a) = 6 \times 10^{-4}$ or $(\delta/a)^2 = 3.3 \times 10^{-7}$. Hence, $\delta D = 0.92 \times 10^{-5} \text{ cm}^{-1}$ and $\delta E = 0.11 \times 10^{-5} \text{ cm}^{-1}$. Taking the magnetic field along

the x- or y-axis, respectively, and considering the Zeeman splitting to be small compared to the zero-field splitting, for the $1/2 \rightarrow -1/2$ transition in first order, the effective g is given by

$$g_{\text{eff}} \approx 6 \left(1 \mp 4 \frac{E}{D} \right). \quad (5-19)$$

But

$$h\nu = g_{\text{eff}} \beta H \approx 6 \left(1 \mp 4 \frac{E}{D} \right) \beta H. \quad (5-20)$$

Therefore,

$$\frac{\delta\nu}{\nu} = - \left(\frac{\delta E}{E} - \frac{\delta D}{D} \right) \frac{E}{D} \left(\frac{1}{4} \mp \frac{E}{D} \right)^{-1}. \quad (5-21)$$

For H parallel to x , $\delta\nu/\nu = 3 \times 10^{-5}$, while for H parallel to y , $\delta\nu/\nu = 1 \times 10^{-5}$, all for 50 kv/cm.

Powell, Gabriel, and Johnson [5-9] have included excited spin doublets as well as the excited quartets in calculating the cubic term $a/6$, but such terms are probably not important for the orthorhombic terms D and E . In the molecular orbital formulation to be presented, the doublets do not contribute at all.

Molecular Orbital Theory for $\text{TiO}_2:\text{Fe}$

Semi-empirical molecular orbital calculations were performed for $\text{Fe}^{+3} (d^5)$ in the TiO_2 lattice using the same program as for Cr^{+3} in TiO_2 and using the same one-electron wave functions as for Cr^{+3} .

The spin-orbit interaction connects the ${}^6A_1, t_2^3 e^2$ ground state only to the ${}^4T_1, t_2^3 e^2$ levels [5-5], resulting in the following expressions for D and E.

$$D = \frac{1}{10} [(\xi_z)^2 - \frac{1}{2}(\xi_x)^2 - \frac{1}{2}(\xi_y)^2] [W({}^6A_1) - W({}^4T_1)]^{-1}, \quad (5-22)$$

$$E = \frac{1}{20} [(\xi_x)^2 - (\xi_y)^2] [W({}^6A_1) - W({}^4T_1)]^{-1}. \quad (5-23)$$

$(\xi_i)^2$ is given by

$$(\xi_i)^2 = \xi^2 \sum_{\alpha < \beta} \langle t_{2\alpha} | l_i | t_{2\beta} \rangle \langle t_{2\beta} | l_i | t_{2\alpha} \rangle. \quad (5-24)$$

For $W({}^4T_1) - W({}^6A_1) = 12,000 \text{ cm}^{-1}$ and $\xi = 270 \text{ cm}^{-1}$ (reduced from the free ion value of 360 cm^{-1} --- see the discussion of a similar reduction in the case of ruby, Chapter IV), Eqs. 5-22 and 5-23 yield $D = 0.31 \text{ cm}^{-1}$ and $E = 0.11 \text{ cm}^{-1}$ as compared to the experimental values of $D = 0.68 \text{ cm}^{-1}$ and $E = 0.073 \text{ cm}^{-1}$. The agreement with experiment seems adequate when it is recalled that no parameter has been fitted to a magnetic resonance result.

The ionic electric field effect was calculated for 50 kv/cm using the assumption that the ionic polarizability of iron in the TiO_2 lattice is the same as that of titanium, as was done in the previous section. The parameters of Table 4-1 for TiO_2 were used. The results are $\delta D = 0.94 \times 10^{-4} \text{ cm}^{-1}$ and $\delta E = 0.02 \times 10^{-4} \text{ cm}^{-1}$. Using Eq. 5-21 yields $\delta\nu/\nu = 2 \times 10^{-4}$ for H parallel to x and $\delta\nu/\nu = 1 \times 10^{-4}$ for H parallel to y.

Note that as might have been expected from the ruby calculations, these figures are an order of magnitude larger than those obtained in the crystal field calculation. Experimentally, for H along x, $\delta\nu/\nu \leq 1 \times 10^{-5}$, twenty times smaller than the calculated value. This is probably an indication that the ionic polarizability of the iron in the TiO_2 lattice is considerably less than the polarizability of titanium in that lattice.

Recently, Wemple [5-10] has observed a large quadratic effect on the iron paramagnetic resonance in $\text{KTaO}_3:\text{Fe}^{+3}$. He observed $\delta D = 10^{-3} \text{ cm}^{-1}$ for 13 kv/cm. Since the material is paraelectric, the ionic polarizability of the iron in the KTaO_3 lattice would seem to be large, as is the tantalum polarizability. This is somewhat different from the result for $\text{TiO}_2:\text{Fe}$. Wemple has explained the large effect as arising from electrostriction rather than the optical mode distortion considered in this work.

Chapter VI

ON THE ELECTRIC DIPOLE MOMENT OF THE ELECTRON

The implications of the existence of an electric dipole moment for the electron have been examined by Salpeter [6-1] and by Feinberg [6-2], who have calculated the resultant change in the Lamb shift. From experimental measurements of the Lamb shift they have placed an upper bound on the value of the electronic electric dipole moment. Salpeter has also calculated upper bounds for the dipole moment from the absence of $K \rightarrow L_1$ x-ray transitions in heavy atoms, the hyperfine splitting of the positronium ground state, and the metastable $2s$ -state in hydrogen. When this work was started, the lowest previous upper bound had been set by the free electron experiment of Nelson et al. [6-3]. Since then Wilkinson et al. [6-4] have repeated Nelson's experiment obtaining the lowest upper bound so far set. Table 6-I summarizes these results.

Landau and Lee and Yang [6-5] have shown that for an elementary particle to possess an electric dipole moment there is required the non-conservation of both parity and time-reversal symmetry. In view of this fact it seems desirable to determine the experimental upper bound on the dipole moment of the various elementary particles as accurately as possible. An upper bound on the electric dipole moment of the proton has been set by Sternheimer [6-6], on the neutron by Smith, Purcell and Ramsey [6-7], on the muon by Berley, et al. [6-8], and on the positron by Salpeter [6-1]. The limits set for the neutron and muon are from free particle experiments, while the proton limit was set by considerations of the Lamb shift. The results are listed in Table 6-II.

A new upper bound was set for the electric dipole moment of the electron by the use of the electric field effect in ruby. The existence of an electronic electric dipole moment should cause a lifting of the Kramers degeneracy and hence, a shift in the resonance frequency under the application of an electric field. By verifying the Kramers degeneracy it was possible to show that the dipole moment is zero to the accuracy of the experiment. The electric field effect described previously in ruby will be termed the ordinary electric field effect (Chapters III and IV). This experiment separates the ordinary effect from the dipole-dependent effect by reversing the polarity of the applied electric and magnetic fields, since the two effects have different dependences on these field polarities.

Theoretical Considerations

Sachs and Schwebel [6-10] have treated the implications of an electronic electric dipole moment on the energy levels of a paramagnetic ion. The following treatment is an elaboration of their work. Consider the usual Hamiltonian for an electron bound to an atom in a predominantly ionic crystal.

$$\mathcal{H} = - (\hbar^2/2m) \nabla^2 + e\phi - iek \underline{2s} \cdot (\nabla\phi) \times \underline{\nabla}. \quad (6-1)$$

The terms are, respectively, the kinetic, potential, and spin-orbit energies, $k = (\hbar/2mc)^2$. The potential energy may be divided into terms arising from the nuclear charge, from the charges of other electrons, and from the crystalline electric field.

$$\phi = \phi_{\text{nuc}} + \phi_{\text{el}} + \phi_{\text{cr}}^g + \phi_{\text{cr}}^u \quad (6-2)$$

Table 6-I . Electronic electric dipole moment

<u>Experiment</u>	<u>Reference</u>	
Metastable 2s-state in atomic hydrogen	6-1	$< 1.2 \times 10^{-12}$ cm e
Hyperfine splitting of positronium ground state	6-1	$< 8 \times 10^{-13}$ cm e
Absence of $K \rightarrow L_1$ transitions in heavy atoms	6-1	$< 2 \times 10^{-13}$ cm e
Lamb shift	6-1, 6-2	$< 1.5 \times 10^{-13}$ cm e
Kramers degeneracy	6-11	$< 1.4 \times 10^{-13}$ cm e
Free electron	6-3	$< 4 \times 10^{-15}$ cm e
Kramers degeneracy	this work	$< 1.4 \times 10^{-15}$ cm e
Electron scattering	6-9	$< 1 \times 10^{-15}$ cm e
Free electron	6-4	$< 5 \times 10^{-16}$ cm e

Table 6-II. Electric dipole moments of the elementary particles

<u>Particle</u>	<u>Reference</u>	
Electron	6-4	$< 5 \times 10^{-16}$ cm e
Positron	6-1	$< 8 \times 10^{-13}$ cm e
Proton	6-6	$< 1.3 \times 10^{-13}$ cm e
Neutron	6-7	$< 5 \times 10^{-20}$ cm e
Muon	6-8	$< 2 \times 10^{-15}$ cm e

The first three terms have even parity; the last has odd parity. The usual procedure for simplifying the spin-orbit term is to consider $\nabla\phi$ to be predominantly radial. This gives

$$\begin{aligned} -iek \underline{2s} \cdot \left(\frac{1}{r} \frac{\partial\phi}{\partial r} \right) \underline{r} \times \underline{\nabla} \\ = \xi \underline{s} \cdot \underline{l} \end{aligned} \quad (6-3)$$

where

$$\xi = \left\langle 2ek \left(\frac{1}{r} \frac{\partial\phi}{\partial r} \right) \right\rangle \quad (6-4)$$

Now consider a set of wave functions which are eigenfunctions of the Hamiltonian

$$\mathcal{H}_0 = -(\hbar^2/2m)\nabla^2 + e\phi^g - iek \underline{2s} \cdot (\nabla\phi^g) \times \underline{\nabla} \quad (6-5)$$

This Hamiltonian commutes with the parity operator and is all of even parity. Hence, the resulting eigenfunctions will also be eigenfunctions of the parity operator. Consider further the perturbing Hamiltonian

$$\mathcal{H}' = -\xi\mu_0 \underline{2s} \cdot (\nabla\phi) + e\phi_{cr}^u - iek \underline{2s} \cdot (\nabla\phi_{cr}^u) \times \underline{\nabla} \quad (6-6)$$

The last two terms result simply from the addition of the odd part of the crystal field. The first term comes from assuming the electron to have an intrinsic electric dipole moment $\underline{P} = 2\xi\mu_0 \underline{s}$, where μ_0 is the Bohr magneton. This term will lift the Kramers degeneracy. Equation 6-6 may be rewritten following Sachs and Schwebel

$$\begin{aligned} \mathcal{H}' = -\xi\mu_0 e^{-1} \left\{ [2\underline{s} \cdot \underline{\nabla}, \mathcal{H}_0] + iek [2\underline{s} \cdot \underline{\nabla}, 2\underline{s} \cdot (\nabla\phi^g) \times \underline{\nabla}] + \right. \\ \left. + [2\underline{s} \cdot \underline{\nabla}, e\phi_{cr}^u] \right\} + e\phi_{cr}^u - iek \underline{2s} \cdot (\nabla\phi_{cr}^u) \times \underline{\nabla} \quad (6-7) \end{aligned}$$

To see this, note that

$$[2\underline{s} \cdot \underline{\nabla}, -(\hbar^2/2m)\nabla^2] = 0, \quad (6-8)$$

and that

$$\begin{aligned} [2\underline{s} \cdot \underline{\nabla}, e\phi] &= 2\underline{e}\underline{s} \cdot \underline{\nabla}\phi - 2\underline{e}\underline{s} \cdot \phi\underline{\nabla} \\ &= 2\underline{e}\underline{s} \cdot (\underline{\nabla}\phi) \end{aligned} \quad (6-9)$$

In first order evaluate \mathcal{H}' between the eigenfunctions of \mathcal{H}_0 , which are also eigenfunctions of the parity operator since \mathcal{H}_0 commutes with the parity operator. Terms one, two, four, and five of Eq. 6-7 are all of odd parity, and hence, cannot yield a non-zero diagonal element. The third term gives a contribution

$$\Delta W = -\xi\mu_0 2\underline{s} \cdot \underline{\nabla}\phi_{cr}^u \quad (6-10)$$

In second order, use the odd terms in pairs, keeping in mind that the only contributions of interest are those linear in ξ and s . The dominant term of this form is

$$\begin{aligned} \Delta W &= -\xi\mu_0 e^{-1} \left\{ \langle n | [2\underline{s} \cdot \underline{\nabla}, \mathcal{H}_0] | n' \rangle \langle n' | e\phi_{cr}^u | n \rangle + \right. \\ &\quad \left. + \text{complex conjugate} \right\} (W_n - W_{n'})^{-1} \\ &= -\xi\mu_0 e^{-1} \left\{ (W_{n'} - W_n) \langle n | 2\underline{s} \cdot \underline{\nabla} | n' \rangle \langle n' | e\phi_{cr}^u | n \rangle + \right. \\ &\quad \left. + (W_n - W_{n'}) \langle n | e\phi_{cr}^u | n' \rangle \langle n' | 2\underline{s} \cdot \underline{\nabla} | n \rangle \right\} \times \\ &\quad \times (W_n - W_{n'})^{-1} \\ &= \xi\mu_0 \left\{ \langle n | 2\underline{s} \cdot \underline{\nabla}\phi_{cr}^u | n \rangle - \langle n | \phi_{cr}^u 2\underline{s} \cdot \underline{\nabla} | n \rangle \right\} \\ &= \xi\mu_0 \langle n | 2\underline{s} \cdot (\underline{\nabla}\phi_{cr}^u) | n \rangle \end{aligned} \quad (6-11)$$

Note that this just cancels the contribution from 6-10.

The only other second-order contribution of importance comes from the spin-orbit interactions as shown below. Other second-order terms have been evaluated but are not discussed here since they are much smaller.

$$\Delta W = -\xi\mu_0 e^{-1} (iek) \left\{ \langle n | [2\mathbf{s} \cdot \nabla, 2\mathbf{s} \cdot (\nabla\phi^g) \times \nabla] | n' \rangle \times \right. \\ \left. \times \langle n' | e\phi_{cr}^u | n \rangle + c.c. \right\} (W_n - W_{n'})^{-1} \quad (6-12)$$

But also, Sachs and Schwebel give the identity

$$(2\mathbf{s} \cdot \mathbf{a})(2\mathbf{s} \cdot \mathbf{b}) = \mathbf{a} \cdot \mathbf{b} + i2\mathbf{s} \cdot \mathbf{a} \times \mathbf{b}, \quad (6-13)$$

which reduces Eq. 6-12 to

$$\Delta W = \xi\mu_0 k (W_n - W_{n'})^{-1} \left\{ \langle n | 2\mathbf{s} \cdot \nabla \times [(\nabla\phi^g) \times \nabla] | n' \rangle - \right. \\ \left. - \langle n | 2\mathbf{s} \cdot [(\nabla\phi^g) \times \nabla] \times \nabla | n' \rangle \right\} \langle n' | e\phi_{cr}^u | n \rangle + \\ + \langle n | e\phi_{cr}^u | n' \rangle \left\{ \langle n' | 2\mathbf{s} \cdot \nabla \times [(\nabla\phi^g) \times \nabla] | n \rangle - \right. \\ \left. - \langle n' | 2\mathbf{s} \cdot [(\nabla\phi^g) \times \nabla] \times \nabla | n \rangle \right\} \quad (6-14)$$

The last two terms are the complex conjugate written out explicitly. Working with real wave functions, these terms may be omitted if the remaining terms are multiplied by two. Apparently, the second and fourth terms, arising from the commutator, have been omitted by Sachs and Schwebel. The use of Eqs. 6-3 and 6-4 gives

$$\Delta W = 2\xi\mu_0 (W_n - W_{n'})^{-1} \left\{ \langle n | \mathbf{s} \cdot \nabla \times i\zeta_{cr} | n' \rangle - \right. \\ \left. - \langle n | \mathbf{s} \cdot i\zeta_{cr} \times \nabla | n' \rangle \right\} \langle n' | \phi_{cr}^u | n \rangle \quad (6-15)$$

Taking the z-axis along s allows 6-15 to be written in component form.

$$\begin{aligned} \Delta W = 2\xi\mu_0 (W_n - W_{n'})^{-1} s_z \left\{ \langle n | \frac{\partial}{\partial x} | n'' \rangle \langle n'' | i\xi l_y | n' \rangle - \right. \\ \left. - \langle n | \frac{\partial}{\partial y} | n'' \rangle \langle n'' | i\xi l_x | n' \rangle - \right. \\ \left. - \langle n | i\xi l_x | n'' \rangle \langle n'' | \frac{\partial}{\partial y} | n' \rangle + \right. \\ \left. + \langle n | i\xi l_y | n'' \rangle \langle n'' | \frac{\partial}{\partial x} | n' \rangle \right\} \langle n' | \phi_{cr}^u | n \rangle. \quad (6-16) \end{aligned}$$

In this form, Eq. 6-15 was evaluated numerically using parameters derived from optical spectra and using the Slater type wave functions of Chapter IV to evaluate matrix elements of z . The crystal field was evaluated at the nucleus from a purely electrostatic model.

Define a tensor \underline{A} by the relation

$$\begin{aligned} \langle \nabla \phi_{cr}^u - \underline{E} \rangle \cdot \underline{A}_{nn} = -e^{-1} \left\{ \langle 3d_n | \nabla_{xi} l | u \rangle (\xi_u/3) - \right. \\ \left. - \langle 3d_n | i l_x \nabla | u \rangle (\xi_{3d}/3) \right\} \langle u | e \phi_{cr}^u - e E r | 3d_n \rangle \times \\ \times (W_d - W_u)^{-1}, \quad (6-17) \end{aligned}$$

where \underline{E} is a possible applied electric field. The tensor \underline{A} has only diagonal elements non-zero, and furthermore $A_{xx} = A_{yy} \neq A_{zz}$. Now consider the three unpaired chromium 3d electrons,

$$\begin{aligned} \Delta W = -2\xi\mu_0 \sum_{n=1}^3 s_n \cdot (3\underline{A}_{nn}) \cdot \langle \nabla \phi_{cr}^u - \underline{E} \rangle \\ = -2\xi\mu_0 \underline{S} \cdot (\sum \underline{A}_{nn}) \cdot \langle \nabla \phi_{cr}^u - \underline{E} \rangle. \quad (6-18) \end{aligned}$$

In the spin Hamiltonian formulation describing the spin-dependent energy levels of the ground state, simply add this term to the Hamiltonian. For ruby, $\nabla\phi_{cr}^u$ is predominantly directed along the c- or z-axis, so only $(\sum_n A_n)_{zz}$ is of interest. From equation (6-16), this is calculated to be 1.15×10^{-3} , with a probable error of a factor of two. Note that because $\langle \nabla\phi_{cr}^u \rangle_z$ dominates, the largest effect of the electric dipole will come if the applied magnetic field is also along the z-axis. The major contributions to A_n come when the odd state u is a 3p-, 4p-, or 4f-state. Other chromium states have larger energy denominators and smaller matrix elements to the ground state. Odd wave functions made up of oxygen molecular orbitals as in Chapter IV were found to give a negligible contribution because of small matrix elements.

Experimental Procedure and Results

The electric field effects are introduced into the usual spin Hamiltonian by the addition of the following perturbation.

$$\mathcal{H}' = \sum_i \sum_{j < k} (1/2) R_{ijk} E_i (S_j S_k + S_k S_j) - \sum_{ij} 2 \xi \mu_o (\sum_n A_n)_{ij} S_i \langle \nabla\phi_{cr}^u \rangle_j - E_j \quad (6-19)$$

The first term represents the ordinary electric field effect, and the second is the dipole induced effect, which lifts the Kramers degeneracy. Browne [6-9] has attempted to detect the dipole induced effect experimentally by applying a uniform electric field to a paramagnetic salt. He modulated

the resonance of Cr^{3+} in alum with an applied electric field but could detect no effect. It is not clear, however, that any effect observed in his experiment would not be due to the ordinary electric field effect.

However, the term $\nabla\phi_{\text{Cr}}^u$ is much larger than any possible applied electric field if the paramagnetic site lacks inversion symmetry, as is the case in ruby. If the $-1/2 \rightarrow -3/2$ transition of Cr^{3+} in ruby is observed with the magnetic field along the z- or c-axis, there should be a shift in frequency of

$$\delta\nu = h^{-1} \left\{ 3R_{zzz} E_z - 2g\mu_0 \left(\sum_n A_n \right)_{zz} \langle \nabla\phi_{\text{Cr}}^u \rangle_z \right\}. \quad (6-20)$$

Assume the dominant part of $\nabla\phi_{\text{Cr}}^u$ to be along the c-axis and take the applied electric field along the c-axis as well. Now for both electric and magnetic fields along the c-axis, the four sites in the Al_2O_3 lattice become equivalent in pairs. Both terms in (6-20) are of opposite sign for one of these pairs of sites as compared to the other pair. This is true because $\nabla\phi_{\text{Cr}}^u$ changes sign on inversion, the two pairs of sites being related by inversion. R is proportional to $\nabla\phi_{\text{Cr}}^u$, whereas $\sum_n A_n$ is not. Thus, $\delta\nu$ in (6-20) produces a splitting of the observed resonance line in ruby since the resonance frequency for the two pairs shifts in opposite directions.

If the direction of the applied magnetic field is reversed, only the second term in (6-20) will reverse in sign since it is proportional to S . The first term is proportional to S^2 . On the other hand, reversing the sign of the applied electric field reverses the sign of only the first term

if one assumes $\nabla\phi_{cr}^u \gg E$. Thus, on reversal of either the applied electric or the applied magnetic field, the splitting ($= 2|\delta\nu|$) changes by four times the second term in Eq. (6-20). If Δ represents the change on reversal of either the applied electric or magnetic field,

$$\Delta (2|\delta\nu|) = 8h^{-1} \xi \mu_0 (\sum_n A_n)_{zz} \langle \nabla\phi_{cr}^u \rangle_z \quad (6-21)$$

Any possible additional splitting due to the T-tensor terms of Chapter III would have the same symmetry as the R-tensor terms as regards the reversal in sign of either applied field. Hence, possible effects of a T-tensor term may be lumped with the first term of Eq. 6-20.

One may inquire as to why any electric field was applied, thereby introducing the complication of the ordinary electric field effect. The dipole induced splitting by itself must be assumed to be much smaller than one line-width, and from the discussion of Chapter III the observed additional broadening of the line produced by the dipole effect would be proportional to the square of the effect. Also, there would be no way to "turn off" the induced broadening. The ordinary electric field effect is used initially to split the line, in which case the additional splitting arising from the dipole effect is directly observable.

In this work the procedure was to observe the electrically induced line splitting for four cases: (1) electric and magnetic fields normal, (2) magnetic field reversed, electric field normal, (3) both fields reversed, and (4) electric field reversed, magnetic field normal. The difference between the line splittings for the second and fourth cases on the one hand and the

first and third cases on the other hand is $\Delta(2\delta \nu)$ in Eq. (6-21). Experimentally, this quantity was found to be (0.025 ± 0.125) gauss or (0.07 ± 0.35) Mc/sec.

The uncertainty quoted is based on the standard deviation of the results of eight runs. (See Chapter II). In Eq. (6-21) $(\sum_n A_n)_{zz} = 1.15 \times 10^{-3}$, and from a purely electrostatic model $\nabla \phi_{cr}^u = 3.6 \times 10^8$ v/cm, which yields $|\xi| = (0.5 \pm 2.3) \times 10^{-5}$. (Taking into account only nearest neighbor oxygen ions gives $\nabla_{cr}^u = 6 \times 10^8$ v/cm, but a lattice sum [6-12] gives the value used.) Remembering the possible uncertainty in $(\sum_n A_n)_{zz}$ of a factor of two, it is possible to say only that $|\xi|$ is probably less than 3.5×10^{-5} and almost certainly less than 7×10^{-5} . The latter corresponds to a dipole moment of 1.4×10^{-15} cm e. This upper bound on the electric dipole moment of the electron is three times better than the best previous published upper bound set by Nelson, et al., but not as good as the bound of 5×10^{-16} cm e set by Wilkinson, et al.

In view of the extensive molecular orbital theory developed in Chapter IV, it may seem strange to use simple crystal field theory in calculating the dipole effect. Unfortunately, while the semi-empirical molecular orbital theory used is very good in treating the chromium ligand interactions, it is unsatisfactory in treating the 3d-4p interaction on the chromium, and it is just this interaction which is needed in calculating the dipole effect. The electrostatic model used in evaluating 6-16 is probably conservative, so that using it is to err on the safe side.

The experimental limitations which prevented a better upper bound to be set on the electric dipole moment of the electron arise mainly from instrumental instabilities over the period of a run. More fundamental, however, is the limitation that this measurement depends on calculation of effective fields in a solid, a problem whose solution is beset with considerable uncertainty. The approximations used in the calculations here are quite crude, but a better calculation must await better wave functions and energy levels for excited states of an atom in a solid, and a better theory of the crystalline field.

ACKNOWLEDGMENTS

I would like first to express my indebtedness to Professor N. Bloembergen for his interest, encouragement, and advice in this work. I also thank him for valuable criticism in the preparation of this report.

The assistance of L. L. Lohr, Jr., in the theoretical part of this work is gratefully acknowledged. The semi-empirical molecular orbital procedure is due to him, and he has programmed all of the computer runs reported here. I have also profited greatly from conversations with F. A. Collins and L. C. Kravitz.

The assistance of many members of the staff of the Gordon McKay Laboratory in the experimental parts of this work and in the preparation of this manuscript is acknowledged with thanks.

I thank Dr. J. O. Artman and Dr. M. Weger for sending me copies of their work prior to publication.

I am indebted to the National Science Foundation for a pre-doctoral fellowship from 1957 to 1961 .

REFERENCES

- 1-1 B. Bleaney and K. W. H. Stevens, *Rep. Prog. Phys.* 16, 108 (1953);
K. D. Bowers and J. Owen, *Rep. Prog. Phys.* 18, 304 (1955);
M. H. L. Pryce, *Nuovo Cimento, Supp.* 6, 817 (1957);
W. Gordy, W. V. Smith, and R. E. Trambarulo, Microwave Spectroscopy (John Wiley and Sons, Inc., New York, 1953);
D. J. E. Ingram, Spectroscopy at Radio and Microwave Frequencies (Butterworths, London, 1955);
W. Low, Paramagnetic Resonance in Solids (Academic Press, New York, 1960);
G. E. Pake, Paramagnetic Resonance (W. A. Benjamin, Inc., New York, 1962).
- 1-2 Elementary texts covering the material of reference 1-1:
- C. Kittel, Introduction to Solid State Physics (John Wiley and Sons, Inc., New York, 1956);
L. F. Bates, Modern Magnetism (Cambridge Univ. Press, Cambridge, 1951);
M. Kotani, *Supp. Prog. Theoret. Phys. (Kyoto)* 14, 1 (1960).
- See also:
- G. E. Pake, *Am. J. Phys.* 18, 438, 473 (1950).
- 1-3 H. A. Lorentz, Theory of Electrons (Teubner, Leipzig, 1909);
H. Fröhlich, Theory of Dielectrics, (Oxford Univ. Press, Oxford, 1949);
B. Szigeti, *Trans. Faraday Soc.* 45, 155 (1949);
C. J. F. Böttcher, Theory of Electric Polarisation (Elsevier, Amsterdam, 1952).
- 1-4 W. M. Walsh, Jr., *Phys. Rev.* 114, 1485 (1959);
— *Phys. Rev. Letters* 4, 507 (1960);
— *Phys. Rev.* 122, 762 (1961).

- 1-5 G. D. Watkins and E. Feher, *Bull. Am. Phys. Soc.* 7, 29 (1962).

Optical pressure experiments in MgO have also been carried out:

A. L. Schawlow, A. H. Piksis and S. Sugano, *Phys. Rev.* 122, 1469 (1961);

S. Minomura and H. G. Drickamer, *J. Chem. Phys.* 35, 903 (1961).

- 1-6 P. L. Donoho and R. B. Hemphill, *Bull. Am. Phys. Soc.* 7, 306 (1962);

R. B. Hemphill and P. L. Donoho, *Bull. Am. Phys. Soc.* 8, 133 (1963).

Optical experiments have also been carried out:

A. L. Schawlow, *Advances in Quantum Electronics* (J. R. Singer, ed., Columbia Univ. Press, 1961, p. 60);

D. R. Stevens, S. Minomura and H. G. Drickamer, *J. Chem. Phys.* 35, 424, 427, 429, 903 (1961).

- 1-7 M. Date and Y. Miyako, *First International Conference on Paramagnetic Resonance*, The Hebrew University, Jerusalem, Israel, 1962 (to be published).

- 1-8 T. Deutsch, G. A. DeMars and L. Rimai, *Bull. Am. Phys. Soc.* 7, 538 (1962).

- 1-9 D. F. Wait and R. H. Sands, *Bull. Am. Phys. Soc.* 7, 538 (1962).

- 1-10 N. Bloembergen, *Science* 133, 1363 (1961).

- 1-11 T. Kushida and K. Saiki, *Phys. Rev. Letters* 7, 9 (1961).

- 1-12 J. Armstrong, N. Bloembergen and D. Gill, *Phys. Rev. Letters* 7, 11 (1961).

- 1-13 J. Armstrong, N. Bloembergen and D. Gill, *J. Chem. Phys.* 35, 1132 (1961),

N. Bloembergen, *J. Chem. Phys.* 35, 1131 (1961).

- 1-14 R. Dixon, private communication.

See also:

N. Bloembergen, *Proceedings of Conference on Electric and Magnetic Resonance (Colloque Ampere)*, Eindhoven, Netherlands, 1962 (to be published).

- 1-15 D. Gill and N. Bloembergen, Bull. Am. Phys. Soc. 7, 84 (1962); and Phys. Rev. (to be published).

See also:

N. Bloembergen, Ref. 1-14.

- 1-16 G. W. Ludwig and H. H. Woodbury, Phys. Rev. Letters 7, 240 (1961);
F. S. Ham, Phys. Rev. Letters 7, 242 (1961).
- 1-17 G. W. Ludwig and F. S. Ham, Phys. Rev. Letters 8, 210 (1962);
G. W. Ludwig, First International Conference of Paramagnetic Resonance, The Hebrew University, Jerusalem, Israel, 1962 (to be published).

For a review of the spectra of impurities in silicon, see:

G. W. Ludwig and H. H. Woodbury, Solid State Physics 13, 223 (1962).

- 1-18 J. E. Wertz and P. Auzins, Phys. Rev. 106, 484 (1957).

See also:

J. H. E. Griffiths and J. W. Orton, Proc. Phys. Soc. 73, 948 (1959).

- 1-19 For the structure of ruby, see:

W. G. Wyckoff, Crystal Structures, Vol. II (Interscience Publishers, New York, 1960), and references therein;

L. Pauling, Z. Krist. 69, 415 (1928);

S. Geschwind and J. P. Remeika, J. Appl. Phys. 33, 370 (1962).

While the cell parameters quoted by Wyckoff are probably correct, the interatomic distances quoted are probably not.

- 1-20 For the magnetic resonance spectrum of ruby, see:

G. M. Zverev and A. M. Prokhorov, Soviet Physics--JETP 7, 354 (1958);

A. A. Manenkov and A. M. Prokhorov, Soviet Physics--JETP 1, 611 (1955);

J. E. Geusic, Phys. Rev. 102, 1252 (1956).

1-21 J. O. Artman and J. C. Murphy, Bull. Am. Phys. Soc. 7, 14 (1962).

For a theoretical discussion see:

J. O. Artman and J. C. Murphy, Bull. Am. Phys. Soc. 7, 196 (1962);

—First International Conference on Paramagnetic Resonance, The Hebrew University, Jerusalem, Israel, 1962 (to be published).

1-22 E. B. Royce and N. Bloembergen, Bull. Am. Soc. 7, 200 (1962).

1-23 N. Bloembergen and E. B. Royce, First International Conference on Paramagnetic Resonance, The Hebrew University, Israel, 1962 (to be published).

1-24 D. L. Carter and A. Okaya, Phys. Rev. 118, 1485 (1960).

1-25 M. Weger and E. Feher, First International Conference on Paramagnetic Resonance, The Hebrew University, Jerusalem, Israel, 1962 (to be published).

1-26 M. Sachs and S. Schwebel, Annals of Physics 8, 475 (1959);

M. Sachs, Annals of Physics 6, 244 (1959).

1-27 M. E. Browne, Phys. Rev. 121, 1699 (1961).

1-28 D. F. Nelson, A. A. Schupp, R. W. Pidd and H. R. Crane, Phys. Rev. Letters 2, 492 (1959).

2-1 See references 1-1 and 1-2.

2-2 The reader unfamiliar with microwave techniques is referred to any of the texts on that subject, such as:

D. J. E. Ingram, Spectroscopy at Radio and Microwave Frequencies (Butterworths, London, 1955);

S. Ramo and J. R. Winnery, Fields and Waves in Modern Radio (John Wiley and Sons, Inc., New York, 1953);

E. L. Ginzton, Microwave Measurements (McGraw-Hill Book Co., Inc., New York, 1957);

T. Moreno, Microwave Transmission Design Data (Dover, New York, 1948).

For a discussion of magnetic resonance spectrometers, see:

G. Feher, Bell System Tech. J. 36, 449 (1957), and references therein.

2-3 G. D. Watkins, Thesis, Harvard University, 1952.

2-4 A. M. Portis, Phys. Rev. 91, 1071 (1953).

2-5 For a discussion of the various cases of adiabatic rapid and fast passage and the resultant signals on phase detections, see:

A. M. Portis, Magnetic Resonance in Systems with Spectral Distributions, Tech. Note No. 1, Sarah Mellon Scaife Radiation Laboratory, University of Pittsburgh (1955);

M. Weger, Bell System Tech. J. 39, 1013 (1960).

In nuclear magnetic resonance, similar phenomena arising from inhomogeneous broadening due to magnetic field inhomogeneities have been discussed by:

N. Bloembergen, E. M. Purcell and R. V. Pound, Phys. Rev. 73, 679 (1948);

A. G. Redfield, Phys. Rev. 98, 1782 (1955).

The case discussed by Redfield differs from the usual paramagnetic case in that he considers tightly coupled spins.

Adiabatic rapid passage is most clearly discussed in the paper:

F. Bloch, Phys. Rev. 70, 460 (1946).

- 2-6 See reference 1-18.
- 2-7 See reference 1-24.
- 2-8 See reference 1-16. Other impurities in silicon have also shown electric field effects; see reference 1-17.
- 2-9 G. Feher, Phys. Rev. 114, 1219 (especially p. 1239) (1955).
- 2-10 I. Solomon and J. Ezratty, Phys. Rev. 127, 78 (1962).

- 3-1 See reference 1-21.
- 3-2 See reference 1-22.
- 3-3 See reference 1-23.
- 3-4 See reference 1-20.
- 3-5 See reference 1-19.
- 3-6 W. Kaiser, S. Sugano and D. L. Wood, Phys. Rev. Letters 6, 605(1961).
- 3-7 W. S. Chang and A. E. Siegman, Stanford Electronics Laboratory, Tech. Report 156-2;

Reproduced in:

- J. Weber, Rev. Mod. Phys. 31, 681 (1959).
- 3-8 S. Geschwind and J. P. Remeika, Phys. Rev. 122, 757 (1961).

- 4-1 See for example: J. S. Griffith, The Theory of Transition Metal Ions (Cambridge Univ. Press, Cambridge, 1961), or references listed under 1-1.

For reviews of crystal field theory and optical spectra, see:

- W. A. Runciman, Rep. Prog. Phys. 21, 30 (1958);
- D. S. McClure, Solid State Physics, 9, 400 (1959).

For an illuminating comparison of the 3d transition and 4f rare earth groups, see:

- G. Burns, Phys. Rev. 128, 2121 (1962).
- 4-2 Y. Tanabe and S. Sugano, J. Phys. Soc. Japan 9, 753, 766 (1954) (I and II).
- 4-3 R. Finkelstein and J. H. Van Vleck, J. Chem. Phys. 8, 787, 790 (1940).
- 4-4 R. L. Belford and M. Karplus, J. Chem. Phys. 31, 394 (1959).
- 4-5 T. S. Piper and R. L. Carlin, J. Chem. Phys. 33, 1208 (1960).
- 4-6 W. H. Kleiner, J. Chem. Phys. 20, 1784 (1952).
- 4-7 Y. Tanabe and S. Sugano, J. Phys. Soc. Japan 11, 864 (1956)(III);
S. Sugano, J. Appl. Phys. Supp. 33, (1962).
- 4-8 J. H. Van Vleck, J. Chem. Phys. 3, 803 (1935).
- 4-9 J. H. E. Griffiths, J. Owen and I. M. Ward, Proc. Roy. Soc. A219 526 (1953);
K. W. H. Stevens, Proc. Roy. Soc. A219 ; 542 (1953);
J. H. E. Griffiths and J. Owen, Proc. Roy. Soc. A226, 96 (1954).
- 4-10 M. Tinkham, Proc. Roy. Soc. A227, 183 (1955).
- 4-11 MnF_2 : R. G. Shulman and V. Jaccarino, Phys. Rev. 108, 1219 (1957);
Ibid. 109, 1084 (1958).
 FeF_2 : J. W. Stout and R. G. Shulman, Phys. Rev. 118, 1136 (1960).
 $KMnF_3$: R. G. Shulman and K. Knox, Phys. Rev. 119, 94 (1960).
 $KNiF_3$: R. G. Shulman and K. Knox, Phys. Rev. Letters 4, 603 (1960).
- 4-12 R. G. Shulman and S. Sugano, Phys. Rev. Letters 7, 157 (1961).
- 4-13 J. H. Van Vleck, J. Chem. Phys. 7, 61, 72 (1939).
- 4-14 R. Schlapp and W. G. Penney, Phys. Rev. 42, 666 (1932).
- 4-15 A. Siegert, Physica 4, 138 (1957).

- 4-16 S. Sugano and Y. Tanabe, J. Phys. Soc. Japan 13, 880 (1958) .
- 4-17 S. Sugano and M. Peter, Phys. Rev. 122, 381 (1961).
- 4-18 D. S. McClure, J. Chem. Phys. 36, 2757 (1962).
- 4-19 See reference 1-21 .
- 4-20 L. L. Lohr, Jr. and W. N. Lipscomb, J. Chem. Phys., to be published.
- 4-21 See reference 1-3 .
- 4-22 S. L. Adler, Phys. Rev. 126, 413 (1962).
- 4-23 R. M. Sternheimer, Phys. Rev. 96, 951 (1954);
Ibid. 107, 1565 (1957);
Ibid. 115, 1198 (1959);
Ibid. 127, 1220 (1962).
- 4-24 E. E. Havinga, Phys. Rev. 119, 1193 (1960).
- 4-25 M. H. Brodsky and E. Burstein, Bull. Am. Phys. Soc. 7, 214 (1962).
- 4-26 See reference 1-15.
- 4-27 R. W. Dixon, see reference 1-14 .
- 4-28 G. G. Belford, R. A. Bernheim and H. S. Gutowsky, J. Chem. Phys. 35, 1032 (1961).
- 4-29 J. R. Tessman, A. H. Kahn and W. Shockley, Phys. Rev. 92, 890 (1953).
- 4-30 S. Roberts, Phys. Rev. 76, 1215 (1949).
- 4-31 G. O. Jones, D. H. Martin, P. A. Mower and C. H. Perry, Proc. Roy. Soc. A261, 10 (1961);
B. Szigeti (ref. 1-3) .

- 4-32 A. R. Von Hippel, ed., Dielectric Materials and Applications (John Wiley and Sons, Inc., New York, 1954);
Handbook of Chemistry and Physics, C. D. Hodgman, ed. (Chemical Rubber Pub. Co., Cleveland, 1950).
- 4-33 W. Kaiser, S. Sugano and D. L. Wood, Phys. Rev. Letters 6, 605 (1961).
- 4-34 C. E. Moore, Atomic Energy Levels, National Bureau of Standards, Circular No. 467.
- 4-35 K. W. H. Stevens, Proc. Roy. Soc. A219, 542 (1953);

See also:

- J. Owen, Proc. Roy. Soc. A227, 183 (1955).
- 4-36 S. Koide and M. H. L. Price, Phil. Mag. 3, 607 (1958).
- 4-37 J. W. Stout, J. Chem. Phys. 31, 709 (1959).
- 4-38 R. Pappalardo, J. Chem. Phys. 31, 1050 (1959).
- 4-39 J. C. Zahner and H. G. Drickamer, J. Chem. Phys. 35, 1483 (1961).
- 4-40 W. Marshall and R. Stuart, Phys. Rev. 123, 2048 (1961).
- 4-41 Y. Tanabe and H. Kamimura, J. Phys. Soc. Japan 13, 394 (1958)(IV);
T. Tanabe, Supp. Prog. Theoret. Phys. (Kyoto) 14, 17 (1960);
W. A. Runciman and K. A. Schroeder, Proc. Roy. Soc. A265, 489 (1962);
J. S. Griffith, The Irreducible Tensorial Method for Molecular Symmetry Groups (Prentice-Hall, Englewood Cliffs, New Jersey (1962)).
- 4-42 R. Lacroix, Comp. Rend. 252, 1768 (1961).
- 4-43 H. Kamimura, Phys. Rev. 128, 1077 (1962).
- 4-44 N. Laurence, E. C. McIrvine and J. Lamb, J. Phys. Chem. Solids 23, 515 (1962).

- 4-45 P. H. Fang and W. S. Brower, *Phys. Rev.*, to be published.
- 4-46 See reference 1-25 .
- 5-1 See for example B. Szigeti, reference 1-3 .
- 5-2 W. G. Wyckoff, Crystal Structures (Interscience Publishers, New York, 1960) .
- 5-3 See reference 4-20 .
- 5-4 J. H. Gerritsen, S. E. Harrison, H. R. Lewis and J. P. Wittke, *Phys. Rev. Letters* 2, 153 (1959).
Radio Corporation of America Laboratories, Molecular Amplifiers and Generators, Progress Reports Feb. 15, 1960 and Oct. 15, 1960.
- 5-5 See reference 4-41 .
- 5-6 See reference 1-24.
- 5-7 H. Watanabe, *Prog. Theoret. Phys. (Kyoto)* 18, 405 (1957) .

See also:

- C. A. Huntington, B. R. Judd and D. F. O. Pope, *Proc. Phys. Soc.* B70, 514 (1957).
- 5-8 G. Racah, *Phys. Rev.* 61, 186 (1942);
 Ibid. 62, 438 (1942) ;
 Ibid. 63, 367 (1943);
- U. Fano and G. Racah, Irreducible Tensorial Sets (Academic Press, New York, 1959);
- E. U. Condon and G. H. Shortly, Theory of Atomic Spectra (Cambridge University Press, Cambridge, 1959).
- 5-9 M. J. D. Powell, J. R. Gabriel and D. F. Johnson, *Phys. Rev. Letters* 5, 145 (1960);
 J. R. Gabriel, D. F. Johnson and M. J. D. Powell, *Proc. Roy. Soc.* A264, 503 (1961).

- 5-10 S. H. Wemple, Bull. Am. Phys. Soc. 8, 62 (1963).
- 6-1 E. E. Salpeter, Phys. Rev. 112, 1642 (1958).
- 6-2 G. Feinberg, Phys. Rev. 112, 1637 (1958).
- 6-3 See reference 1-28.
- 6-4 D. T. Wilkinson, result quoted in Harvard colloquium.
- 6-5 L. Landau, Nuclear Physics 3, 127 (1957);
— Soviet Physics--JETP 5, 336 (1957);
T. D. Lee and C. N. Yang, Phys. Rev. 104, 254 (1956);
— Brookhaven National Laboratory Report BNL-443 (1957);
T. D. Lee, R. Oehme and C. N. Yang, Phys. Rev. 106, 340 (1957).

See also:

- N. Ramsey, Phys. Rev. 109, 225 (1958).
- 6-6 R. M. Sternheimer, Phys. Rev. 113, 828 (1959).
- 6-7 Smith, E. M. Purcell and N. Ramsey, Phys. Rev. 108, 120 (1957).
- 6-8 Berley, Garwin, Gidal and Lederman, Phys. Rev. Letters 1, 144 (1958).
- 6-9 J. Goldemberg and Y. Torizuka, Phys. Rev.; to be published.
- 6-10 See reference 1-26.
- 6-11 See reference 1-27.
- 6-12 See reference 4-18.